JOURNAL OF GEOPHYSICAL RESEARCH, VOL. 113, E12S42, doi:10.1029/2008JE003201, 2008

Iron mineralogy and aqueous alteration from Husband Hill through Home Plate at Gusev Crater, Mars: Results from the Mössbauer instrument on the Spirit Mars Exploration Rover

R. V. Morris,[1] G. Klingelhöfer,[2] C. Schröder,[1] I. Fleischer,[2] D. W. Ming,[1] A. S. Yen,[3] R. Gellert,[4] R. E. Arvidson,[5] D. S. Rodionov,[2,6] L. S. Crumpler,[7] B. C. Clark,[8] B. A. Cohen,[9] T. J. McCoy,[10] D. W. Mittlefehldt,[1] M. E. Schmidt,[10] P. A. de Souza Jr.,[11] and S. W. Squyres[12]

Received 20 May 2008; accepted 8 October 2008; published 23 December 2008.

[1] Spirit's Mössbauer (MB) instrument determined the Fe mineralogy and oxidation state of 71 rocks and 43 soils during its exploration of the Gusev plains and the Columbia Hills (West Spur, Husband Hill, Haskin Ridge, northern Inner Basin, and Home Plate) on Mars. The plains are predominantly float rocks and soil derived from olivine basalts. Outcrops at West Spur and on Husband Hill have experienced pervasive aqueous alteration as indicated by the presence of goethite. Olivine-rich outcrops in a possible mafic/ultramafic horizon are present on Haskin Ridge. Relatively unaltered basalt and olivine basalt float rocks occur at isolated locations throughout the Columbia Hills. Basalt and olivine basalt outcrops are found at and near Home Plate, a putative hydrovolcanic structure. At least three pyroxene compositions are indicated by MB data. MB spectra of outcrops Barnhill and Torquas resemble palagonitic material and thus possible supergene aqueous alteration. Deposits of Fe^{3+}-sulfate soil, located at Paso Robles, Arad, and Tyrone, are likely products of acid sulfate fumarolic and/or hydrothermal activity, possibly in connection with Home Plate volcanism. Hematite-rich outcrops between Home Plate and Tyrone (e.g., Montalva) may also be products of this aqueous activity. Low water-to-rock ratios (isochemical alteration) are implied during palagonite, goethite, and hematite formation because bulk chemical compositions are basaltic (SO_3-free basis). High water-to-rock ratios (leaching) under acid sulfate conditions are implied for the high-SiO_2 rock and soil in Eastern Valley and the float rock FuzzySmith, which has possible pyrite/marcasite as a hydrothermal alteration product.

Citation: Morris, R. V., et al. (2008), Iron mineralogy and aqueous alteration from Husband Hill through Home Plate at Gusev Crater, Mars: Results from the Mössbauer instrument on the Spirit Mars Exploration Rover, *J. Geophys. Res.*, *113*, E12S42, doi:10.1029/2008JE003201.

1. Background

[2] The Mars Exploration Rover (MER) Spirit traversed the plains of 160 km diameter Gusev Crater eastward from its landing site (sol 0; 14.5692°S, 175.4729°E in International Astronomical Union 2000 coordinates on 4 January 2004 UTC [*Squyres et al.*, 2004; *Arvidson et al.*, 2004]) to the Columbia Hills (sol ∼155). Spirit encountered the Columbia Hills at West Spur (Figure 1), climbed up and over West Spur (sol ∼329) and up the NW slope of Husband Hill to its summit (sol ∼618), descended Husband Hill via Haskin Ridge (sol ∼705) and the El Dorado ripple field (sol ∼710), and drove into the northern Inner Basin of the Columbia Hills. The rover proceeded to the NW corner of Home Plate (sol ∼742) and completed its first encounter with the structure by exiting to the east (sol ∼772). Spirit crisscrossed the area to the east and SE of Home Plate, including an aborted attempt to climb McCool

[1]NASA Johnson Space Center, Houston, Texas, USA.
[2]Institut fur Anorganische und Analytische Chemie, Johannes Gutenberg Universität, Mainz, Germany.
[3]Jet Propulsion Laboratory, California Institute of Technology, Pasadena, California, USA.
[4]Department of Physics, University of Guelph, Guelph, Ontario, Canada.
[5]Department of Earth and Planetary Sciences, Washington University, St. Louis, Missouri, USA.
[6]Space Research Institute, Moscow, Russia.
[7]New Mexico Museum of Natural History and Science, Albuquerque, New Mexico, USA.
[8]Lockheed Martin Corporation, Littleton, Colorado, USA.
[9]NASA Marshall Space Flight Center, Huntsville, Alabama, USA.
[10]Department of Mineral Sciences, Smithsonian Institution, Washington, D.C., USA.
[11]Tasmanian ICT Centre, CSIRO, Hobart, Tasmania, Australia.
[12]Department of Astronomy, Cornell University, Ithaca, New York, USA.

0148-0227/08/2008JE003201$09.00

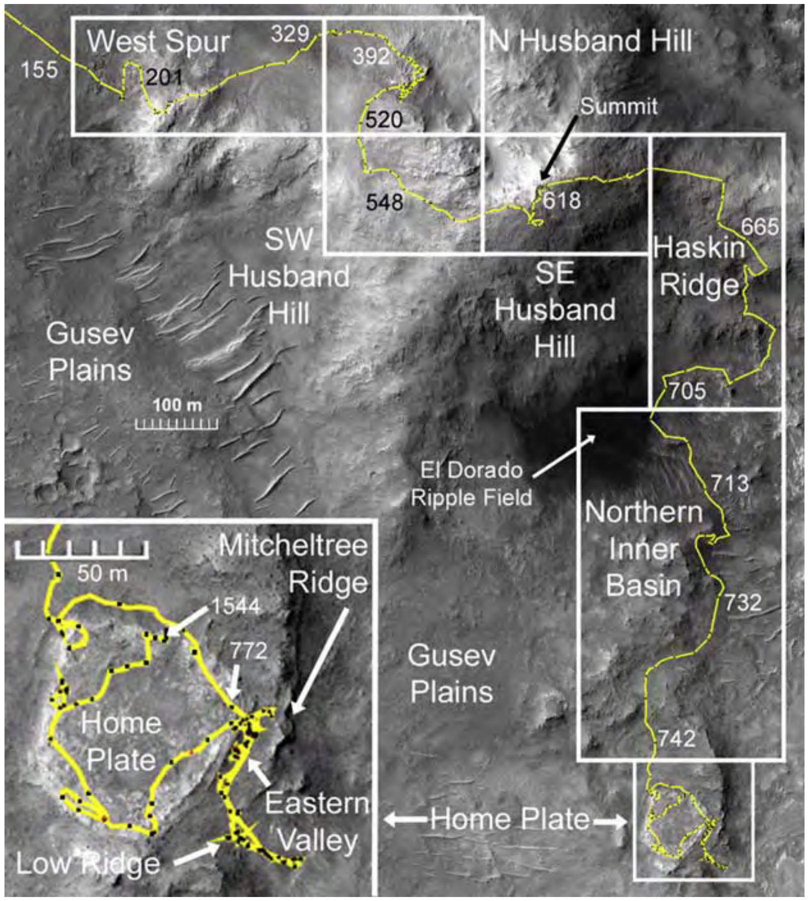

Figure 1. Image showing the Columbia Hills region of Gusev Crater explored by the Spirit rover. The boxes (modeled after *Arvidson et al.* [2008]) are keyed to text discussion. Selected sol numbers are located along the traverse for reference. A sol is a Martian solar day and is equal to 2439:35.244 UT.

Hill and exploration of Low Ridge and Eastern Valley, and then climbed back onto Home Plate to begin its second encounter on sol ~1315. As of sol 1544, Spirit was parked on a north facing slope of Home Plate to optimize solar power generation for its third winter on Mars. Spirit spent its first two winters on north facing slopes at West Spur on the NW side of Husband Hill and at Low Ridge. A discussion of Spirit's traverse and measurement campaigns and maps showing details of traverses overlain onto a HiRISE map base are found by *Arvidson et al.* [2006, 2008].

[3] Spirit and its twin Opportunity on the other side of Mars at Meridiani Planum each carry six science instruments [*Squyres et al.*, 2003; *Klingelhöfer et al.*, 2003]. The stereo, multispectral panoramic imager (Pancam) and the Mini-Thermal Emission Spectrometer (Mini-TES) are mast-mounted remote sensing instruments. Mounted on the Instrument Deployment Device (IDD) at the end of the 5 degree of freedom robotic arm are the four contact instruments: the MIMOS II Mössbauer Spectrometer (MB), the Alpha Particle X-Ray Spectrometer (APXS), the Microscopic Imager (MI), and the Rock Abrasion Tool (RAT). As of sol 1544, all science instruments are functional except that the RAT is limited to brushing activities because its grinding pads have worn away (last use sol ~420), and Mini-TES is compromised by a spectrally thick covering of dust on the mirror that reflects middle-infrared energy into the instrument (since sol 1370). The MB instrument has full functionality, with a source strength of ~2 mCi (~150 mCi at sol 0). Rover mobility is also impaired because one of its six wheels is immobile (beginning sol ~799); the frozen wheel, however, is a good trenching tool, revealing subsurface material.

[4] The primary scientific objective of Spirit's exploration of Gusev Crater is to characterize the surface and atmosphere, searching for evidence of water and clues for assessing past and current climates and their suitability for life [*Squyres et al.*, 2004]. The focus of this paper relative to that objective is the results of the Mössbauer spectrometer. The instrument provides quantitative information about the distribution of Fe among its coordination states and oxidation states (ratio of Fe^{3+} to total Fe; Fe^{3+}/Fe_T), the identification of Fe-bearing phases, and the relative distribution of Fe among coordination states, oxidation states, and Fe-bearing phases. Mössbauer spectra do not directly provide information about the concentration of Fe-bearing phases (e.g., olivine); rather, MB spectra provide information about the amount of Fe associated with Fe-bearing phases. Thus, a sample could be 100% olivine as Mg_2SiO_4, but that olivine would not be detected by MB.

[5] Despite the Fe-centric view of Mössbauer spectroscopy, a MB instrument is a key mineralogical exploration

Table 1. Mössbauer Parameters δ, ΔE_Q, and FWHM for Fe2D1 (Ol), Fe2D2 (Px), and Fe3D1 (npOx) Doublet Subspectra[a]

	Generic Phase Name (Assignment)									
	Fe2D1 (Ol)			Fe2D2 (Px)			Fe3D1 (npOx)			
Target Name[b]	δ (mm/s)	ΔE_Q (mm/s)	FWHM (mm/s)	δ (mm/s)	ΔE_Q (mm/s)	FWHM (mm/s)	δ (mm/s)	ΔE_Q (mm/s)	FWHM (mm/s)	T (K)
North, SW, and SE Husband Hill and Haskin Ridge										
A534RB0 (Independence_Livingston)[c]	–	–	–	[1.13][d]	[2.14]	[0.59]	0.38[e]	0.95	0.86	210–290
A540RS0 (Independence_Penn2)[c]	–	–	–	1.19	2.45	0.90	0.38	0.76	0.96	210–290
A555RB0 (Descartes_Discourse)	[1.15]	[3.00]	[0.42]	1.17	2.12	0.46	0.37	0.91	0.66	210–280
A559RB0 (Bourgeoisie_Chic)	1.17	2.98	0.40	1.16	2.11	0.37	[0.37]	0.77	0.74	210–270
A562RB0 (Bourgeoisie_Gentle Matrice)[c]	[1.15]	[3.00]	[0.42]	1.17	2.15	0.44	0.38	0.99	0.59	210–270
A568RU0 (Assemblee_Gruyere)[c]	–	–	–	1.05	2.39	0.64	0.34	1.16	0.63	200–270
A585SU0 (Lambert_Whymper)	1.15	2.99	0.42	1.14	2.11	0.58	0.39	0.83	0.82	200–270
A602RU0 (Irvine_Shrewsbury)	1.15	2.95	0.34	1.16	2.13	0.46	[0.37]	0.82	0.53	200–270
A609SU0 (Cliffhanger_Hang2)	1.15	3.01	0.35	1.16	2.22	0.62	0.38	0.89	0.72	200–270
A611SD0 (Cliffhanger_Lands End)	1.15	3.04	0.38	1.17	2.17	0.57	0.36	0.91	0.68	200–270
A629RU0 (Hillary_Khumjung)	[1.15]	[3.00]	[0.39]	1.14	2.15	0.42	0.39	1.06	0.71	210–270
A631RU0 (Hillary_Namche Bazaar)	[1.15]	[3.00]	[0.39]	[1.15]	[2.18]	[0.49]	0.39	1.03	0.54	210–270
A648RB0 (Kansas_Kestrel)	–	–	–	1.17	2.11	0.43	0.38	1.08	0.58	200–270
A662RB0 (Larrys Bench_Thrasher)	1.15	3.03	0.39	[1.15]	[2.06]	[0.49]	0.37	0.90	0.60	210–270
A674RB0 (Seminole_Osceola)	1.15	3.04	0.40	1.18	2.18	0.40	0.38	0.92	0.67	210–270
A677RB0 (Seminole_Abiaka)	1.15	3.02	0.39	1.17	2.14	0.36	0.36	0.89	0.65	210–270
A690RB0 (Algonquin_Iroquet)	1.15	3.05	0.39	1.15	2.14	0.43	0.33	0.90	0.70	210–270
A699RU0 (Comanche Spur_Horse Back)	1.15	3.05	0.40	1.23	1.94	0.42	0.34	0.94	0.83	210–270
A702RB0 (Comanche Spur_Palimino)	1.16	3.07	0.41	1.24	1.93	0.42	0.33	1.07	0.82	210–270
A708SU0 (El Dorado Scuff_Shadow)	1.15	3.02	0.39	1.13	2.12	0.61	[0.37]	0.86	0.71	200–270
Northern Inner Basin										
A723SD0 (Arad_Samra)	[1.15]	[2.95]	[0.39]	[1.16]	[2.17]	[0.56]	–	–	–	190–270
A737RU0 (Bu Zhou_Gong Gong)	[1.14]	[2.97]	[0.41]	1.15	2.11	0.41	0.36	0.84	0.53	190–270
Home Plate										
A748RU0 (Barnhill_Ace)	1.14	2.99	0.40	1.15	2.09	0.47	0.36	0.88	0.63	200–260
A754RB0 (Posey_Manager)	1.15	3.04	0.35	1.15	2.16	0.53	0.38	0.94	0.70	200–260
A762RB0 (James Cool Papa Bell_Stars)	1.14	3.02	0.37	1.16	2.15	0.55	0.37	0.91	0.62	190–270
A769RU0 (Home Plate_Fuzzy Smith)[f]	[1.14]	[3.01]	[0.38]	1.17	2.13	0.50	–	–	–	190–250
Low Ridge and Eastern Valley										
A810RU0 (Enderbyland_Halley)	[1.15]	[3.03]	[0.39]	1.14	2.14	0.59	[0.38]	[0.92]	[0.76]	190–260
A817SU0 (Enderbyland_Mawson)	1.15	3.05	0.38	1.15	2.15	0.54	0.36	0.89	0.66	190–250
A826SU0 (Enderbyland_Progress)	1.16	3.03	0.39	1.15	2.12	0.53	0.39	0.85	0.70	190–250
A836RU0 (Enderbyland_Halley Offset)	[1.15]	[3.03]	[0.39]	[1.14]	[2.13]	[0.57]	0.37	0.73	0.55	190–250
A840SB0 (Enderbyland_Progress1)	1.15	3.03	0.41	1.15	2.10	0.53	0.38	0.86	0.64	190–250
A853SB0 (Enderbyland_Progress2)	1.16	3.04	0.42	1.15	2.12	0.53	0.39	0.88	0.71	190–240
A880RU0 (Enderbyland_Halley Brunt)	1.16	3.00	0.36	1.15	2.09	0.51	[0.38]	[0.92]	[0.76]	200–250
A948RU0 (Endebyland_Halley Brunt Offset3)	[1.15]	[3.03]	[0.39]	[1.14]	[2.13]	[0.57]	[0.38]	[0.92]	[0.76]	220–250
A1015SD0 Tyrone_Berkner Island1) Model A	[1.14]	[3.01]	[0.41]	[1.16]	[2.13]	[0.64]	–	–	–	190–250
A1015SD0 Tyrone_Berkner Island1) Model B	[1.14]	[3.01]	[0.41]	[1.16]	[2.13]	[0.64]	[0.37]	[0.86]	[0.65]	190–250
A1018SD0 (Bear Island_Bear Island)	1.15	3.01	0.40	1.16	2.12	0.56	[0.37]	0.86	0.65	190–260
A1029RU0 (Graham Land_King George)	1.18	3.01	0.37	1.14	2.13	0.49	0.38	0.80	0.63	190–260
A1033RB0 (Graham Land_King George)	1.17	[3.03]	0.39	1.15	2.10	0.49	0.36	0.84	0.67	190–260
A1056RU0 (Esperanza_Palma)	[1.16]	[3.01]	[0.39]	1.15	2.09	0.45	[0.37]	0.82	0.50	250–280
A1073RU0 (Troll_Montalva)	–	–	–	[1.14]	[2.13]	[0.57]	[0.38]	0.77	0.50	200–270
A1082RU0 (Troll_Riquelme3)	[1.15]	[3.01]	[0.39]	1.12	2.15	0.52	0.33	0.89	0.59	190–270
A1101SD0 (Tyrone_Mount Darwin) Model A	[1.14]	[3.01]	[0.41]	[1.16]	[2.13]	[0.64]	–	–	–	190–270
A1101SD0 (Tyrone_Mount Darwin) Model B	[1.14]	[3.01]	[0.41]	[1.16]	[2.13]	[0.64]	[0.37]	[0.86]	[0.65]	190–270
A1145RB0 (Torquas_Torquas2)	[1.14]	[2.97]	[0.41]	1.16	2.12	0.38	0.35	0.82	0.60	200–270
A1155RU0 (Elizabeth Mahon_Elizabeth Mahon)	[1.14]	[3.01]	[0.41]	[1.17]	[2.10]	[0.54]	0.33	0.91	0.49	200–270
A1170RU0 (Madeline English_Madeline EnglishIDD)	[1.14]	[3.01]	[0.41]	1.17	2.13	0.40	0.39	0.82	0.61	200–270
A1174RS0 (Examine This_Everett)	[1.14]	[3.01]	[0.38]	1.16	2.15	0.43	0.34	0.79	0.71	210–270
A1177RB0 (Examine This_Slide)	[1.14]	[2.97]	[0.41]	1.16	2.10	0.41	0.37	0.82	0.54	210–270
A1180RU0 (Examine This_Good Question)	1.17	2.99	[0.41]	1.17	2.08	0.42	0.34	0.90	0.54	210–270
A1191SD0 (Gertrude Weise_Kenosha Comets)	[1.16]	[3.00]	[0.41]	[1.15]	[2.11]	[0.52]	[0.37]	[0.86]	[0.64]	200–270
A1200SD0 (Gertrude Weise_Lefty Ganote)	[1.16]	[3.00]	[0.41]	[1.15]	[2.11]	[0.52]	[0.37]	[0.86]	[0.64]	210–270
Home Plate										
A1207RB0 (Home Plate_Pesapallo1)	[1.14]	[2.97]	[0.41]	1.15	2.13	0.46	0.38	0.96	0.60	210–270
A1213RB0 (Home Plate_June Emerson)	[1.14]	[2.97]	[0.41]	1.16	2.11	0.44	0.36	0.92	0.52	210–270
A1217RB0 (Home Plate_Elizabeth Emery)	[1.14]	[2.97]	[0.41]	1.16	2.11	0.48	0.38	0.81	0.62	210–270
Eastern Valley										
A1228RU0 (Eastern Valley_Nancy Warren)	[1.14]	[2.97]	[0.41]	1.16	2.08	0.43	[0.37]	0.72	0.71	200–270
A1245SD0 (Eastern Valley_Eileen Dean)	[1.14]	[2.97]	[0.41]	1.14	2.11	0.47	[0.35]	0.95	0.63	210–270
A1255RD0 (Eastern Valley_Innocent Bystander)	[1.14]	[2.97]	[0.41]	[1.17]	[2.11]	[0.37]	[0.35]	0.92	0.73	210–260

Table 1. (continued)

	Generic Phase Name (Assignment)									
	Fe2D1 (Ol)			Fe2D2 (Px)			Fe3D1 (npOx)			
Target Name[b]	δ (mm/s)	ΔE_Q (mm/s)	FWHM (mm/s)	δ (mm/s)	ΔE_Q (mm/s)	FWHM (mm/s)	δ (mm/s)	ΔE_Q (mm/s)	FWHM (mm/s)	T (K)
				Home Plate						
A1328RB0 (Home Plate_Texas Chili)	[1.14]	[2.97]	[0.41]	1.15	2.14	0.46	0.32	.96	0.65	210–270
A1343RU0 (Home Plate_Humboldt Peak)	1.14	3.03	0.41	[1.14]	[2.08]	[0.48]	[0.36]	[0.88]	[0.63]	210–270
A1370RB0 (Home Plate_Pecan Pie)	[1.14]	[2.97]	[0.41]	1.14	2.09	0.45	0.37	0.84	0.66	200–270
A1411RU0 (Home Plate_Chanute)	[1.14]	[2.97]	[0.41]	1.16	2.12	0.40	0.34	0.90	0.66	200–260
				All Gusev Crater Targets[g]						
Average all targets	1.15	3.00	0.39	1.16	2.14	0.50	0.37	0.90	0.67	190–270
Standard deviation (2σ)	0.02	0.07	0.04	0.04	0.16	0.18	0.04	0.18	0.20	190–270
Average Px-A	–	–	–	1.16	2.12		–	–	–	200–270
Standard deviation	–	–	–	0.02	0.04		–	–	–	200–270
Average Px-B	–	–	–	1.16	2.28		–	–	–	200–270
Standard deviation	–	–	–	0.13	0.10		–	–	–	200–270
Average Px-C	–	–	–	1.23	1.93		–	–	–	200–270
Standard deviation	–	–	–	0.02	0.02		–	–	–	200–270

[a]Parameters were calculated from spectra summed over the temperature interval. The values of δ are referenced to metallic iron foil at the same temperature as the sample. FWMH is full width at half maximum.

[b]Target naming convention is Awwwwxyz (Feature-name_Target-name). A, MER-A (Gusev Crater); wwww, Gusev Crater sol number that data product was returned to Earth (for integrations covering multiple sols, the sol of the first returned data product is used); x, R (rock) or S (soil); y, U (undisturbed), D (disturbed), T (trench), B (RAT brushed surface), R (RAT ground surface), G (RAT grindings), or S (Scuff or scrape on rock surface made with rover wheel); z, 0 by default; z = 1, 2, 3... for multiple analyses of the same target on the same sol. For AxxxSTz, z = 1, 2, 3... with increasing number corresponding to increasing depth. Alphanumeric strings before parentheses are unique target identifiers.

[c]From *Clark et al.* [2007].

[d]MB parameters in brackets are constraints used in the fitting procedure.

[e]Unless otherwise noted, MB parameter uncertainty is ±0.02 mm/s.

[f]From *Squyres et al.* [2007].

[g]Average includes values for Gusev Crater targets from *Morris et al.* [2006a].

tool in a Fe-rich environment like Mars because important rock-forming minerals (e.g., olivine (Ol), pyroxene (Px), ilmenite (Ilm), and (titano)magnetite (Mt)) and secondary minerals (e.g., serpentine, Fe-sulfates, and oxides/oxyhydroxides like hematite (Hm), goethite (Gt), and ferrihydrite) are Fe bearing. For unaltered or weakly altered rocks, the Fe^{3+}/Fe_T ratio provided by MB is necessary to perform normative calculations [e.g., *McSween et al.*, 2006a, 2006b, 2008; *Ming et al.*, 2006], and the distribution of Fe among Fe-bearing phases distinguishes between different types of rock (e.g., presence or absence of olivine in basalt). For altered basaltic materials, MB provides information about the distribution of Fe-bearing phases among alteration products (e.g., nanophase ferric oxide (npOx), jarosite, and phyllosilicates), which constrain the type and extent of alteration and weathering (e.g., neutral versus acid chloride versus acid sulfate aqueous process under ambient or hydrothermal conditions [e.g., *Morris et al.*, 2000a]).

[6] Mössbauer results for Gusev Crater were published by the MER team for the first 90 sols in a special issue on Spirit at Gusev Crater (*Science, 305*, 793–845, 2004) [*Morris et al.*, 2004] and for the first 520 sols in a special issue on Results From the Mars Exploration Rover Spirit Mission (*J. Geophys. Res., 111,* 2006) [*Morris et al.*, 2006a]. Several topical articles have initial release of MB data since sol 520 [*Clark et al.*, 2007; *McSween et al.*, 2008; *Schmidt et al.*, 2008a; *Squyres et al.*, 2007, 2008]. Ten Fe-bearing phases were identified outright or constrained in mineralogical composition. Identified outright are olivine, pyroxene, ilmenite, and (titano)magnetite as primary igneous phases and hematite, goethite, and nanophase ferric oxide (npOx) as Fe^{3+}-bearing alteration products. A Fe^{3+}-bearing sulfate was identified in three soils, but its stoichiometry is not known. Fe^{3+}-sulfate may be more common than the number of analyses indicates, because it is present in the subsurface and only detected when exposed by the churning action of rover wheels [e.g., *Yen et al.*, 2008]. Evidence for minor Fe-bearing chromite was developed for one rock (Assemblee), but the identification relied heavily on its unusually high Cr concentration (2.7 wt % Cr_2O_3 versus <0.9 wt % in all other rock and soil targets [*Clark et al.*, 2007]). A major Fe-bearing component in one rock (FuzzySmith) was assigned to pyrite/marcasite, but the assignment is equivocal [*Squyres et al.*, 2007].

[7] During the first 520 sols, Spirit traversed the Gusev plains, entered the Columbia Hills at West Spur, and climbed West Spur and the NW slope of Husband Hill to a point near its summit. The Gusev plains are generally characterized by relatively unaltered olivine basalt float rocks and soils derived from olivine basalt. In contrast, West Spur and the NW slope of Husband Hill are generally characterized by strongly altered outcrops and relatively unaltered basalt and olivine basalt float rocks [e.g., *Morris et al.*, 2006a].

2. This Work

[8] Mössbauer results subsequent to *Morris et al.* [2006a] (sols 520 to 1544) are reported here. Spirit encountered olivine basalt soils similar to the Gusev plains, occasional subsurface and sulfate-rich soils, new varieties of relatively unaltered float and outcrop rocks that are very rich in

Table 2. Mössbauer Parameters δ, ΔE_Q, and FWHM for Fe2D3 (Ilmemite), Fe3D2 (Fe^{3+}-sulfate), and Fe?D1 Doublet Subspectra[a]

	Generic Phase Name (Assignment)									
	Fe2D3 (Ilm)			Fe3D2 (Fe^{3+}-sulfate)			Fe?D1			
Target Name	δ (mm/s)	ΔE_Q (mm/s)	FWHM (mm/s)	δ (mm/s)	ΔE_Q (mm/s)	FWHM (mm/s)	δ (mm/s)	ΔE_Q (mm/s)	FWHM (mm/s)	T (K)
North, SW, and SE Husband Hill and Haskin Ridge										
A530RB (Independence_Franklin)	[1.07][b]	[0.80]	[0.51]	–	–	–	–	–	–	210–290
A534RB0 (Independence_Livingston)	[1.07]	[0.80]	[0.45]	–	–	–	–	–	–	210–290
A540RS0 (Independence_Penn2)	[1.07]	[0.80]	[0.51]	–	–	–	–	–	–	210–290
A559RB0 (Bourgeoisie_Chic)	1.08[c]	0.81	0.52	–	–	–	–	–	–	210–270
A562RB0 (Bourgeoisie_Gentle Matrice)	1.05	0.82	0.32	–	–	–	–	–	–	210–270
A631RU0 (Hillary_Namchebazaar)	1.03	0.80	0.42	–	–	–	–	–	–	210–270
A648RB0 (Kansas_Kestrel)	1.06	0.92	0.45	–	–	–	–	–	–	200–270
A662RB0 (Larrys Bench_Thrasher)	1.06	0.83	0.32	–	–	–	–	–	–	210–270
Northern Inner Basin										
A723SD0 (Arad_Samra)	–	–	–	0.41	0.51	0.54	–	–	–	190–270
Home Plate										
A769RU0 (Home Plate_Fuzzy Smith)	[1.07]	[0.79]	[0.50]	–	–	–	0.28	0.68	0.76	190–250
Low Ridge and Eastern Valley										
A1015SD0 (Tyrone_Berkner Island1) Model A	–	–	–	0.42	0.81	0.63	–	–	–	190–250
A1015SD0 (Tyrone_Berkner Island1) Model B	–	–	–	0.44	0.79	0.63	–	–	–	190–250
A1101SD0 (Tyrone_Mount Darwin) Model A	–	–	–	[0.42]	0.78	0.57	–	–	–	190–270
A1101SD0 (Tyrone_Mount Darwin) Model B	–	–	–	[0.44]	0.75	0.55	–	–	–	190–270
A1155RU0 (Elizabeth Mahon_Elizabeth Mahon)	[1.07]	[0.79]	[0.50]	–	–	–	–	–	–	200–270
A1191SD0 (Gertrude Weise_Kenosha Comets)	[1.07]	[0.79]	[0.50]	–	–	–	–	–	–	200–270
A1255RD0 (Examine This_Innocent Bystander)	[1.06]	[0.81]	[0.50]	–	–	–	–	–	–	210–260
All Gusev Crater Targets[d]										
Average	1.07	0.80	0.38	0.43	0.58	0.64	–	–	–	190–270
Standard deviation (1σ)	0.02	0.06	0.07	0.02	0.05	0.06	–	–	–	190–270

[a]Parameters were calculated from spectra summed over the temperature interval. Values of δ are with respect to metallic iron foil at the same temperature as the sample.
[b]MB parameters in brackets are constraints used in the fitting procedure.
[c]Unless otherwise stated, MB parameter uncertainties are ±0.03 mm/s for Fe2D3 and ±0.02 mm/s for Fe3D2 and Fe?D1.
[d]Average includes values for Gusev Crater targets from *Morris et al.* [2006a].

pyroxene, olivine, and/or (titano)magnetite, and heavily altered outcrop rocks that are very rich in hematite. The procedures for calculation of Mössbauer parameters by least squares methods are described by *Morris et al.* [2006a] and are not repeated here. The derived Mössbauer parameters for each Fe speciation are the isomer shift (δ), quadrupole splitting (ΔE_Q), hyperfine field strength (B_{hf}), and subspectral area (A). The values of δ, ΔE_Q, and B_{hf} provide information about the coordination, oxidation, and mineralogical state of a subspectrum, and A is the percentage of total Fe (Fe_T) associated with specific Fe-bearing phases. The MB peak positions for doublet and sextet subspectra are characterized by δ and ΔE_Q and by δ, ΔE_Q, and B_{hf}, respectively. The remainder of this paper is divided into eight major sections: (1) identification of Fe-bearing phases; (2) classification of Gusev Crater rocks and soils; (3) the Fe mineralogy of rocks and soils along the traverse of Spirit; (4) Fe-bearing mineralogical markers for aqueous alteration; (5) isochemical aqueous alteration at low water-to-rock ratios; (6) acid sulfate alteration at high water-to-rock ratios; (7) aqueous processes and magnetite and pyroxene; and (8) the hydrothermal system at Home Plate.

3. Identification of Fe-Bearing Phases

[9] Values for the speciation sensitive Mössbauer parameters δ, ΔE_Q, and B_{hf} are compiled in Tables 1–4 or are previously published [*Morris et al.*, 2006a; *Clark et al.*, 2007; *Squyres et al.*, 2007]. Phase identification diagrams (δ versus ΔE_Q for doublets; δ versus ΔE_Q and B_{hf} versus ΔE_Q for sextets) for MB measurements through sol 1544 are shown in Figures 2 and 3 (updated from *Morris et al.* [2006a]). Seven and possibly nine different Fe-bearing phases that have doublet subspectra are now identified. The difference in potential number of phases is a result of the large range for the MB parameters of the Fe2D2 doublet (Figure 2a) as discussed in section 3.2. Three Fe-bearing phases that have sextet subspectra are identified. We now have multiple occurrences of each sextet phase, which confirms previous phase assignments and shows the natural variations for their MB parameters.

[10] Generic names for the doublet and sextet subspectra and specific mineralogical assignments, which are based largely on literature [e.g., *Burns and Solberg*, 1990; *McCammon*, 1995; *Stevens et al.*, 1998] and in-house compilations of room temperature Mössbauer parameters, are shown in Figures 2 and 3 and discussed in this section. Room temperature MB data are applicable to the Martian measurements made at lower temperatures (typically 200 to 270 K) because the difference in temperature between the MB source and the measurement target is approximately zero in both cases [e.g., *Morris et al.*, 2006a]. An important exception is the presence of a magnetic transition that occurs between room temperature and Martian surface temperatures (e.g., the Morin transition of hematite).

Table 3. Mössbauer Parameters δ, ΔE_Q, and B_{hf} for Magnetite Sextet Subspectra[a]

	Generic Phase Name (Assignment)						
	Fe3S1 (Mt tet-Fe^{3+})			Fe2.5S1 (Mt oct-$Fe^{2.5+}$)			
Target Name	δ (mm/s)	ΔE_Q (mm/s)	B_{hf} (T)	δ (mm/s)	ΔE_Q (mm/s)	B_{hf} (T)	T (K)
	North, SW, and SE Husband Hill and Haskin Ridge						
A602RU0 (Irvine_Shrewsbury)	0.30[b]	0.03	50.1	0.64	−0.03	46.6	200–270
	Northern Inner Basin						
A737RU0 (Bu Zhou_Gong Gong)	0.31	−0.01	50.0	0.65	0.00	46.8	190–270
	Home Plate						
A748RU0 (Barnhill_Ace)	0.29	0.05	49.9	0.64	−0.02	47.1	200–260
A754RB0 (Posey_Manager)	0.31	−0.03	50.6	0.66	−0.07	47.3	200–260
	Low Ridge and Eastern Valley						
A1056RU0 (Esperanza_Palma)	0.30	−0.01	49.8	0.69	0.01	45.9	250–280
A1145RB0 (Torquas_Torquas2)	0.32	−0.07	49.8	[0.65][c]	−0.05	46.2	200–270
A1170RU0 (Madeline English_Madeline EnglishIDD)	0.33	0.05	50.5	0.68	0.04	47.1	200–270
A1174RS0 (Examine This_Everett)	0.31	0.00	50.0	0.66	−0.02	47.2	210–270
A1177RB0 (Examine This_Slide)	0.33	−0.01	49.9	0.66	−0.04	46.6	210–270
	Home Plate						
A1207RB0 (Home Plate_Pesapallo1)	0.28	0.02	50.1	0.65	0.06	46.2	210–270
A1213RB0 (Home Plate_June Emerson)	0.30	0.03	50.1	0.66	−0.05	46.7	210–270
A1217RB0 (Home Plate_Elizabeth Emery)	0.30	0.01	50.1	0.64	−0.03	46.6	210–270
	Eastern Valley						
A1245SD0 (Eastern Valley_Eileen Dean)	0.33	0.02	49.5	0.67	0.07	46.7	210–270
A1255RD0 (Eastern Valley_Innocent Bystander)	0.31	0.04	50.0	0.66	−0.02	46.9	210–260
	All Gusev Crater Targets[d]						
Average	0.31	0.01	50.0	0.66	−0.01	46.7	190–270
Standard deviation (2σ)	0.03	0.03	0.5	0.06	0.08	0.8	190–270
	Parameter Constraints When Needed for Fitting Proecdures						
Mt constraint	[0.31][b]	[0.06]	[50.1]	[0.64]	[0.00]	[46.9]	190–270

[a]Parameters were calculated from spectra summed over the temperature interval. Values of δ are with respect to metallic iron foil at the same temperature as the sample.
[b]MB parameter errors are ±0.02 mm/s for δ and ΔE_Q and ±0.8 T for B_{hf}.
[c]MB parameters in brackets are constraints used in the fitting procedure.
[d]Average includes values for Gusev Crater targets from *Morris et al.* [2006a].

3.1. Fe2D1 (Olivine)

[11] The Fe2D1 doublet from octahedral (oct)-Fe^{2+} is common in rock and soil spectra throughout the Gusev plains and the Columbia Hills (Figure 4). The calculated Mössbauer parameters are very similar (Figure 2a), with average values (103 measurements) of 1.15 ± 0.02 and 3.00 ± 0.07 mm/s for δ and ΔE_Q, respectively (Table 1). We assign the doublet to Mg-rich olivine (Ol; $(Mg,Fe)_2SiO_4$) [*Morris et al.*, 2004, 2006a].

3.2. Fe2D2 (Pyroxene)

[12] The Fe2D2 doublet from oct-Fe^{2+} is also common in rock and soil spectra throughout the region of Gusev Crater explored by Spirit (Figure 4). The Mössbauer parameters for the Fe2D2 group, however, form a diffuse group compared to the Fe2D1 doublet (Figure 2a), implying differences in mineralogical composition. By visual examination, the Fe2D2 MB data can be divided into three subgroups (Px-A, Px-B, and Px-C) (Figure 2a). We discuss these three pyroxene subgroups next.

3.2.1. Fe2D2-A (Pyroxene-A)

[13] Most data for rocks and all data for soils occur within the region labeled Px-A in Figure 2a. The average values (92 measurements) of δ and ΔE_Q for Px-A are 1.16 ± 0.02 and 2.12 ± 0.04 mm/s, respectively (Table 1). We assign the Px-A doublet to pyroxene (Px; (Mg, Ca, Fe)SiO_3 [*Morris et al.*, 2006a] whose mineralogical composition (e.g., orthopyroxene, high-Ca clinopyroxene, or pigeonite) is not currently constrained.

3.2.2. Fe2D2-B (Pyroxene-B or Possible Fe^{2+} Alteration Products)

[14] The Fe2D2 doublet Mössbauer parameters for Clovis Class and Independence Class rocks plot within the region labeled Px-B (Figure 2a). The average values (19 measurements) of δ and ΔE_Q are 1.16 ± 0.03 and 2.28 ± 0.10 mm/s, respectively (Table 1). Both rock classes are highly altered on the basis of Fe mineralogy and chemical compositions [e.g., *Morris et al.*, 2006a; *Ming et al.*, 2006; *Clark et al.*, 2007]. For example, Clovis Class rocks have goethite and little or no olivine as Fe-bearing phases and Independence Class rocks have low total Fe concentrations (~6 wt % total Fe as FeO) and ilmenite or chromite (Chr) as residual Fe-bearing phases. Because Px-B is associated only with highly altered rocks, we consider that an Fe^{2+}-bearing alteration product is a viable alternate assignment to pyroxene. Nevertheless, we will refer to the phase as Px-B for shorthand notation.

3.2.3. Fe2D2-C (Pyroxene-C or Some Other Fe^{2+}-Bearing Phase)

[15] The Fe2D2 Mössbauer parameters for one Ol-rich outcrop, Comanche Spur on Haskin Ridge, are distinct from the values for all other rocks and soils (Px-C in Figure 2a).

Table 4. Mössbauer Parameters δ, ΔE_Q, and B_{hf} for Goethite and Hematite Sextet Subspectra[a]

Target Name	δ (mm/s)	ΔE_Q (mm/s)	B_{hf} (T)	T (K)
Fe3S3 (Goethite, oct-Fe^{3+}) North, SW, and SE Husband Hill and Haskin Ridge				
A648RB0 (Kansas_Kestrel)	0.37[b]	−0.26	39.4[b]	200–270
Gt average for all Gusev targets[c]	0.38	−0.19	37.3	200–270
Gt standard deviation (2σ)	0.02	0.10	2.9	200–270
Fe3S2 (Hematite,oct-Fe^{3+}) for $\Delta E_Q < -0.10$ mm/s Low Ridge and Eastern Valley				
A810RU0 (Enderbyland_Halley)	0.37	−0.16	52.2	190–260
A817SU0 (Enderbyland_Mawson)	0.36	−0.15	51.9	190–250
A836RU0 (Enderbyland_Halley Offset)	0.37	−0.16	52.2	190–250
A880RU0 (Enderbyland_Halley Brunt)	0.39	−0.17	52.1	200–250
A1029RU0 (Graham Land_King George)	0.39	−0.20	52.2	190–260
A1033RB0 (Graham Land_King George)	0.38	−0.21	52.2	190–260
A1073RU0 (Troll_Montalva)	0.38	−0.17	52.0	200–270
A1082RU0 (Troll_Riquelme3)	0.38	−0.18	51.7	190–270
Hm average all Gusev targets[c]	0.37	−0.17	52.2	190–270
Hm standard deviation (2σ)	0.03	0.06	1.0	190–270
Fe3S2 (Hematite,oct-Fe^{3+}) for $-0.10 < \Delta E_Q < 0.10$				
Hm average all Gusev targets[c]	0.37	−0.02	52.4	190–270
Hm standard deviation (2σ)	0.03	0.09	0.9	190–270
Hm all PasoRobles Class soil MER-A sol >520	[0.37]	[0.03]	[53.0]	190–270
Fe3S2 (Hematite,oct-Fe^{3+}) for $\Delta E_Q > 0.10$				
Hm average all Gusev targets[c]	0.37	0.25	53.6	190–270
Hm standard deviation (2σ)	0.04	0.12	0.06	190–270
Parameter Constraints When Needed for Fitting Proecdures				
Gt constraint	[0.38][d]	[−0.17]	[36.5]	200–270
Hm constraint for Gusev rocks	[0.37]	[−0.16]	[51.7]	190–270
Hm constraint for all Laguna Class soil	[0.37]	[−0.16]	[51.7]	190–270
Hm constraint for PasoRobles Class soil	[0.37]	[0.03]	[53.0]	190–270

[a]MB parameters were calculated from spectra summed over the temperature interval. Values of δ are with respect to metallic iron foil at the same temperature as the sample.
[b]MB parameter errors are ±0.02 mm/s for δ and ΔE_Q and ±0.8 T for B_{hf}.
[c]Average includes values for Gusev Crater targets from *Morris et al.* [2006a].
[d]MB parameters in brackets are constraints used in the fitting procedure.

The average values (2 measurements) of δ and ΔE_Q are 1.23 ± 0.02 and 1.93 ± 0.02 mm/s, respectively (Table 1). The difference implies either a pyroxene whose mineralogical composition is unique to Comanche Spur or some other Fe-bearing (oct-Fe^{2+}) phase that is unique to the outcrop. This phase could either be a product of igneous activity or a product of secondary mineralization. Mini-TES and Pancam spectra for Comanche Spur are also distinct from those for the other Ol-rich rocks on Haskin Ridge (Larrys Bench, Seminole, and Algonquin) [*McSween et al.*, 2008; *Farrand et al.*, 2008]. The origin of the difference is not known, although it seems reasonable to couple it to the presence of Px-C.

3.3. Fe2D3 (Ilmenite)

[16] The Fe2D3 doublet from oct-Fe^{2+} (Figure 2a) generally occurs with low subspectral areas in the spectra of rocks and soils on Husband Hill, Home Plate, and Eastern Valley (Figure 4). Its Mössbauer parameters form a distinct group that has average values (19 measurements) of δ and ΔE_Q equal to 1.07 ± 0.02 and 0.80 ± 0.06 mm/s, respectively (Table 2). We assign the doublet to ilmenite (Ilm; $FeTiO_3$) [*Morris et al.*, 2006a]. Figure 5 shows the expected correlation between the Ti concentration and the concentration of Fe associated with ilmenite. The three solid lines correspond to calculated lines for stoichiometric ilmenite ($FeTiO_3$) plus 0.0, 0.1, and 0.2 moles/24(O + Cl) of Ti in one or more phases other than ilmenite (e.g., magnetite or pyroxene). It follows for individual rocks that Algonquin (Aqn), Independence (Ind), and Bourgeoisie Chic (BC), which plot near y = x, have Ti predominantly associated with ilmenite and that Watchtower (Wt), Champagne (Ch), and Wishstone (Wi), which plot at y > (x + 0.15), have Ti mostly associated with phases other than ilmenite.

3.4. Fe2D4 and Fe3D5 (Fe^{2+} and Fe^{3+} in Chromite)

[17] One rock (Assemblee) has an anomalously high Cr_2O_3 concentration (~2.7 wt %) compared to all other Gusev rocks (<0.9 wt %) [*Clark et al.*, 2007]. Because of the high Cr_2O_3 concentration and a relatively low TiO_2 concentration (~0.9 wt %), both chromite (Chr; $Fe^{2+}(Cr\text{-}Fe^{3+})_2O_4$ and ilmenite were considered as Fe-bearing phases during least squares fitting procedures. A better fit to the experimental data was made with a chromite model, resulting in the assignment of that phase [*Clark et al.*, 2007].

3.5. Fe3D1 (npOx)

[18] The Fe3D1 doublet from oct-Fe^{3+} is ubiquitous in the spectra of rocks and soils at Gusev Crater, and its Mössbauer parameters form a diffuse group (Figures 2a and 2b). The average values of δ and ΔE_Q for all Gusev rock and soil spectra are 0.37 ± 0.04 and 0.90 ± 0.18 mm/s, respectively (Table 1). The large standard deviations of the average, especially for ΔE_Q, imply a complex and variable mineralogical and chemical assemblage. We assign the doublet to nanophase ferric oxide (npOx), which is a generic

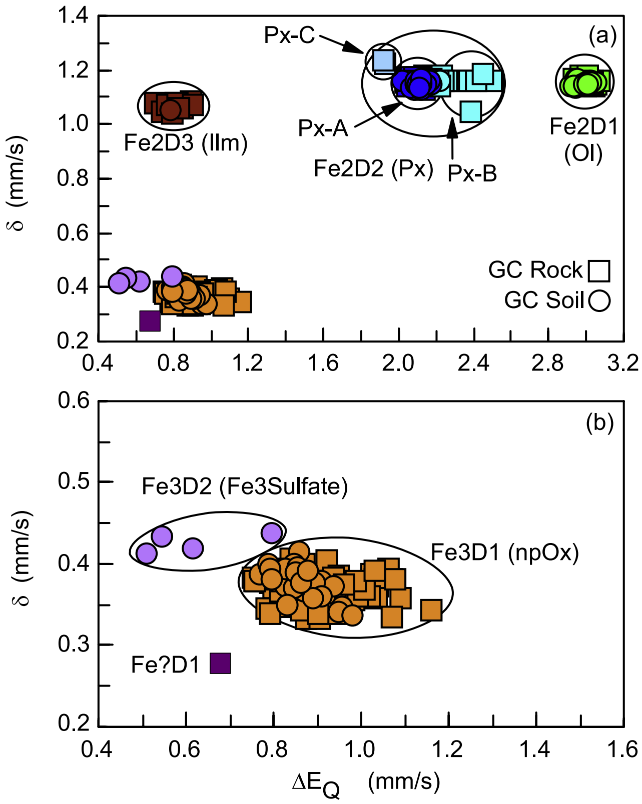

Figure 2. Doublet identification diagrams: isomer shift (δ) versus quadrupole splitting (ΔE_Q). The isomer shift is referenced with respect to metallic iron foil at the same temperature as the Martian surface target (200–270 K). (a) Six groups of doublet spectra are observed: three from octahedral (oct)-Fe^{2+} (Fe2D1, Fe2D2, and Fe2D3), two from oct-Fe^{3+} (Fe3D1 and Fe3D2), and one from Fe (Fe?D1) whose coordination and oxidation states are equivocal. In Figure 2a the Fe2D1, Fe2D2, and Fe2D3 doublets are assigned to olivine (Ol), pyroxene (Px), and ilmenite (Ilm), respectively. The pyroxene group is subdivided into three groups. Px-A includes most rocks and all soils. Px-B includes the rocks Independence and Assemblee, and Ebenezer, Uchben, and other members of Clovis Class. Px-C is a singular occurrence for the rock Comanche Spur. (b) The Fe3D1 and Fe3D2 doublets are assigned to nanophase ferric oxide (npOx) and Fe^{3+}-sulfate (Fe3Sulfate). Fe?D1, a singular occurrence for the rock Fuzzy Smith, is either low-spin Fe^{2+} or tetrahedral (tet)-Fe^{3+}. The preferred assignment is the former as pyrite/marcasite (Pyr/Mar).

name for poorly crystalline or short-range order products of oxidative alteration/weathering that have oct-Fe^{3+} (MB doublet) and are predominantly oxide/oxyhydroxide in nature [*Morris et al.*, 2006a]. Depending on local conditions, npOx (as encountered on the Earth) can be any combination of superparamagnetic hematite and goethite, lepidocrocite, ferrihydrite, schwertmannite, akaganéite, hisingerite, and the oct-Fe^{3+} rich particles that pigment iddingsite and palagonite. NpOx can also incorporate anions like SO_4^{2-}, Cl^-, and PO_4^{3-} through specific chemical adsorption. Because of different local conditions, it is possible that one or more forms of npOx on Mars are uncommon or not present on Earth.

3.5.1. Fe3D1 (npOx) for Basaltic Soils

[19] A good correlation (R^2 = 0.71) between Cl and SO_3 is present for Martian basaltic soils (Laguna Class soil) and two measurements of undisturbed and relatively thick dust coatings on the basaltic rock Mazatzal (Mazatzal Oregon and Mazatzal NewYork) (Figure 6a). The molar concentrations of Cl and S individually correlate (R^2 = 0.66 and 0.43, respectively) with the molar concentration of Fe associated with npOx ($A_{npOx}Fe_T/100$) (Figures 6b and 6c). The chemical concentrations are from APXS measurements [*Gellert et al.*, 2006; *Ming et al.*, 2006, 2008; *Clark et al.*, 2007; *Squyres et al.*, 2007], and the values A_{npOx} from MB measurements are compiled in Table 5 and *Morris et al.* [2006a]. The solid lines are linear least squares fits. The straightforward interpretation of Figures 6b and 6c from the y-intercepts is that the end-member (A_{npOx} = 0%) for basaltic soils has average concentrations of Cl = 0.11 moles/24(O + Cl) (~0.43 wt % Cl) and S = 0.35 moles/24(O + Cl)

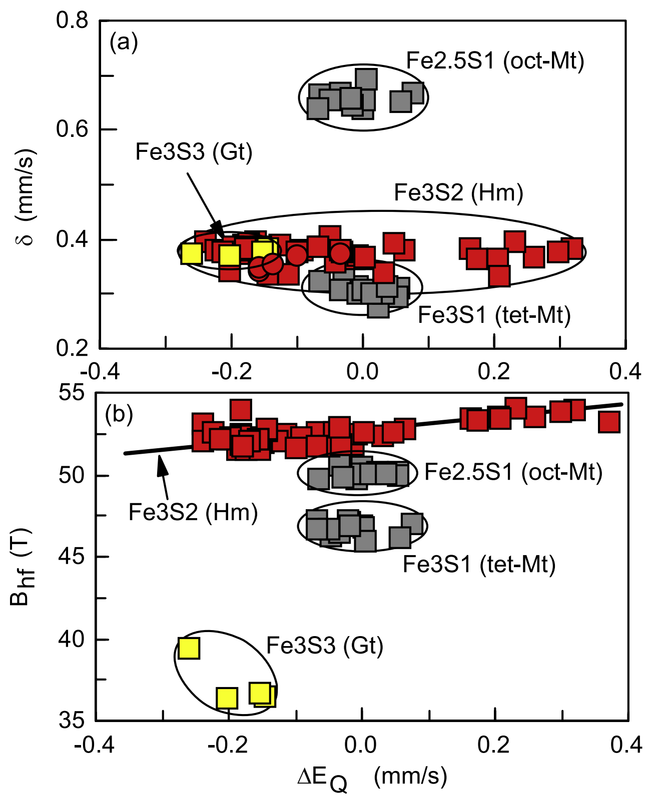

Figure 3. Sextet identification diagrams: (a) isomer shift (δ) versus quadrupole splitting (ΔE_Q) and (b) hyperfine field strength (B_{hf}) versus ΔE_Q. The isomer shift is referenced with respect to metallic iron foil at the same temperature as the Martian surface target (200–270 K). Four groups of sextet spectra are observed: one from tet-Fe^{3+} (Fe3S1), two from oct-Fe^{3+} (Fe3S2 and Fe3S3), and one from oct-$Fe^{2.5+}$ (Fe2.5S1). Fe3S1 and Fe2.5S1 are assigned to the tetrahedral and octahedral sites of magnetite, respectively. Fe3S2 is assigned to hematite, and Fe3S3 is assigned to goethite. A range of values is present for Hm because Martian diurnal temperatures are proximate to its Morin transition temperature (~260 K).

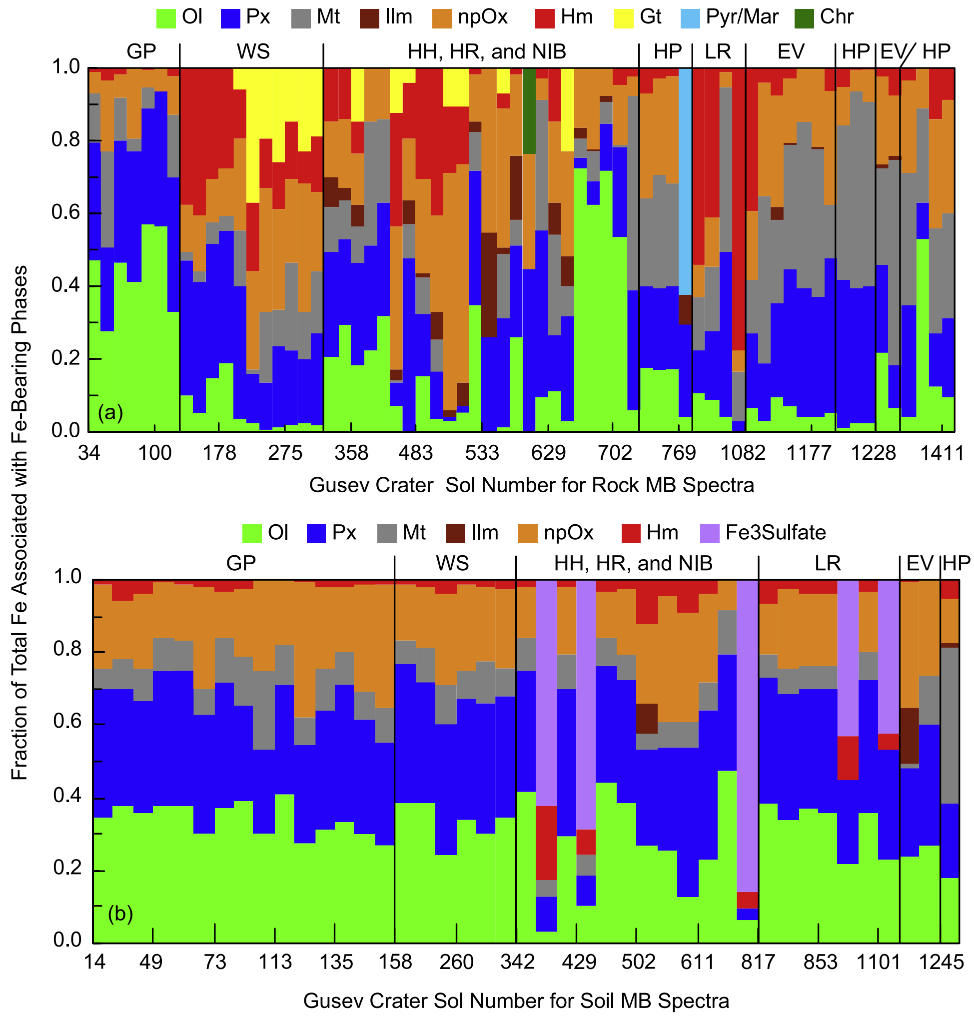

Figure 4. Histograms showing fraction of total Fe associated with Fe-bearing phases for Gusev Crater (a) rocks and (b) soils from landing through sol 1544. Note that the *x* axis is not linear in sol number. Fe-bearing phase names are Ol, olivine; Px, pyroxene; Mt, magnetite; Ilm, ilmenite; npOx, nanophase ferric oxide; Hm, hematite; Gt, goethite; Pyr/Mar, pyrite/marcasite; Chr, chromite; and Fe3Sulfate, Fe^{3+}-bearing sulfate. Location names are GP, Gusev plains; WS, West Spur; HH, Husband Hill; HR, Haskin Ridge; NIB, northern Inner Basin; HP, Home Plate; LR, Low Ridge; and EV, Eastern Valley.

(~3.1 wt % SO_3). Similarly, the interpretation from the slopes is that the Cl/Fe^{3+} and S/Fe^{3+} ratios for Fe associated with npOx are 0.14 and 0.66, respectively. Molar S/Fe ratios for typical sulfates and sulfides are 0.13 (schwertmannite), 0.67 (jarosite), 1.00 (troilite and binary Fe^{2+}-sulfates), 1.00 to 1.20 (pyrrhotite), 1.67 (binary Fe^{3+}-sulfates), and 2.0 (pyrite and marcasite).

[20] S and Cl either do not correlate or negatively correlate with other sulfate- and chloride-forming elements (Mg, Ca, Al, and Fe not associated with npOx) (Figure 7). These observations are additional evidence that S, Cl, and Fe from npOx occur together in the same phase in Martian Laguna Class soil. An updated plot (not shown) of $A_{Px}Fe_T/100$ versus $A_{npOx}Fe_T/100$ [*Morris et al.*, 2006a] continues to show a negative correlation, consistent with the Fe3D1 assignment to npOx as opposed to Fe^{3+} in pyroxene.

[21] Additional information concerning the mineralogical composition of npOx associated with Martian soil is provided by multispectral data (~0.4–1.1 μm) of bright dust from the Imager for Mars Pathfinder (IMP) and the MER Panoramic Camera (Pancam) and by hyperspectral data (~0.4 to >2.5 μm) from the Observatoire pour la Minéralogie, l'Eau, les Glaces et l'Activité (OMEGA) and the Compact Reconnaissance Imaging Spectrometer for Mars (CRISM). Bright dust spectra [e.g., *Bell et al.*, 2000, 2004; *Bibring et al.*, 2006; *Lichtenberg et al.*, 2007; *Arvidson et al.*, 2008] are characterized by a featureless absorption edge between ~0.4 and ~0.75–0.80 μm and relatively flat reflectance between 0.75 and 0.80 μm and 2.5 μm. The featureless ferric absorption edge of high-albedo soils is consistent with npOx (as opposed to well crystalline Fe^{3+}-bearing compounds like hematite, goethite, and jarosite). The absence of detectable spectral features from H_2O near 1.4 and 1.9 μm and from M-OH (M = Fe, Mg, Al, Si) near 1.4 and 2.1–2.4 μm imply the bright dust is anhydrous and not hydroxylated [e.g., *Bell et al.*, 2000, 2004; *Morris et al.*, 2000a; *Bibring et al.*, 2006]. A caveat is that H_2O and M-OH could be present if hydrogen bonding is suffi-

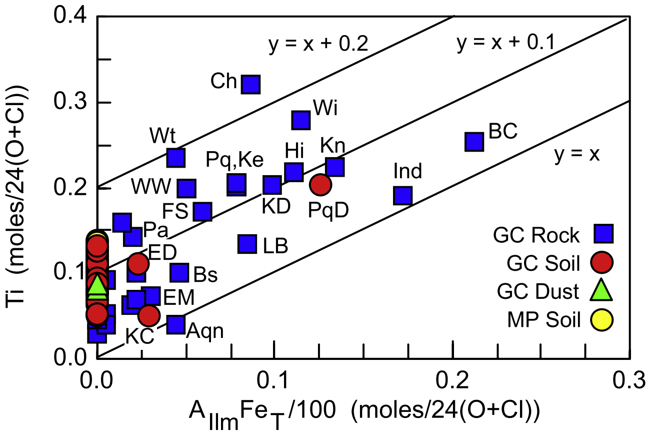

Figure 5. Molar concentration of Ti (total Ti) versus molar concentration of Fe associated with ilmenite ($A_{Ilm}Fe_T/100$) for Gusev Crater rock, soil, and dust and Meridiani Planum soil. Location names are GC, Gusev Crater; and MP, Meridiani Planum. Rock names are Aqn, Algonquin; Bs, Backstay; BC, Bourgoisie Chic, Ch, Champagne; EM, Elizabeth Mahon; Hi, Hillary; Ind, Independence; KD, Keel Davis; Kn, Kansas; Ke, Keystone; FS, Fuzzy Smith; LB, Larrys Bench; Pa, Paros; Pq, Pequod; Wi, Wishstone; Wt, Watchtower; and WW, Wishing Well. Soil names are ED, Eileen Dean; KC, Kenosha Comets; and PqD, Pequod Doubloon.

ciently strong to suppress below detection limits the H_2O and M-OH spectral features. The presence of a spectral feature near 3 μm in all Mars spectra analyzed to date is evidence that some H_2O/OH is present [e.g., *Yen et al.*, 1998; *Jouglet et al.*, 2007; *Milliken et al.*, 2007].

3.5.2. Fe3D1 (npOx) for Rocks

[22] An issue for both APXS and MB measurements on rocks is the extent to which dust and soil on rock surfaces contribute to the measured values. For measurements of interior rock surfaces exposed by grinding with the RAT, this contribution is not present in the absence of fallback of RAT tailings and addition of material by the wind. Since sol 420, only RAT brushing has been done because the grinding pads wore out. The datum for each rock in Figure 8 corresponds to analysis of a RAT grind surface when available, to a RAT brush surface when a RAT grind analysis was not done, or to an undisturbed surface when neither a RAT grind nor a RAT brush analysis was done. An additional complicating factor is the different sampling depths for APXS and MB, with the latter being deeper. An analysis of an undisturbed rock surface with soil/dust coating intermediate in thickness between the APXS and MB sampling depths would yield a soil analysis for APXS and a soil-rock analysis for MB [*Morris et al.*, 2006b].

[23] In contrast to soils, the concentrations of Cl and SO_3 for all rocks are not well correlated (Figure 8a) and neither are the molar concentrations of both Cl and S with $A_{npOx}Fe_T/100$ (Figures 8b and 8c). These observations are explained if rocks have different intrinsic Cl and S concentrations and/or have been acted upon by Cl- and S-bearing fluids/vapors having different Cl and S concentrations. For purposes of discussion, the rock data are divided

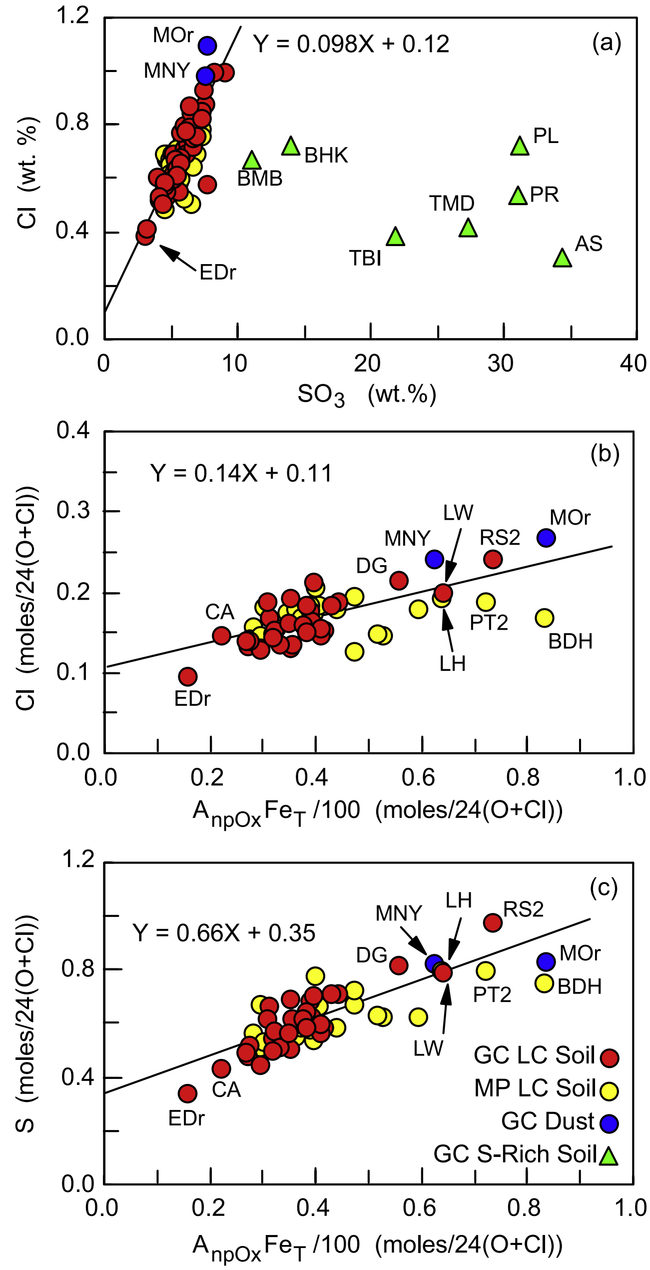

Figure 6. Cl, S, and npOx relationships for soils: (a) Cl versus SO_3, (b) molar Cl concentration versus molar concentration of Fe associated with npOx ($A_{npOx}Fe_T/100$), and (c) molar S concentration versus molar concentration of Fe associated with npOx. Equations and solid lines describe linear least squares fit of Laguna Class soil and dust from Gusev Crater and Meridiani Planum. Location and class names are GC, Gusev Crater; MP, Meridiani Planum; and LC, Laguna Class. Soil names are AS, Arad Samra; BDH, Big Dig Hema Trench1; BHK, Boroughs Hells Kitchen; BMB, Boroughs Mill Basin; CA, Crumble Almonds; DG, Desert Gobi; EDr, El Dorado Scuff Shadow; LH, Mont Blanc Les Hauches; LW, Lambert Whymper; MNY, Mazatzal NewYork; MOr, Mazatzal Oregon; PL, Paso Robles Paso Light1; PR, Pasadena Paso Robles; PT2, Purgatory Track2; RS2, Bighole RS2; TBI, Tyrone Berkner Island; and TMD, Tyrone Mount Darwin.

Table 5. Mössbauer Areas for Component Subspectra, Fe^{3+}/Fe_T, and Temperature Measurement Interval for Mössbauer Spectra of Rock and Soil Targets at Gusev Crater for Sols A534 Through Sol A1411[a]

	Phase Assignment														
	Ol (%)	Px (%)	Ilm (%)	Chr (%)	npOx (%)	Sulfate (%)		Mt (%)	Mt(3) (%)	Mt(2.5) (%)	Hm (%)	Gt (%)	Sum (%)	Fe^{3+}/Fe_T	T (K)
Generic name	Fe2D1	Fe2D2	Fe2D3	–	Fe3D1	Fe3D2	Fe?D1	–	Fe3S1	Fe2.5S1	Fe3S2	Fe3S3	–	–	–
Revised From Morris et al. [2006a]															
A350RU0 (WishingWell_Dreaming)	25	25	2	0	17	0	0	0	0	0	22	9	100	0.48	210–260
A353RU0 (Champagne_Lip)	14	30	5	0	16	0	0	0	0	0	16	19	100	0.51	210–250
A358RR0 (Champagne_RAT2)	22	24	9	0	11	0	0	0	0	0	20	15	100	0.46	210–250
North, SW, and SE Husband Hill and Haskin Ridge															
A534RB0 (Independence_Livingston)[b]	0[c]	20	24	0	56	0	0	0	0	0	0	0	100[d]	0.56[e]	210–290
A540RS0 (Independence_Penn2)[b]	0	32	33	0	35	0	0	0	0	0	0	0	100	0.35	210–290
A555RB0 (Descartes_Discourse)	1	27	0	0	43	0	0	18	11	6	5	7[f]	100	0.68	210–280
A559RB0 (Bourgeoisie_Chic)	26	25	18	0	23	0	0	7	4	3	2	0	100	0.31	210–270
A562RB0 (Bourgeoisie_GentleMatrice)	1	33	3	0	35	0	0	18	10	8	3	7[g]	99	0.59	210–270
A568RU0 (Assemblee_Gruyere)[b]	0	44	0	23	32	0	0	0	0	0	0	0	100	0.37	200–270
A585SU0 (Lambert_Whymper)	26	28	0	0	34	0	0	8	4	3	4	0	100	0.45	200–270
A602RU0 (Irvine_Shrewsbury)	9	46	0	0	6	0	0	36	17	20	3	0	100	0.35	200–270
A609SU0 (Cliffhanger_Hang2)	13	41	0	0	30	0	0	7	3	4	9	0	100	0.45	200–270
A611SD0 (Cliffhanger_LandsEnd)	25	40	1	0	24	0	0	9	5	4	3	0	100	0.33	200–270
A629RU0 (Hillary_Khumjung)	11	17	6	0	27	0	0	27	11	16	12	0	100	0.58	200–270
A631RU0 (Hillary_Namchebazaar)	11	13	11	0	18	0	0	29	9	20	17	0	100	0.54	210–270
A648RB0 (Kansas_Kestrel)	3	28[f]	9	0	29	0	0	8	5	3	0	23	100	0.59	200–270
A662RB0 (LarrysBench)	72	3	3	0	16	0	0	5	3	2	0	0	100	0.20	210–270
A674RB0 (Seminole_Osceola)	57	7	1	0	23	0	0	11	5	7	0	0	100	0.31	210–270
A677RB0 (Seminole_Abiaka)	67	6	1	0	21	0	0	5	3	3	0	0	100	0.25	210–270
A690RB0 (Algonquin_Iroquet)	71	13	2	0	8	0	0	6	1	5	0	0	100	0.11	210–270
A699RU0 (ComancheSpur_HorseBack)	57	22	0	0	16	0	0	0	0	0	5	0	100	0.21	210–270
A702RB0 (ComancheSpur_Palimino)	51	27	0	0	16	0	0	1	0	1	5	0	100	0.22	210–270
A708SU0 (ElDoradoScuff_Shadow)	47	32	0	0	8	0	0	12	5	7	0	0	100	0.17	200–270
Northern Inner Basin															
A723SD0 (Arad_Samra)	7	3	0	0	0	86	0	0	0	0	4	0	100	0.90	190–270
A737RU0 (BuZhou_GongGong)	6	33	0	0	5	0	0	54	21	33	2	0	100	0.45	190–270
Home Plate															
A748RU0 (Barnhill_Ace)[h]	18	22	0	0	29	0	0	24	9	15	7	0	100	0.53	200–260
A754RB0 (Posey_Manager)[h]	17	23	0	0	27	0	0	31	15	16	3	0	100	0.53	200–260
A762RB0 (JamesCoolPapaBell_Stars)[h]	17	23	0	0	29	0	0	28	12	15	3	0	100	0.52	190–270
A769RU0 (HomePlate_FuzzySmith)[h]	4	26[f]	8	0	0	0	63	0	0	0	0	0	100	0.00	190–250
Low Ridge and Eastern Valley															
A810RU0 (Enderbyland_Halley)	12	12	0	0	8	0	0	15	5	10	54[f]	0	100	0.72	190–260
A817SU0 (Enderbyland_Mawson)	39	34	0	0	14	0	0	7	1	6	7	0	100	0.24	190–250
A826SU0 (Enderbyland_Progress)	34	35	0	0	22	0	0	7	3	4	3	0	100	0.29	190–250
A836RU0 (Enderbyland_HalleyOffset)	2	3	0	0	8	0	0	15	4	11	72[f]	0	100	0.88	190–250
A840SB0 (Enderbyland_Progress1)	37	32	0	0	20	0	0	7	3	4	4	0	100	0.29	190–250
A853SB0 (Enderbyland_Progress2)	36	35	0	0	20	0	0	6	3	3	4	0	100	0.29	190–240
A880RU0 (Enderbyland_HalleyBrunt)	14	17	0	0	9	0	0	11	2	8	48	0	100	0.64	200–250
A948RU0 (Endebyland_HalleyBruntOffset3)	14	17	0	0	11	0	0	16	9[d]	7	42[g]	0	100	0.66	220–250
A1015SD0 (Tyrone_BerknerIsland1) Model A	22[g]	23[g]	0	0	0	43[g]	0	0	0	0	12[g]	0	100	0.56	190–250
A1015SD0 (Tyrone_BerknerIsland1) Model B	22[g]	23[g]	0	0	[9][i]	34[g]	0	0	0	0	12[g]	0	100	0.56	190–250
A1018SD0 (BearIsland_BearIsland)	36	37	0	0	16	0	0	8	4	4	3	0	100	0.26	190–260
A1029RU0 (GrahamLand_KingGeorge)	8	20	0	0	13	0	0	17	6	10	43	0	100	0.67	190–260
A1033RB0 (GrahamLand_KingGeorge)	9	19	0	0	15	0	0	18	7	11	40	0	101	0.67	190–260
A1056RU0 (Esperanza_Palma)	4	45	0	0	4	0	0	45	25	20	1	0	100	0.40	250–280
A1073RU0 (Troll_Montalva)	0	3	0	0	5	0	0	14	5	9	78	0	100	0.93	200–270
A1082RU0 (Troll_Riquelme3)	6	20	0	0	19	0	0	15	8[c]	7	39[f]	0	100	0.70	190–270
A1101SD0 (Tyrone_MountDarwin) Model A	23[g]	30[g]	0	0	0	42[g]	0	0	0	0	5[g]	0	100	0.47	190–270
A1101SD0 (Tyrone_MountDarwin) Model B	22[g]	31[g]	0	0	[12]	30[g]	0	0	0	0	5[g]	0	100	0.47	190–270
A1145RB0 (Torquas_Torquas2)	3	16	0	0	31	0	0	46	25[g]	21	4[f]	0	100	0.71	200–270

Table 5. (continued)

	Phase Assignment														
	Ol (%)	Px (%)	Ilm (%)	Chr (%)	npOx (%)	Sulfate (%)		Mt (%)	Mt(3) (%)	Mt(2.5) (%)	Hm (%)	Gt (%)	Sum (%)	Fe^{3+}/Fe_T	T (K)
A1155RU0 (ElizabethMahon_ElizabethMahon)	10	25	4	0	30	0	0	23	9	14	8	0	100	0.54	200–270
A1170RU0 (MadelineEnglish_ Madeline EnglishIDD)	7	37	0	0	18	0	0	35	16	18	3	0	100	0.46	200–270
A1174RS0 (ExamineThis_Everett)	4	35	0	0	15	0	0	46	18	28	0	0	100	0.47	210–270
A1177RB0 (ExamineThis_Slide)	4	33	0	0	22	0	0	41	18	23	0	0	100	0.51	210–270
A1180RU0 (ExamineThis_GoodQuestion)	5	42	0	0	31[f]	0	0	15	6	9[g]	6	0	100	0.47	210–270
A1191SD0 (GertrudeWeise_KenoshaComets)	24[f]	24	16[f]	0	35	0	0	1	0	1	1	0	100	0.36	200–270
A1200SD0 (GertrudeWeise_LeftyGanote)	27	33	0	0	26	0	0	14	6	7[f]	0	0	100	0.36	210–270
Home Plate															
A1207RB0 (HomePlate_Pesapallo1)	1	41	0	0	11	0	0	42	20	22	5	0	100	0.48	210–270
A1213RB0 (HomePlate_JuneEmerson)	2	37	0	0	6	0	0	54	21	33	1	0	100	0.44	210–270
A1217RB0 (HomePlate_ElizabethEmery)	2	38	0	0	8	0	0	51	23[f]	28	1	0	100	0.46	210–270
Eastern Valley															
A1228RU0 (EasternValley_NancyWarren)	22	24	1	0	24	0	0	26	7	20	2[g]	0	100	0.44	200–270
A1245SD0 (EasternValley_EileenDean)	18	20	2	0	12	0	0	43	17	26	5	0	100	0.47	210–270
A1255RD0 (EasternValley_InnocentBystander)	7	12	1	0	17	0	0	54	24	30	7	0	100	0.64	210–260
Home Plate															
A1328RB0 (HomePlate_TexasChili)	4	30	0	0	25	0	0	34	16	18	7	0	100	0.56	210–270
A1343RU0 (HomePlate_HumboldtPeak)	53	10	0	0	11	0	0	26	13	13	0	0	100	0.31	200–270
A1370RB0 (HomePlate_PecanPie)	12	15	0	0	30	0	0	29	11	18	14	0	100	0.64	200–260
A1411RU0 (HomePlate_Chanute)	9	22	0	0	31	0	0	29	14	15	9	0	100	0.62	200–260

[a]Subspectral areas were calculated from spectra summed over the temperature interval. Component subspectra are *f* factor corrected.
[b]From *Clark et al.* [2007].
[c]Uncertainty in subspectral area is ±2% absolute unless otherwise noted.
[d]Because Mt = Mt(3) + Mt(2.5), Sum = Ol + Px + Ilm + Chr+ npOx + Fe3D2 + Fe?D1 + Mt + Hm + Gt.
[e]Uncertainty in Fe^{3+}/Fe_T is ±0.03.
[f]Uncertainty in subspectral area is ±3% absolute.
[g]Uncertainty in subspectral area is ±4% absolute.
[h]From *Squyres et al.* [2007].
[i]Subspectral areas in brackets are constraints used in the fitting procedure.

into five groups (Table 6) on the basis of Figure 8. Group one (nine rocks; red squares) has Cl and SO_3 concentrations that are the lowest among rocks and are also less than measured in any soil (Figure 8a). The analyzed rock surfaces have undergone, relative to other rocks, minimal alteration by Cl- and S-bearing fluids/vapors. Group two (12 rocks; blue triangles) has values of Cl, SO_3, and $A_{npOx}Fe_T/100$ that generally overlap corresponding data for soils. These rocks thus have any combination of soil/dust coatings that are thick compared to both APXS and MB penetration depths and intrinsic values that are within the range observed for soils.

[24] Group three (six rocks; purple squares) has high S concentrations compared to soils and rocks with comparable $A_{npOx}Fe_T/100$ concentrations (Figure 8c). The high S concentrations for Alligator (All) and Peace (Pe) are attributed to cementation of porous rock by $MgSO_4{\bullet}nH_2O$ [*Ming et al.*, 2006], and the same explanation may hold for the other rocks (String Of Pearls, Pot Of Gold, Bread Box, and Halley) which, with one exception (Halley), are all located at Hank's Hollow on West Spur.

[25] Group four (five rocks; green circles) has soil-like Cl concentrations but is depleted in S relative to soils and rocks with comparable $A_{npOx}Fe_T/100$ concentrations (Figure 8c). Group five (30 rocks; light blue inverted triangles) has soil-like to depleted concentrations of S and is enriched in Cl relative to soils with comparable values of SO_3 and $A_{npOx}Fe_T/100$ (Figure 8). The rocks with exceptionally high Cl concentrations (1.6 to 2.2 wt %) include Clovis (Cl), Slide (Sl), TexasChili (TC), Uchben (Uc), Posey (Po), Kansas (Kn), and Lutefisk (Lu). The rocks in Groups four and five presumably reacted with or were invaded by solutions/vapors having different Cl/S ratios than other rocks. Note that the high-Cl rocks include rocks from highly altered (Gt-bearing) Clovis Class and the relative unaltered Barnhill Class. Unfortunately, we were not able to RAT grind Barnhill Class rock, so the Cl may just have high concentrations in near-surface regions.

[26] In summary, the complex relationship among S, Cl, and Fe associated with npOx in rocks (Figures 8b and 8c) compared to soils (Figures 6b and 6c) results from the diversity of Cl and S concentrations in rocks compared to

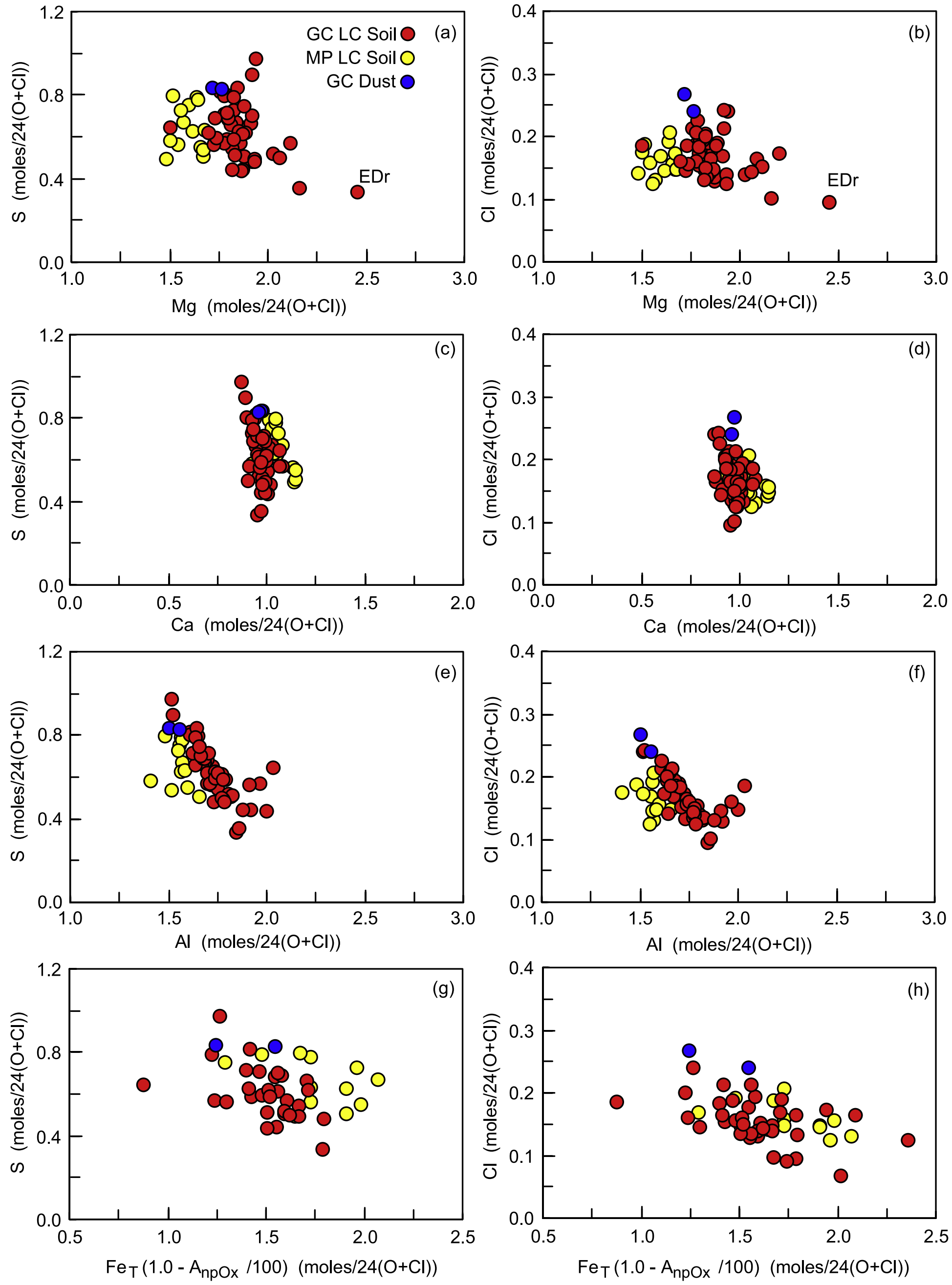

Figure 7. Plots of molar concentrations of S and Cl versus molar concentrations of (a and b) Mg, (c and d) Ca, (e and f) Al, and (g and h) Fe not associated with npOx ($Fe_T(1.0\text{-}A_{npOx}/100)$) for Laguna Class soil and dust from Gusev Crater and Meridiani Planum. The absence of positive correlation is evidence for the view that S and Cl are speciated with npOx in Laguna Class soils (see text). Location and class names are GC, Gusev Crater; MP, Meridiani Planum; and LC, Laguna Class. EDr is soil El Dorado Scuff Shadow.

Gusev basaltic soil. The data suggest that the primary carrier of Cl, S, and npOx in basaltic soil is the bright dust component that mixes in variable proportions with basaltic comminuted basaltic rocks that have low levels of intrinsic Cl, S, and npOx (e.g., Group one rocks like Adirondack, Backstay, and Irvine Class rocks).

[27] Additional information on the nature of npOx in rocks is obtained from the values of ΔE_Q (Figure 9). The values of ΔE_Q for soil fall in the range ~0.75 to ~0.95 mm/s. This range overlaps the ΔE_Q range for terrestrial and synthetic forms of npOx (~0.54 to 0.96 mm/s [e.g., *Johnson*, 1977; *Morris et al.*, 1989, 2000a]), although most values are <0.80 mm/s. The ΔE_Q = 0.96 mm/s value is reported for akaganéite (Fe(O, OH, Cl) [*Johnson*, 1977]). For the synthetic samples, ΔE_Q correlates with particle diameter, with smaller npOx particles having larger values of ΔE_Q. We suggest that the generally higher values of ΔE_Q for Martian npOx in soils compared to terrestrial occurrences and synthetic samples may be related to the high concentrations of Cl and S associated with Martian npOx.

[28] Fourteen rocks have values of ΔE_Q that are larger (>0.97 mm/s) than those observed for soils (Figure 9). Is it reasonable to assign their ferric doublets to the alteration phase npOx, or are the high values evidence for a different Fe^{3+}-bearing phase? We suggest that npOx is an appropriate assignment because, with the possible exception of Comanche Spur, these rocks are heavily altered [*Morris et al.*, 2006a]. Seven rocks (Clovis, Kansas, Ebenezer, Uchben, Tetl, Temples, and Lutefisk) have Gt and Hm as major Fe-bearing phases and high Cl concentrations (Figures 8b and 9b and Table 5). Three (Watchtower, Paros, and Pequod) likewise have Gt and Hm as major Fe-bearing phases, but have soil-like Fe concentrations of Cl and are depleted in S relative to soils. Hillary has Hm as a major Fe-bearing phase and is modestly enriched in Cl. Pot Of Gold has Hm as a major Fe-bearing phase, has a soil-like Cl concentration, and is enriched in S relative to soils. Assemblee does not have detectable Mt, Gt, and Hm and has soil-like Cl and S concentrations, but does have a low total Fe concentration (~6.5 wt % as FeO) and a high Cr concentration (~2.7 wt % as Cr_2O_3) [*Clark et al.*, 2007].

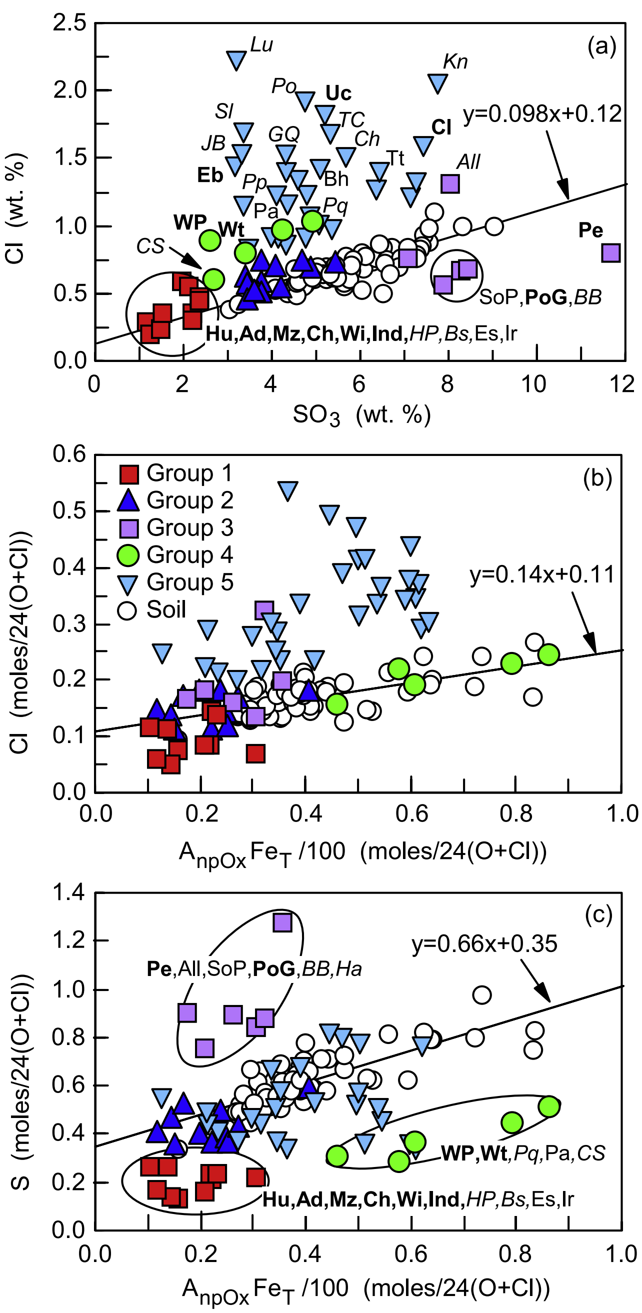

[29] Comanche Spur has olivine as its major Fe-bearing phase, which is not a characteristic of an altered rock. However, until the identity of Px-C is clearly resolved, it is premature to address the origin of the large value of ΔE_Q for its npOx doublet.

[30] In summary, the Fe3D1 doublet for rocks is reasonably assigned to the generic Fe^{3+} alteration product npOx. The wide range in the values of ΔE_Q for npOx in rocks (0.70 to 1.15 mm/s) is attributed to different forms of npOx produced in response to variable local conditions, including Fe, Cl, and S concentrations, availability of substitutional impurities (e.g., Al^{3+}), water to rock ratio, pH, and temperature. The higher values of ΔE_Q may, for example, reflect the high Cl concentrations for rocks like Clovis, Kansas, and Ebenezer or, as suggested by *Morris et al.* [2007], a composition approaching hydronium jarosite. The values of ΔE_Q for npOx are significantly lower than the values reported for the jarosite encountered at Meridiani Planum (average ΔE_Q = 1.20 ± 0.02 mm/s [*Morris et al.*, 2006b]). *Van Cromphaut et al.* [2007] have suggested that the large values of ΔE_Q in Clovis Class rocks result from Fe^{3+} in glass. We show in section 3.11 that Fe^{3+}-bearing glass is not a viable interpretation on the basis of Mössbauer data and geologic context.

3.6. Fe3D2 (Fe^{3+}-Sulfate)

[31] The Fe3D2 doublet from oct-Fe^{3+} (Figure 2b) is present only in the spectra of 5 soil targets in the Columbia Hills (Pasadena Paso Robles, Paso Robles2 Paso Light1, Arad Samra, Tyrone Berkner Island, and Tyrone Mount Darwin) (Figure 4). The average values of δ and ΔE_Q are 0.43 ± 0.02 and 0.58 ± 0.05 mm/s, respectively (Table 2). We assign the doublet to a Fe^{3+}-bearing sulfate (Fe3Sulfate) [*Morris et al.*, 2006a].

Figure 8. Cl, S, and npOx relationships for rocks: (a) Cl versus SO_3, (b) molar Cl concentration versus molar concentration of Fe associated with npOx ($A_{npOx}Fe_T/100$), and (c) molar S concentration versus molar concentration of Fe associated with npOx. On the basis of these data, Gusev rocks cluster into five groups (see text). Equations and solid lines describe linear least squares fits of Laguna Class soil and dust from Gusev Crater and Meridiani Planum (see Figure 6). Rock names are Ad, Adirondack; All, Alligator; BB, Bread Box; Bh, Barnhill; Bs, Backstay; Ch, Champagne; Cl, Clovis; CS, Comanche Spur; Eb, Ebenezer; Es, Esperanza; GQ, Good Question; Ha, Halley; HP, Humboldt Peak; Hu, Humphrey; Ind, Independence; Ir, Irvine; JB, James CP Bell; Kn, Kansas; Lu, Lutefisk; Mz, Mazatzal; Pa, Paros; Pe, Peace; Po, Posey; PoG, Pot Of Gold; Pp, Pesapallo; Pq, Pequod; Sl, Slide; SoP, String Of Pearls; TC, Texas Chili; Tt, Tetl; Uc, Uchben; Wi, Wishstone; WP, Wooly Patch; and Wt, Watchtower. Bold, RAT grind surface; italic, RAT brush surface; normal, undisturbed surface.

Table 6. Grouping of Rocks According to Concentrations of Cl, S, and A_{npOx} in Figure 7[a]

				Group 5	
Group 1	Group 2	Group 3	Group 4	WS and HH[b]	EV and HP[b]
Adirondack	Mimi Shoe	Bread Box	**Wooly Patch**	**Clovis**	Barnhill
Humphrey	*Route 66*	**Pot Of Gold**	**Watchtower**	**Uchben**	*James Cool-Papa Bell*
Mazatzal	Joshua	String Of Pearls	*Pequod*	**Ebenezer**	*Posey*
Champagne	Wishing Well	*Alligator*	Paros	Tetl	*Texas Chili*
Independence	Fuzzy Smith	**Peace**	*Comanche Spur*	Temples	*Chanute*
Backstay	Nancy Warren	*Halley*		*Lutefisk*	Good Question
Irvine	Elizabeth Mahon			*Descartes*	*Everett*
Wishstone	**Innocent Bystander**			*Keystone*	*Slide*
Esperanza	*June Emerson*			*Keel Davis*	*Torquas*
Humboldt Peak	*Elizabeth Emery*			Hillary	Riquelme
	Pesapallo			*Kansas*	Montalva
	King George			*Seminole*	Madeline English
				Keel Reef	*Pecan Pie*
				Assemblee	
				Bourgeoisie Chic	
				Larrys Bench	
				Algonquin	

[a]Only includes rocks with both APXS and MB data. Bold typeface, RAT grind, wheel scuff (Independence), or broken rock (Innocent Bystander); italic typeface, RAT brush; normal typeface, undisturbed. Group 1, low S and low $A_{npOx}Fe_T/100$; group 2, soil-like Cl, S, and $A_{npOx}Fe_T/100$; group 3, high S and intermediate $A_{npOx}Fe_T/100$; group 4, low S and high $A_{npOx}Fe_T/100$; group 5, high Cl.
[b]WS, West Spur; HH, Husband Hill; EV, Eastern Valley; HP, Home Plate.

3.7. Fe?D1 (Possible Fe^{2+} Sulfide–Pyrite/Marcasite)

[32] The Fe?D1 doublet from low-spin Fe^{2+} or perhaps tetrahedral (tet)-Fe^{3+} (Figure 2b) is present only in the spectrum of the rock Fuzzy Smith on Home Plate (Figure 4). Its values of δ and ΔE_Q are 0.28 ± 0.02 and 0.68 ± 0.02 mm/s, respectively (Table 2), and it is a major Fe-bearing component (63% of total Fe). The doublet is assigned to an FeS_2 assemblage (pyrite and marcasite; pyr/mar), although the assignment is not unequivocal [*Squyres et al.*, 2007]. Pyrrohotite is not a viable assignment.

3.8. Fe3S1 (Magnetite tet-Fe^{3+}) and Fe2.5S1 (Magnetite oct-$Fe^{2.5+}$)

[33] The Fe3S1 and Fe2.5S1 sextet pair (Figure 3) are common in the spectra of rocks and soil, although particularly high subspectral areas are found in float rocks in the Columbia Hills and in outcrop rocks at Home Plate (Figure 4). Their average values of δ, ΔE_Q, and B_{hf} are 0.31 ± 0.03 mm/s, 0.01 ± 0.03 mm/s, and 50.0 ± 0.5 T for Fe3S1 and 0.66 ± 0.06 mm/s, −0.01 ± 0.08 mm/s, and 46.7 ± 0.8 T for Fe2.5S1, respectively (Table 3). We assign the sextet pair to magnetite (Mt: Fe_3O_4 for stoichiometric magnetite) where Fe3S1 is the tet-Fe^{3+} site and Fe2.5S1 oct-$Fe^{2.5+}$ site [*Morris et al.*, 2006a]. For stoichiometric magnetite, octahedral (Fe^{3+} + Fe^{2+}) to tetrahedral (Fe^{3+}) site occupancy ratio is 2.0. Deviations from stoichiometry commonly occur in terrestrial materials because of substitutional impurities (particularly Ti, Cr, and Al) and partial oxidation of Fe^{2+}.

3.9. Fe3S2 (Hematite)

[34] The Fe3S2 sextet from oct-Fe^{3+} (Figure 3) occurs in the spectra of many rocks at West Spur, on Husband Hill, and at Home Plate (Figure 4). We assign the sextet to hematite (Hm; α-Fe_2O_3) [*Morris et al.*, 2006a]. The large range for ΔE_Q (Figure 3a) and the systematic variation of B_{hf} with ΔE_Q (Figure 3b) are manifestations of the proximity of the Hm Morin transition temperature and Martian diurnal temperatures [*Morris et al.*, 2006a]. The Morin transition temperature occurs at ~260 K for chemically pure, bulk, well-crystalline Hm, but it can occur over a wide range of temperatures and sometimes can be suppressed depending on impurities and particle size [e.g., *Murad and Johnston*, 1987; *Dang et al.*, 1998]. The average values of δ, ΔE_Q, and B_{hf} are (1) 0.37 ± 0.03 mm/s, −0.17 ± 0.06 mm/s, and 52.2 ± 1.0 T for spectra having ΔE_Q < −0.10 mm/s, (2) 0.37 ± 0.03 mm/s, −0.02 ± 0.09 mm/s, and 52.4 ± 0.8 T for spectra having −0.10 < ΔE_Q < 0.10 mm/s, and (3) 0.37 ± 0.04 mm/s, 0.25 ± 0.12 mm/s, and 53.6 ± 0.6 T for spectra having ΔE_Q > 0.10 mm/s, respectively (Table 4). The outcrop rock Montalva at Low Ridge has the highest percentage of Fe from Hm (A_{Hm} = 78%) for any Martian sample analyzed to date, including the lag deposits of Hm-bearing blueberries at Meridiani Planum [*Morris et al.*, 2006b].

3.10. Fe3S3 (Goethite)

[35] The Fe3S3 sextet (oct-Fe^{3+}) occurs in rocks (Clovis Class and Watchtower Class) at West Spur and Husband Hill (Figure 4). We assign the sextet to goethite (Gt; α-FeOOH) [*Morris et al.*, 2006a]. This assignment is confirmed by *Van Cromphaut et al.* [2007], and they also calculated a mean particle diameter of ~10 nm for the Gt particles in Clovis Class rocks. The average values of δ, ΔE_Q, and B_{hf} are 0.38 ± 0.02 mm/s, −0.19 ± 0.10 mm/s, and 39.4 ± 2.9 T, respectively (Table 4). The outcrop rock Clovis at West Spur has the highest percentage of Fe from Gt (A_{Gt} = 37%).

3.11. Fe-Bearing Glass

[36] Fe-bearing glass can be produced on the Martian surface as a product of volcanic activity and meteoritic impact [e.g., *Allen et al.*, 1981; *Bouska and Bell*, 1993]. From a process perspective, there is thus a reasonable expectation for Fe-bearing glass to form on the Martian surface. How much Fe-bearing glass is currently present on the Martian surface depends on the unknown balance

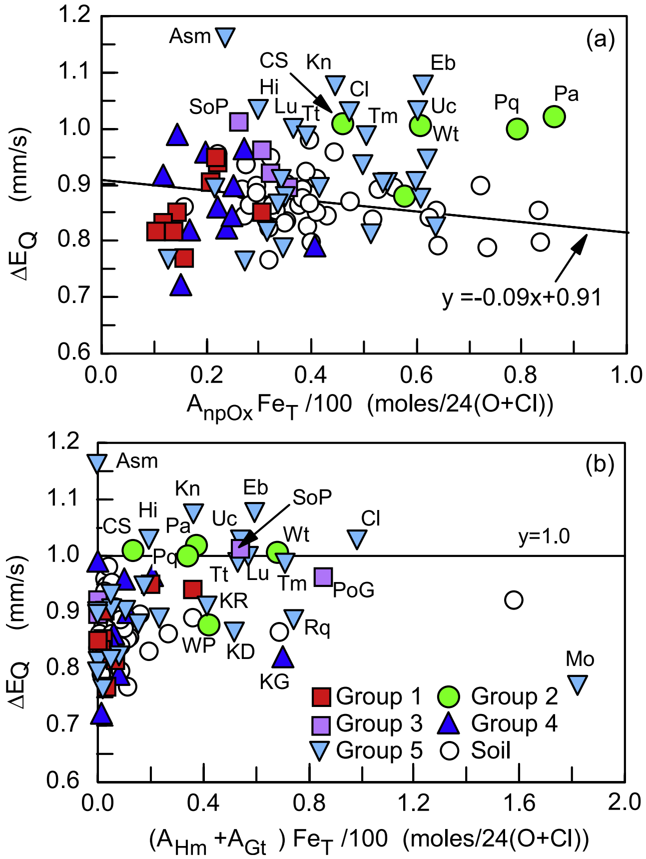

Figure 9. Quadrupole splitting ΔE_Q for npOx versus (a) A_{npOx} and (b) $(A_{Hm} + A_{Gt})Fe_T/100$ for Gusev Crater rocks. Corresponding data for soils are shown for reference. The solid line and equation in Figure 9a refers to the linear least squares fit of the soil data. The solid line in Figure 9b at y = 1.0 is drawn for reference. Rock names are Asm, Assemblee; Cl, Clovis; CS, Comanche Spur; Eb, Ebenezer; Hi, Hillary; KD, Keel Davis; KG, King George; Kn, Kansas; KR, Keel Reef; Lu, Lutefisk; Mo, Montalva; Pa, Paros; PoG, Pot Of Gold; Pq, Pequod; Rq, Riquelme; SoP, String Of Pearls; Tm, Temples; Tt, Tetl; Uc, Uchben; WP, Wooly Patch; and Wt, Watchtower.

between glass formation times and rates and glass destruction rates (e.g., by aqueous weathering). To evaluate MER MB spectra with respect to the presence or absence of Fe-bearing glass, we obtained transmission MB spectra (295 K) for a Mars composition glass (described by *Morris et al.* [2000b]) that was equilibrated over a range of oxygen fugacities (Figure 10). The MB parameters for the Mars composition glasses and those for several natural basaltic glasses of volcanic origin and other synthetic basaltic glasses are summarized in Table 7. The glass MB parameters were calculated using the same method used for MER MB spectra, except that the linewidths of the Fe^{2+} doublet were not constrained to be equal (Figure 10).

[37] For a plot of δ versus ΔE_Q, the data for Fe^{2+} and Fe^{3+} in synthetic and terrestrial basaltic glasses do not overlap the corresponding data for Gusev MB spectra (Figure 11). On the basis of this observation, we conclude that a clear detection of Fe-bearing basaltic glass has not been made on Mars by MB. This conclusion is contrary to *Van Cromphaut et al.* [2007] who suggested Fe^{3+}-bearing glass as a possible assignment for the Fe3D1 doublet for Clovis Class rocks on the basis of similar values of ΔE_Q. The values of ΔE_Q for Fe^{3+} basaltic glass and the Fe3D1 doublet do overlap, but the values of δ do not, as shown in Figure 11b.

[38] From the perspective of Mini-TES, spectral deconvolutions of Clovis Class and Watchtower Class rocks yield mineralogical compositions that are, respectively, 40–45% and 35–50% unaltered basaltic glass [*Ruff et al.*, 2006]. Spectral deconvolutions of Independence Class rocks and some Home Plate rocks also yield unaltered basaltic glass as a component [*Clark et al.*, 2007; *Squyres et al.*, 2007]. Because basaltic glass is not a good match for the MB data as just discussed, we suggest that there is a component in these highly altered rocks [*Morris et al.*, 2006a; *Ming et al.*, 2006] whose thermal emission spectrum mimics that for basaltic glass and is not included in the spectral library used for deconvolutions. The corundum normative nature of some of these rocks [*Ming et al.*, 2006] suggests allophane as a possibility as suggested by *Arvidson et al.* [2008] for the Voltaire Outcrop. Such a phase could be spectrally important to Mini-TES and be inconsequential for MB because it contains little or no Fe.

4. Classification of Gusev Crater Rocks and Soils

[39] In this section we extend the classification of rocks and soils as previously published [*Squyres et al.*, 2006; *Ming et al.*, 2006; *Morris et al.*, 2006a] to include all samples through sol 1544. The classification scheme is based on APXS chemistry with subclasses created when warranted by large differences in Fe mineralogical composition from MB measurements. New APXS data are published by *Ming et al.* [2008], and Fe mineralogical compositions for individual rocks and soils are listed in Tables 5 and 8. The classification schemes developed here and by *Ming et al.* [2008] are synchronized.

4.1. Gusev Crater Rocks

[40] Gusev Crater rocks are divided into 18 classes on the basis of APXS chemistry, and 8 of the 18 are subdivided into one or more subclasses on the basis of Fe mineralogical composition [*Squyres et al.*, 2006; *Ming et al.*, 2006, 2008; *Morris et al.*, 2006a] (see Table 9). There are 28 named subclasses. Their average Fe mineralogical compositions, Fe^{3+}/Fe_T ratios, and FeO + Fe_2O_3 concentrations are listed in Table 9, and their average values of δ and ΔE_Q, for olivine, pyroxene, and npOx are listed in Table 10. Corresponding APXS chemical compositions are given by *Ming et al.* [2008]. Pie diagrams at the class level for Fe mineralogical compositions are illustrated in Figure 12.

[41] Also compiled in Table 8 are values of the Mineralogical Alteration Index (MAI). This index is the proportion of total Fe associated with Fe-bearing alteration products (MAI = $A_{npOx} + A_{Fe3Sulfate} + A_{Hm} + A_{Gt} + A_{Pyr/Mar}$). Note that we include pyrite/marcasite, which is a Fe^{2+}-bearing mineral and is found only in the rock FuzzySmith, because we consider it to be an alteration product. Magnetite is assumed to be a product of igneous activity and not a product

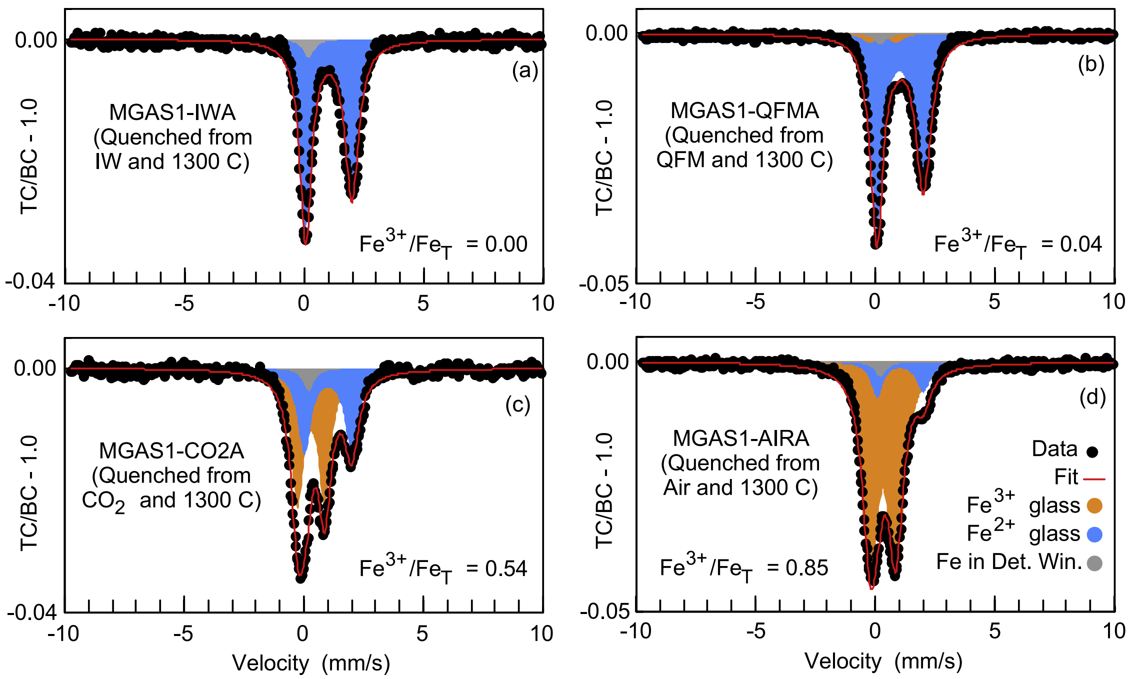

Figure 10. Transmission Mössbauer spectra (295 K) and subspectra obtained by least squares analysis for synthetic basaltic glass formed by quenching after equilibration at 1300°C and oxygen fugacities corresponding to (a) iron wustite (IW), (b) quartz fayalite magnetite (QFM), (c) CO_2 gas, and (d) laboratory air. The basaltic glass is an inferred composition for Mars global average soil at the time of Mars Pathfinder. Note that for oxygen fugacities more reducing than QFM, Fe^{3+}/Fe_T < 0.04. The y axis is the ratio of total counts to baseline counts minus one (TC/BC – 1.0).

Table 7. Mössbauer Parameters (295 K) for Fe-Bearing Basaltic Glass for Natural and Synthetic Samples

	Fe^{3+}		Fe^{2+}			
Sample	δ (mm/s)	ΔE_Q (mm/s)	δ (mm/s)	ΔE_Q (mm/s)	Glass Fe^{3+}/Fe_T	Comments[a]
MGAS1-AIRA	0.31[b]	1.07[b]	[1.03][c]	[1.94]	0.85[d]	Synthetic. 1300 °C in air[e].
MGAS1-CO2A	0.31	1.14	1.01	1.95	0.54	Synthetic. 1300 °C in CO_2[e].
MGAS1-QFMA	[0.31]	[1.15]	1.02	1.95	0.04	Synthetic. 1300 °C at QFM buffer[e].
MGAS1-IWA	–	–	1.03	1.94	0.00	Synthetic. 1300 °C at IW buffer[e].
HARAG1-AIRA	0.31	1.27	[1.06]	[1.97]	0.76	Synthetic. Augite glass. 1400°C in air[f].
HARAG1-QFMA	[0.31]	[1.27]	1.05	1.99	0.06	Synthetic. Augite glass. 1400°C at QFM buffer[f].
HARAG1-IWA	–	–	1.06	1.99	0.00	Synthetic. Augite glass. 1400°C at IW(+1) buffer[f].
HARAG1-IWB	–	–	1.06	1.98	0.00	Synthetic. Augite glass. 1400°C at IW(−1) buffer[f].
QUEGL1-AIRA	0.31	1.12	1.05	1.92	0.73	Synthetic. QUE94201 glass, 1300°C in air[f].
SHILGL1-AIRA	0.30	1.16	1.02	2.00	0.75	Synthetic. Shergotty intercumulus liquid glass. 1350°C in air[g]
EG1-AIRA	0.28	1.20	1.00	2.04	0.81	Synthetic. EET79001 ground mass (lithology A) glass. 1350°C in air[f].
HWKV901, <1 mm	[0.31]	[1.15]	1.07	1.99	0.09	Natural. SW Rift, Kilauea Volcano, Hawaii[i].
HWKV340	[0.31]	[1.15]	1.05	2.01	0.03	Natural. 2002 Flow, Puu Oo, Kilauea Volcano, Hawaii[f,h].
HWPC100, <1 mm	[0.31]	[1.15]	1.10	1.99	0.09	Natural. Kalapana black beach sand, Hawaii[f,h].
KI-CA-01	[0.31]	[1.07]	1.02	1.98	0.05	Natural. Kilauea Iki, Kilauea Volcano, Hawaii[h,i].
HWMK513-MS2, <1 mm	0.28	1.04	1.02	2.08	0.25	Natural. Mauna Kea Volcano, Hawaii[h,j].
HWMK515, 500–1000 μm	–	–	1.11	1.95	–	Natural. Mauna Kea Volcano, Hawaii[k].
Average	0.30	1.14	1.04	1.98	–	
Standard deviation	0.02	0.08	0.03	0.04	–	

[a]All synthetic glasses were quenched to ambient conditions from the indicated temperature and oxygen fugacity. QFM, quartz fayalite magnetite; IW, iron (metallic) wustite.
[b]Uncertainty in δ and ΔE_Q is ±2% absolute unless otherwise noted.
[c]MB parameters in brackets are constraints used in the fitting procedure.
[d]Uncertainty in Fe^{3+}/Fe_T is ±0.03.
[e]*Morris et al.* [2000b] and this study.
[f]This study.
[g]*McKay et al.* [1986] and this study.
[h]Sample also has Fe^{2+} from olivine. All Fe^{3+} associated with glass for calculation of Fe^{3+}/Fe_T.
[i]*Allen et al.* [1993] and this study.
[j]*Morris et al.* [2000a] and this study, nonmagnetic separate.
[k]*Morris et al.* [2000a] and this study. Because 56% of Fe_T is from jarosite, it was not possible to obtain an unconstrained peak area for Fe^{3+} from glass.

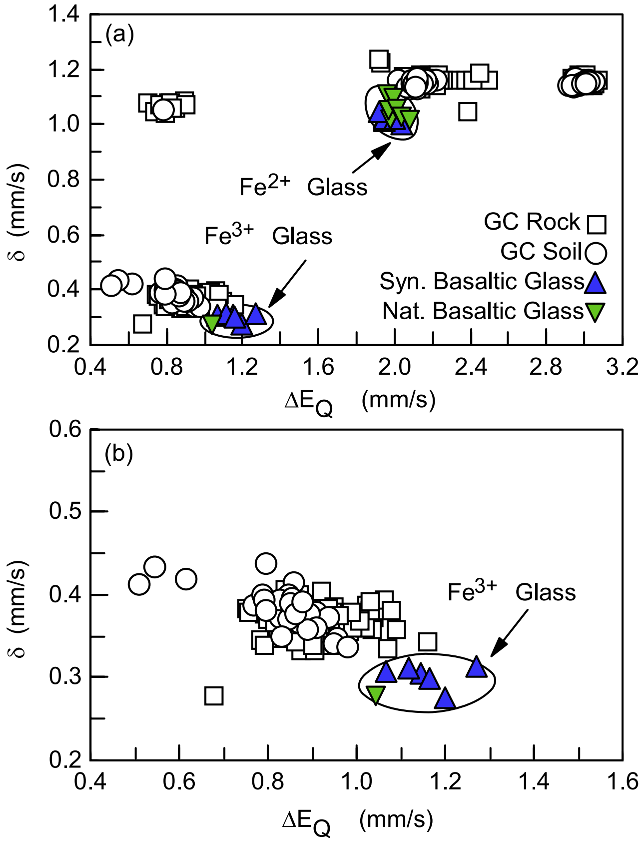

Figure 11. Doublet identification diagrams: isomer shift (δ) versus quadrupole splitting (ΔE_Q). The isomer shift is referenced with respect to metallic iron foil at the same temperature as the target (200–270 K for Gusev Crater (GC) targets and ~295 K for synthetic and natural basaltic glasses). The region near the origin in Figure 11a is expanded in Figure 11b. Note that the glass data do not overlap the data for Martian surface targets, implying no clear detection of basaltic glass on Mars. Data for GC rock and soil are from Figure 1.

of alteration (e.g., by serpentization of olivine). The validity of this assumption is discussed in section 9.

[42] In Figure 13 we plot the Fe^{3+}/Fe_T ratio and the total concentration of Fe as a function of MAI. The solid lines in Figures 13a and 13b represent the special case where $A_{Mt} = A_{Chr} = 0$; that is, all Fe is from any combination of npOx, Fe3Sulfate, Gt, and Hm. The least altered rocks (MAI < 17%) are Adirondack Subclass (Adirondack, Humphrey, Mazatzal, Route66, and Humboldt Peak), Irvine Class (Irvine, Bu Zhou, and Esperanza), Backstay Class (Backstay), Peace Class (Alligator and Peace), and some members of Joshua Subclass (Joshua), Algonquin Class (Larrys Bench and Algonquin), Barnhill Class (Pesapallo, June Emerson, and Elizabeth Emery), and Everett Class (Everett). The most altered rocks (MAI > 50%) are members of Clovis Class (Clovis, Temples, Uchben, Ebenezer, Tetl, and Lutefisk), Watchtower Class (Watchtower, Pequod, Paros, Keel Davis, and Kansas), Descartes Class (Descartes), Pot Of Gold Subclass (Pot Of Gold and Fort Knox), Halley Class (Halley, Riquelme, and King George), Montalva Class (Montalva) and Fuzzy Smith Class (Fuzzy Smith). Because of their low total Fe contents (<8 wt %), Independence Class (Independence and Assemblee) and members of Elizabeth Mahon Class (Elizabeth Mahon and Nancy Warren) are included as most altered rocks (Figure 13c).

4.2. Gusev Crater and Meridiani Planum Soils

[43] Soils at Gusev Crater and Meridiani Planum are divided into five classes on the basis of APXS chemistry, and two of the five are subdivided into subclasses on the basis of mineralogical composition (Table 11). The values of δ and ΔE_Q for olivine, pyroxene, and npOx are listed in Table 12 at the class/subclass level. Pie diagrams for Gusev Crater soils at the subclass level for Fe mineralogical compositions are illustrated in Figure 14.

[44] Laguna Class soils are basaltic soils that are widespread throughout both landing sites, and they are generally mixtures in variable proportions of Ol, Px, and npOx (Panda, Liberty and Gobi Subclasses). The differences among the Panda, Liberty, and Gobi Subclasses are gradational, with Panda Subclass having the least npOx and Gobi Subclass the most. Doubloon Subclass is characterized by enrichments in Ti and P, depletion in Cr, and the presence of ilmenite, which are characteristics inherited from the nearby ilmenite-bearing Watchtower Class and Descartes Class rocks. Mixing with local rock is also suggested by the presence of angular to subangular grains observed in these soils [*Cabrol et al.*, 2008]. The Boroughs Subclass is distinguished by high concentrations of Mg and S, perhaps as a Mg-sulfate salt [e.g., *Wang et al.*, 2006]. Laguna Class soils plot on or near the line for $A_{Mt} = A_{Chr} = 0$ on the Fe^{3+}/Fe_T versus MAI diagram (Figure 13b) because of their generally low Mt content and no detectable Chr.

[45] The two Gertrude Weise Class soils are located in Eastern Valley, which is between Home Plate and Mitcheltree Ridge. Lefty Ganote and Kenosha Comets have very high SiO_2 concentrations (SiO_2 ~75 and ~90 wt %, respectively [*Squyres et al.*, 2008; *Ming et al.*, 2008]), and low total Fe concentrations (Figure 13d). The single-member Eileen Dean Class soil has the highest proportion of Fe from Mt for any soil (A_{Mt} = 43%; Figure 13b). Its Fe mineralogy is comparable to that for Home Plate rocks, so this soil may actually be a very friable rock.

[46] The five soils with MAI > 40% are the Paso Robles Class soils. They are distinguished from all other soils by the presence of Fe^{3+}-bearing sulfate. Soils Paso Robles, Paso Light1, and Samra have 60–86% of total Fe from Fe^{3+}-sulfate (*Morris et al.* [2006a] and Table 5). Berkner Island1 and Mount Darwin have comparatively less Fe from Fe3Sulfate (30%) because both soils are mixtures of local basaltic soil near Low Ridge (Bear Island1) and the light-toned (sulfate-rich) material excavated and transported from Tyrone in the rover wheel wells [*Arvidson et al.*, 2008; *Yen et al.*, 2008]. Therefore, the Tyrone sulfate deposit itself has more than 30% of Fe from Fe^{3+}-sulfate.

[47] In summary, the Panda, Liberty, and Gobi Subclasses of Laguna Class soil represent ubiquitous basaltic soils at both Gusev Crater and Meridiani Planum (Table 11). The Boroughs and Doubloon Subclasses of Laguna Class soil are also basaltic and occur infrequently only at Gusev Crater. Gertrude Weise Class, which encompasses the SiO_2-rich soils, Eileen Dean Class, and the Fe^{3+}-sulfate

Table 8. Average Mössbauer Component Subspectral Areas, Fe^{3+}/Fe_T, Total Fe Concentration as $FeO + Fe_2O_3$, MAI, and Measurement Sol for Rocks at Gusev Crater Through Sol A1544[a]

	Fe-Bearing Phase															
	Ol (%)	Px-A (%)	Px-B (%)	Px-C (%)	Ilm (%)	Chr (%)	Mt (%)	npOx (%)	Fe?D1 (%)	Hm (%)	Gt (%)	Sum (%)	Fe^{3+}/Fe_T	$FeO+Fe_2O_3$ (%)	MAI (%)	Sol
Gusev Plains																
Adirondack (Ad)	47 ± 2[b]	33 ± 2	0	0	0	0	13 ± 2	6 ± 2	0	1 ± 2	0	100	0.17[c]	19.1[d]	7	34
Mimi Shoe (MS)	28 ± 2	23 ± 2	0	0	0	0	26 ± 2	19 ± 2	0	4 ± 2	0	100	0.43	18.0	23	42
Humphrey (Hu)	47 ± 5	34 ± 2	0	0	0	0	11 ± 2	7 ± 2	0	2 ± 2	0	100	0.17	18.9	8	59
Paper Back (PB)	41 ± 2	36 ± 2	0	0	0	0	3 ± 2	19 ± 2	0	0	0	100	0.23	n.d.	20	76
Mazatzal (Mz)	57 ± 2	32 ± 2	0	0	0	0	6 ± 2	5 ± 2	0	0	0	100	0.10	19.0	5	84
Route 66 (R66)	57 ± 2	37 ± 2	0	0	0	0	0	7 ± 2	0	0	0	100	0.07	17.8	7	100
Joshua (Jo)	33 ± 2	37 ± 2	0	0	0	0	17 ± 2	11 ± 2	0	2 ± 2	0	100	0.26	19.1	13	150
West Spur																
Fort Knox (FK)	10 ± 2	37 ± 2	0	0	0	0	2 ± 2	13 ± 2	0	38 ± 2	0	100	0.52	n.d.	51	166
Pot Of Gold (PoG)	5 ± 5	36 ± 2	0	0	0	0	3 ± 2	16 ± 4	0	40 ± 7	0	100	0.58	17.7	56	171
Bread Box (BB)	14 ± 2	37 ± 2	0	0	0	0	6 ± 2	11 ± 2	0	31 ± 2	0	100	0.47	16.0	42	176
String Of Pearls (SoP)	19 ± 2	37 ± 2	0	0	0	0	4 ± 2	13 ± 2	0	27 ± 2	0	100	0.43	17.3	41	178
Wooly Patch (WP)	3 ± 2	37 ± 8	0	0	0	0	15 ± 2	25 ± 5	0	14 ± 4	6 ± 2	100	0.56	18.7	45	198
Clovis (Cl)	2 ± 2	0	14 ± 2	0	0	0	1 ± 2	27 ± 2	0	19 ± 2	37 ± 2	100	0.84	16.9	83	213
Ebenezer (Eb)	1 ± 2	0	13 ± 3	0	0	0	20 ± 2	34 ± 2	0	14 ± 2	20 ± 2	100	0.81	16.8	67	233
Temples (Tm)	1 ± 2	0	22 ± 2	0	0	0	10 ± 2	28 ± 2	0	13 ± 2	26 ± 2	100	0.74	16.5	67	269
Tetl (Tt)	2 ± 2	0	21 ± 2	0	0	0	24 ± 2	23 ± 2	0	16 ± 2	15 ± 2	100	0.70	15.7	53	275
Uchben (Uc)	2 ± 2	0	18 ± 3	0	0	0	13 ± 2	35 ± 4	0	8 ± 2	23 ± 2	100	0.76	14.9	67	288
Lutefisk (Lu)	2 ± 2	0	25 ± 3	0	0	0	17 ± 3	22 ± 3	0	15 ± 4	19 ± 2	100	0.68	15.1	56	303
North, SW, and SE Husband Hill																
Wishstone (Ws)	20 ± 2	29 ± 2	0	0	8 ± 2	0	12 ± 2	16 ± 2	0	14 ± 2	0	100	0.40	12.1	30	336
Wishing Well (WW)	25 ± 2	25 ± 2	0	0	2 ± 2	0	0	17 ± 2	0	22 ± 2	9 ± 2	100	0.48	12.7	33	350
Champagne (Ch)	18 ± 6	27 ± 4	0	0	7 ± 2	0	0	14 ± 3	0	18 ± 3	17 ± 3	100	0.49	13.1	38	358
Peace (Pe)	22 ± 2	29 ± 2	0	0	0	0	34 ± 2	15 ± 2	0	0	0	100	0.39	20.2	15	376
Alligator (All)	32 ± 2	31 ± 2	0	0	0	0	23 ± 2	14 ± 2	0	0	0	100	0.31	19.1	14	385
Watchtower (Wt)	7 ± 2	7 ± 2	0	0	3 ± 2	0	1 ± 2	39 ± 2	0	31 ± 2	12 ± 2	100	0.83	14.3	83	418
Keystone (Ke)	0	47 ± 2	0	0	6 ± 2	0	10 ± 2	17 ± 2	0	15 ± 2	4 ± 2	100	0.43	11.0	37	472
Keel Reef (KR)	15 ± 2	18 ± 2	0	0	1 ± 2	0	10 ± 2	25 ± 2	0	31 ± 2	0	100	0.64	12.2	56	483
Keel Davis (KD)	4 ± 2	13 ± 2	0	0	8 ± 2	0	9 ± 2	27 ± 2	0	40 ± 2	0	100	0.73	11.7	67	486
Paros (Pa)	3 ± 2	1 ± 2	0	0	2 ± 2	0	0	66 ± 2	0	18 ± 2	11 ± 2	100	0.94	12.5	94	491
Pequod (Pq)	5 ± 2	2 ± 2	0	0	6 ± 2	0	0	62 ± 5	0	16 ± 2	11 ± 2	102	0.88	12.1	88	498
Backstay (Bs)	35 ± 2	37 ± 2	0	0	3 ± 2	0	11 ± 2	13 ± 2	0	2 ± 2	0	100	0.23	13.3	15	510
Independence (Ind)	0	26 ± 8	0	0	29 ± 7	0	0	45 ± 15	0	0	0	100	0.45	4.0	45	534
Descartes (De)	1 ± 2	30 ± 4	0	0	1 ± 2	0	18 ± 2	39 ± 6	0	4 ± 2	7 ± 2	100	0.64	14.6	50	552
Bourgeoisie Chic (BC)	26 ± 2	25 ± 2	0	0	18 ± 2	0	7 ± 2	23 ± 2	0	2 ± 2	0	100	0.31	10.5	24	559
Assemblee (Asm)	0	44 ± 2	0	0	0	23 ± 2	0	32 ± 2	0	0	0	100	0.37	6.7	32	568
Irvine (Ir)	9 ± 2	46 ± 2	0	0	0	0	36 ± 2	6 ± 2	0	3 ± 2	0	100	0.35	19.8	9	602
Hillary (Hi)	11 ± 2	15 ± 3	0	0	8 ± 4	0	28 ± 2	23 ± 6	0	15 ± 3	0	100	0.56	11.9	37	629
Kansas (Kn)	3 ± 2	28 ± 2	0	0	9 ± 2	0	8 ± 2	29 ± 2	0	0	23 ± 2	100	0.59	14.1	52	648
Haskin Ridge																
Larrys Bench (LB)	72 ± 2	3 ± 2	0	0	3 ± 2	0	5 ± 2	16 ± 2	0	0	0	100	0.20	20.9	16	662
Seminole (Sm)	62 ± 7	6 ± 2	0	0	1 ± 2	0	8 ± 4	22 ± 2	0	0	0	100	0.28	20.1	22	674
Algonquin (Aqn)	71 ± 2	13 ± 2	0	0	2 ± 2	0	6 ± 2	8 ± 2	0	0	0	100	0.11	21.4	8	690
Comanche Spur (CS)	54 ± 4	0	0	24 ± 3	0	0	1 ± 2	16 ± 2	0	5 ± 2	0	100	0.22	23.0	21	702
Northern Inner Basin																
Bu Zhou (BZ)	6 ± 2	33 ± 2	0	0	0	0	54 ± 2	5 ± 2	0	2 ± 2	0	100	0.45	n.d.	7	737
Home Plate																
Barnhill (Ba)	18 ± 2	22 ± 2	0	0	0	0	24 ± 2	29 ± 2	0	7 ± 2	0	100	0.53	18.6	36	749
Posey (Po)	17 ± 2	23 ± 2	0	0	0	0	31 ± 2	27 ± 2	0	3 ± 2	0	100	0.53	16.1	30	754
James Cool Papa Bell (JB)	17 ± 2	23 ± 2	0	0	0	0	28 ± 2	29 ± 2	0	3 ± 2	0	100	0.52	16.9	32	762
Fuzzy Smith (FS)	4 ± 2	26 ± 2	0	0	8 ± 2	0	0	0	63 ± 2	0	0	100	0.00	6.8	63	769
Low Ridge and Eastern Valley																
Halley (Ha)	10 ± 6	12 ± 6	0	0	0	0	14 ± 3	9 ± 2	0	54 ± 13	0	100	0.73	17.4	63	810
King George (KG)	9 ± 2	19 ± 2	0	0	0	0	17 ± 2	14 ± 2	0	41 ± 2	0	100	0.67	15.3	55	1029
Esperanza (Es)	4 ± 2	45 ± 2	0	0	0	0	45 ± 2	4 ± 2	0	1 ± 2	0	100	0.40	21.0	5	1056
Montalva (Mo)	0	3 ± 2	0	0	0	0	14 ± 2	5 ± 2	0	78 ± 2	0	100	0.93	21.1	84	1073
Riquelme (Rq)	6 ± 2	20 ± 2	0	0	0	0	15 ± 2	19 ± 2	0	39 ± 2	0	100	0.70	17.0	58	1082
Torquas (Tq)	3 ± 2	16 ± 2	0	0	0	0	46 ± 2	31 ± 2	0	4 ± 2	0	100	0.71	18.0	35	1145
Elizabeth Mahon (EM)	10 ± 2	25 ± 2	0	0	4 ± 2	0	23 ± 2	30 ± 2	0	8 ± 2	0	100	0.54	7.3	38	1155
Madeline English (ME)	7 ± 2	37 ± 2	0	0	0	0	35 ± 2	18 ± 2	0	3 ± 2	0	100	0.46	15.3	21	1170
Everett (Ev)	4 ± 2	35 ± 2	0	0	0	0	46 ± 2	15 ± 2	0	0	0	100	0.47	19.9	15	1174

Table 8. (continued)

	Fe-Bearing Phase															
	Ol (%)	Px-A (%)	Px-B (%)	Px-C (%)	Ilm (%)	Chr (%)	Mt (%)	npOx (%)	Fe?D1 (%)	Hm (%)	Gt (%)	Sum (%)	Fe^{3+}/Fe_T	$FeO+Fe_2O_3$ (%)	MAI (%)	Sol
Slide (Sl)	4 ± 2	33 ± 2	0	0	0	0	41 ± 2	22 ± 2	0	0	0	100	0.51	20.1	22	1177
Good Question (GQ)	5 ± 2	42 ± 2	0	0	0	0	15 ± 2	31 ± 2	0	6 ± 2	0	100	0.47	15.5	38	1189
							Home Plate									
Pesapallo (Pp)	1 ± 2	41 ± 2	0	0	0	0	42 ± 2	11 ± 2	0	5 ± 2	0	100	0.48	16.2	16	1207
June Emerson (JE)	2 ± 2	37 ± 2	0	0	0	0	54 ± 2	6 ± 2	0	1 ± 2	0	100	0.44	17.3	7	1213
Elizabeth Emery (EE)	2 ± 2	38 ± 2	0	0	0	0	51 ± 2	8 ± 2	0	1 ± 2	0	100	0.46	17.5	9	1215
							Eastern Valley									
Nancy Warren (NW)	22 ± 2	24 ± 2	0	0	1 ± 2	0	26 ± 2	24 ± 2	0	2 ± 2	0	100	0.44	6.1	27	1228
Innocent Bystander (IBy)	7 ± 2	12 ± 2	0	0	1 ± 2	0	56 ± 2	17 ± 2	0	7 ± 2	0	100	0.64	14.3	24	1255
							Home Plate									
Texas Chili (TC)	4 ± 2	30 ± 2	0	0	0	0	34 ± 2	25 ± 2	0	7 ± 2	0	100	0.56	17.2	29	1325
Humboldt Peak (HP)	53 ± 2	10 ± 2	0	0	0	0	26 ± 2	11 ± 2	0	0	0	100	0.31	17.2	11	1340
Pecan Pie (Pcn)	12 ± 2	15 ± 2	0	0	0	0	29 ± 2	30 ± 2	0	14 ± 2	0	100	0.64	17.7	44	1368
Chanute (Cht)	9 ± 2	22 ± 2	0	0	0	0	29 ± 2	31 ± 2	0	9 ± 2	0	100	0.62	17.2	40	1411

[a]Data used were the first available in the sequence RAT grind surface, RAT brushed surface, and undisturbed surface. Component subspectra are *f* factor corrected. MAI, Mineralogical Alteration Index.
[b]Uncertainty in subspectral area is the larger of the standard deviation of the average and measurement uncertainty. Minimum measurement uncertainty is ±2% absolute.
[c]Uncertainty in Fe^{3+}/Fe_T is ±0.03.
[d]Untertainty in $FeO + Fe_2O_3$ ranges approximately from ±0.05 to 0.3 wt % [*Ming et al.*, 2008].

containing Paso Robles Class soils are present only at Gusev Crater. The only occurrences to date of Paso Robles Class, Gertrude Weise Class, and Eileen Dean Class soils are subsurface. Berry Class soils are present only at Meridiani Planum, and they have high Hm and $FeO + Fe_2O_3$ concentrations resulting from the presence of Hm spherules (a.k.a. blueberries) and their fragments (Table 11 and *Morris et al.* [2006b]).

5. Fe Mineralogy Along the Traverse of the Spirit Rover

[48] The traverse of Spirit through the Columbia Hills is shown in Figure 1 together with names for traverse segments. Detailed discussions of the traverse segments from the landing site through West Spur, north Husband Hill, and partway up SW Husband Hill are previously published [e.g., *Arvidson et al.*, 2006; *Clark et al.*, 2007; *Morris et al.*, 2006a; *Ming et al.*, 2006; *McSween et al.*, 2006a, 2006b; *Squyres et al.*, 2006]. For these segments, short summaries of the Fe mineralogy are given in the discussion that follows.

5.1. Gusev Plains

[49] Spirit traversed the Gusev plains between its landing site and West Spur. All analyzed rocks are olivine basalt float rocks with magnetite (except for Route66) as the Fe oxide phase (Figure 15a). Soils have a similar Fe mineralogical composition and are approximately two-component mixtures of Ol + Px + Mt and npOx + minor Hm (Figure 15b). Bright soils have higher proportion of npOx + Hm than do dark soils.

5.2. West Spur

[50] The Fe mineralogy dramatically changed when Spirit encountered the Columbia Hills at West Spur. Instead of an assemblage of igneous Fe-bearing phases (Ol, Px, and Mt), the rocks have ~20 to 50% of their total Fe associated with the secondary minerals Hm and Gt (Figure 16a). All of the Gt-bearing rocks (Clovis Class) are outcrop rocks, implying that Gt is volumetrically important in the Columbia Hills. In contrast to the rocks, the Fe mineralogy of West Spur soils is equivalent to that for the plains soils (Figure 16b).

5.3. North Husband Hill

[51] This segment marks the appearance of rocks with detectable amounts of the ferrous oxide ilmenite (Figure 17a). All rocks are outcrops except the float rocks Wishstone, Wishing Well, Champagne, and Backstay. Backstay is relatively unaltered (MAI < 15%), and it is the only member of its class investigated in situ with the IDD instruments (Backstay Class). The Fe mineralogical composition of Backstay is characterized by subequal proportions of Ol and Px that total ~70% plus Mt, Ilm, and npOx. Mössbauer spectra for Backstay and Wishstone are shown in Figures 18a and 19a, respectively.

[52] The Wishstone Class rocks (Wishstone, Wishing Well, and Champagne; MAI = 30 to 38%) and especially the Watchtower Class rocks (Watchtower, Keystone, Keel Reef, Keel Davis, Paros, and Pequod; MAI = 37 to 94%) are weakly and pervasively altered, respectively, as evidenced by the presence of Hm, npOx, and, for some rocks, Gt. Watchtower, Paros, and Pequod have >80% of their total Fe in the Fe^{3+}-bearing phases npOx, Hm, and Gt.

[53] According to their Fe mineralogy, Peace Class Outcrop rocks (Peace and Alligator) are relatively unaltered with Ol, Px, and Mt as the dominant Fe-bearing phases and no detectable Hm or Gt (Figure 17a). However, these rocks have high concentrations of Mg and S, implying that the rocks were originally porous material (perhaps tephra) that was invaded and cemented by solutions rich in Mg and sulfate without significant alteration of preexisting silicate and oxide phases [*Ming et al.*, 2006]. Mössbauer spectra for Champagne, Peace, and Watchtower are given in Figure 20.

Table 9. Classification of Gusev Rocks According to Chemical (APXS) and Fe Mineralogical (MB) Data, and Average Values of the Percentage of Total Fe in Specific Fe-Bearing Phases, Oxidation State, and Total Fe as $FeO + Fe_2O_3$ for Each Subclass[a]

Class	Subclass	Rocks in Subclass[b]	Ol(%)	Px(%)	Ilm(%)	Chr(%)	Mt(%)	npOx(%)	Fe?D1(%)	Hm(%)	Gt(%)	Fe^{3+}/Fe_T(%)	$FeO + Fe_2O_3$(%)
Adirondack	Adirondack	**Adirondack, Humphrey, Paperback, Mazatzal, Route 66, Humboldt Peak**	50 ± 6	30 ± 10	0	0	10 ± 9	9 ± 5	0	0 ± 2	0	0.17 ± 0.09	18.6 ± 0.9
	Joshua	**Mimi Shoe, Joshua**	30 ± 4	30 ± 10	0	0	22 ± 7	15 ± 6	0	3 ± 2	0	0.34 ± 0.12	18.6 ± 0.8
Clovis	Clovis	Clovis, Ebenezer, Temples, Tetl, Uchben, Lutefisk	2 ± 2	19 ± 5	0	0	14 ± 8	28 ± 6	0	14 ± 4	23 ± 8	0.76 ± 0.06	15.9 ± 0.9
	Wooly Patch	WoolyPatch	3 ± 2	37 ± 2	0	0	15 ± 2	25 ± 2	0	14 ± 2	6 ± 2	0.56 ± 0.03	18.3 ± 0.3
Wishstone	Wishstone	Wishstone, Wishing Well, Champagne, Bourgeoisie Chic	22 ± 4	26 ± 2	9 ± 7	0	5 ± 6	17 ± 4	0	14 ± 9	6 ± 8	0.42 ± 0.09	12.2 ± 1.1
Peace	Peace	**Peace, Alligator**	27 ± 7	30 ± 2	0	0	28 ± 8	15 ± 2	0	0	0	0.35 ± 0.06	19.8 ± 0.8
Watchtower	Watchtower	Watchtower, Paros, Pequod	5 ± 2	3 ± 3	4 ± 2	0	0	55 ± 14	0	21 ± 8	12 ± 2	0.88 ± 0.06	12.9 ± 1.2
	Keystone	Keystone, Kansas	2 ± 2	38 ± 15	7 ± 2	0	9 ± 2	23 ± 8	0	8 ± 11	14 ± 13	0.51 ± 0.11	11.0 ± 2.2
	Keel	Keel Reef, Keel Davis, Hillary	10 ± 6	15 ± 2	6 ± 4	0	16 ± 11	25 ± 2	0	29 ± 13	0	0.65 ± 0.08	12.5 ± 0.3
Backstay	Backstay	**Backstay**	35 ± 2	37 ± 2	3 ± 2	0	11 ± 2	13 ± 2	0	2 ± 2	0	0.23 ± 0.03	13.3 ± 0.3
Descartes	Descartes	Descartes	1 ± 2	30 ± 2	1 ± 2	0	18 ± 2	39 ± 2	0	4 ± 2	7 ± 2	0.64 ± 0.03	12.5 ± 0.3
Independence	Independence	Independence	0	26 ± 2	29 ± 2	0	0	45 ± 2	0	0	0	0.45 ± 0.03	5.8 ± 0.3
	Assemblee	Assemblee	0	46 ± 2	0	23 ± 2	0	32 ± 2	0	0	0	0.37 ± 0.03	6.7 ± 0.3
Irvine	Irvine	**Irvine, Bu Zhou, Esperanza**	6 ± 3	41 ± 7	0	0	45 ± 9	5 ± 2	0	2 ± 2	0	0.40 ± 0.05	20.4 ± 0.8
Algonquin	Algonquin	**Larrys Bench, Seminole, Algonquin**	69 ± 6	8 ± 5	2 ± 2	0	6 ± 2	15 ± 7	0	0	0	0.20 ± 0.08	20.8 ± 0.7
	Comanche	**Comanche Spur**	54 ± 2	24 ± 2	0	0	1 ± 2	16 ± 2	0	5 ± 2	0	0.22 ± 0.03	22.7 ± 0.3
Barnhill	Barnhill	**Barnhill, Posey, James Cool Papa Bell, Pecan Pie**	16 ± 3	21 ± 4	0	0	28 ± 3	29 ± 2	0	7 ± 6	0	0.55 ± 0.06	17.4 ± 1.1
	Pesapallo	**Madeline English, Pesapallo, June Emerson, Elizabeth Emery, Texas Chili**	3 ± 2	37 ± 4	0	0	43 ± 9	14 ± 8	0	3 ± 3	0	0.48 ± 0.05	16.8 ± 0.9
Fuzzy Smith	Fuzzy Smith	Fuzzy Smith	4 ± 2	26 ± 2	8 ± 2	0	0	0	63 ± 2	0	0	0.00 ± 0.03	6.8 ± 0.3
Halley	Pot Of Gold	Fort Knox, Pot Of Gold, String Of Pearls, Bread Box	12 ± 6	37 ± 2	0	0	4 ± 2	13 ± 2	0	34 ± 6	0	0.50 ± 0.06	16.8 ± 0.9
	Halley	Halley	10 ± 2	12 ± 2	0	0	14 ± 2	9 ± 2	0	54 ± 2	0	0.73 ± 0.03	17.4 ± 0.3
	Grahamland	King George, Riquelme	8 ± 2	20 ± 2	0	0	16 ± 2	16 ± 3	0	40 ± 2	0	0.68 ± 0.02	16.2 ± 1.2
Everett	Everett	**Everett, Slide**	4 ± 2	34 ± 2	0	0	43 ± 3	18 ± 5	0	0	0	0.49 ± 0.03	20.0 ± 0.3
Montalva	Montalva	Montalva	0	3 ± 2	0	0	14 ± 2	5 ± 2	0	78 ± 2	0	0.93 ± 0.03	21.1 ± 0.3
Torquas	Torquas	**Torquas**	3 ± 2	16 ± 2	0	0	46 ± 2	31 ± 2	0	4 ± 2	0	0.71 ± 0.03	18.0 ± 0.3
Good Question	Good Question	Good Question	5 ± 2	42 ± 2	0	0	15 ± 2	31 ± 2	0	6 ± 2	0	0.47 ± 0.03	15.5 ± 0.3
Elizabeth Mahon	Elizabeth Mahon	Elizabeth Mahon, Nancy Warren	16 ± 9	25 ± 2	2 ± 2	0	25 ± 3	27 ± 4	0	5 ± 4	0	0.49 ± 0.07	6.7 ± 0.3
	Innocent Bystander	Innocent Bystander	7 ± 2	12 ± 2	1 ± 2	0	56 ± 2	17 ± 2	0	7 ± 2	0	0.64 ± 0.03	14.3 ± 0.3

[a]Uncertainties are the larger of standard deviation of the average and the measurement uncertainty, which are ±2% for subspectral areas, ±0.03 for Fe^{3+}/Fe_T, and a maximum of ~0.3 wt % for $FeO + Fe_2O_3$. APXS, Alpha Particle X-Ray Spectrometer; MB, Mössbauer.

[b]Bold typeface, unaltered to weakly altered basalt; normal typeface, altered basalt.

Table 10. Average Mössbauer Parameters δ and ΔE_Q and Their Standard Deviations for Ol, Px, and npOx for Gusev Rock Subclasses[a]

		Ol (Fe2D1)				Px (Fe2D2)				npOx (Fe3D1)			
		δ		ΔE_Q		δ		ΔE_Q		δ		ΔE_Q	
Subclass Name	N[b]	Average (mm/s)	SD (mm/s)	Average (mm/s)	SD (mm/s)	Average (mm/s)	SD (mm/s)	Average (mm/s)	SD (mm/s)	Average (mm/s)	SD (mm/s)	Average (mm/s)	SD (mm/s)
Adirondack	5	1.16	0.02	3.00	0.02	1.16	0.02	2.07	0.02	0.37	0.02	0.87	0.08
Joshua	2	1.15	0.02	2.96	0.02	1.16	0.02	2.06	0.03	0.38	0.02	0.82	0.04
Clovis	6	[1.16][c]	–	[3.02]	–	1.16	0.02	2.28	0.11	0.37	0.02	1.02	0.04
Wooly Patch	2	[1.16]	–	[3.02]	–	1.17	0.02	2.15	0.01	0.37	0.02	0.91	0.05
Pot Of Gold	4	[1.16]	–	[3.02]	–	1.16	0.02	2.18	0.03	0.37	0.02	0.97	0.04
Peace	2	1.15	0.02	3.05	0.02	1.15	0.02	2.16	0.02	0.35	0.02	0.91	0.02
Wishstone	4	1.17	0.02	2.97	0.02	1.17	0.02	2.12	0.04	0.37	0.02	0.91	0.09
Watchtower	3	[1.15]	–	[3.01]	–	[1.16]	–	[2.20]	–	0.36	0.02	1.01	0.02
Keystone	1	–	–	–	–	1.16	0.02	2.19	0.02	0.35	0.02	0.89	0.02
Keel	2	1.15	0.02	3.06	0.02	1.15	0.02	2.20	0.04	0.36	0.02	0.89	0.03
Backstay	1	1.15	0.02	3.00	0.02	1.16	0.02	2.12	0.02	0.34	0.02	0.90	0.02
Descartes	2	1.17	0.02	2.98	0.02	1.16	0.02	2.12	0.02	0.37	0.02	0.86	0.13
Independence	1	–	–	–	–	1.19	0.02	2.45	0.02	0.38	0.02	0.85	0.02
Assemblee	1	–	–	–	–	1.05	0.02	2.39	0.02	0.34	0.02	1.16	0.02
Irvine	3	1.15	0.02	2.95	0.02	1.15	0.02	2.11	0.02	0.39	0.02	0.82	0.02
Algonquin	3	1.15	0.02	3.03	0.02	[1.15]	–	[2.06]	–	0.35	0.02	0.91	0.02
Comanche	1	1.15	0.02	3.06	0.02	1.23	0.02	1.92	0.02	0.34	0.02	1.01	0.02
Barnhill	3	1.15	0.02	3.02	0.02	1.16	0.02	2.13	0.04	0.37	0.02	0.91	0.03
Pesapallo	2	[1.14]	–	[3.01]	–	1.16	0.02	2.12	0.01	0.38	0.02	0.86	0.05
Fuzzy Smith	1	[1.14]	–	[3.01]	–	–	–	–	–	–	–	–	–
Halley	1	[1.15]	–	[3.03]	–	[1.14]	–	[2.13]	–	[0.38]	–	[0.92]	–
Grahamland	2	1.18	0.02	3.06	0.02	1.13	0.02	2.13	0.04	0.34	0.02	0.86	0.04
Everett	2	[1.14]	–	[2.97]	–	1.16	0.02	2.12	0.03	0.35	0.02	0.80	0.02
Montalva	1	–	–	–	–	[1.14]	–	[2.13]	–	[0.37]	–	0.77	0.02
Torquas	1	[1.14]	–	[2.97]	–	1.16	0.02	2.12	0.02	0.35	0.02	0.82	0.02
Good Question	1	[1.14]	–	[2.97]	–	1.17	0.02	2.08	0.02	0.34	0.02	0.90	0.02
Elizabeth Mahon	1	[1.14]	–	[3.01]	–	1.17	0.02	1.99	0.02	0.34	0.02	0.79	0.10
Innocent Bystander	1	[1.14]	–	[2.97]	–	[1.17]	–	[2.11]	–	[0.35]	–	0.90	0.02

[a]Values of δ are with respect to metallic iron foil at the same temperature as the sample. Table is ordered by increasing sol number for the first appearance of a rock in each subclass.
[b]Number of rocks used to calculate the average; not the number of rocks in a subclass.
[c]MB parameters in brackets are constraints used in the fitting procedure.

[54] Most soils analyzed during the traverse up Husband Hill (Figure 17b) are typical Ol-Px-Mt-npOx basaltic soils (e.g., Laguna Class soil). Doubloon (Doubloon Subclass) is a basaltic soil but is distinct on the basis of detectable ilmenite (Figure 21a). The oxide was probably inherited from the nearby Ilm-bearing rocks (e.g., Wishstone Class). The PasoRobles soil (Figure 21b) is the first occurrence of sulfate-rich soil (Paso Robles Class) whose Fe mineralogical composition has more than ~30 to 86% of its total Fe present as a Fe^{3+}-bearing sulfate. The Paso Robles locale was analyzed twice, on sols 401 and 429.

5.4. Southwest Husband Hill

[55] All rocks are outcrop, except Bourgeoisie Chic, which is a clast in the outcrop rock Descartes. The clast has a very different Fe mineralogical composition from Descartes in which it is imbedded (Figure 22a). Specifically, the clast has significantly more Ol and Ilm and less npOx and no Gt. The chemical composition of Bourgeoisie Chic is similar to that for Wishstone rocks, so that the Voltaire Outcrop may be a conglomerate composed of Descartes and Wishstone material [*Arvidson et al.*, 2008]. Mössbauer spectra for Descartes and Bourgeoisie Chic are shown in Figures 19b and 19c, respectively.

[56] The outcrop rocks Independence and Assemblee (Independence Class) are strongly altered as evidenced by their low Fe concentration (5.8 and 6.7 wt %, respectively, as FeO + Fe_2O_3). This is consistent with their unusual Fe mineralogy (Figure 22a). Independence is a npOx, Px, and Ilm assemblage, and the rock has the highest proportion of total Fe from Ilm for any Gusev or Meridiani sample analyzed to date (A_{Ilm} = 29%). Assemblee, which has ~2.7 wt % Cr_2O_3, is the only rock with evidence for chromite (A_{Chr} = 23%). Unlike the altered rocks in Clovis Class, Wishstone Class, and Watchtower Class, the Independence Class rocks do not have detectable Hm and Gt. Mössbauer spectra for Independence and Assemblee are shown in Figures 23a and 23b, respectively. No soils were analyzed by MB on SW Husband Hill.

5.5. Southeast Husband Hill

[57] Three rocks were analyzed by MB on the SE side of the Husband Hill summit (Figure 22a). The float rock Irvine is relatively unaltered (MAI < 15%), and it is the first occurrence of a class of rocks (Irvine Class) whose Fe mineralogical composition is dominated by Px and Mt. The outcrop rocks Hillary and Kansas are Watchtower Class with detectable Fe from Ilm. Kansas has detectable Gt, so that the oxyhydroxide is detected by MB on both sides of Husband Hill. The Mössbauer spectrum for Irvine is shown in Figure 18b.

[58] Soils analyzed on SE Husband Hill are typical Laguna Class basaltic soils (i.e., Fe mineralogy is Ol-Px-Mt-npOx). Whymper (Gobi Subclass) has among the highest values of Fe from npOx detected to date (A_{npOx} = 34%) and is a good example of a bright soil. Hang2 and Lands End (which has

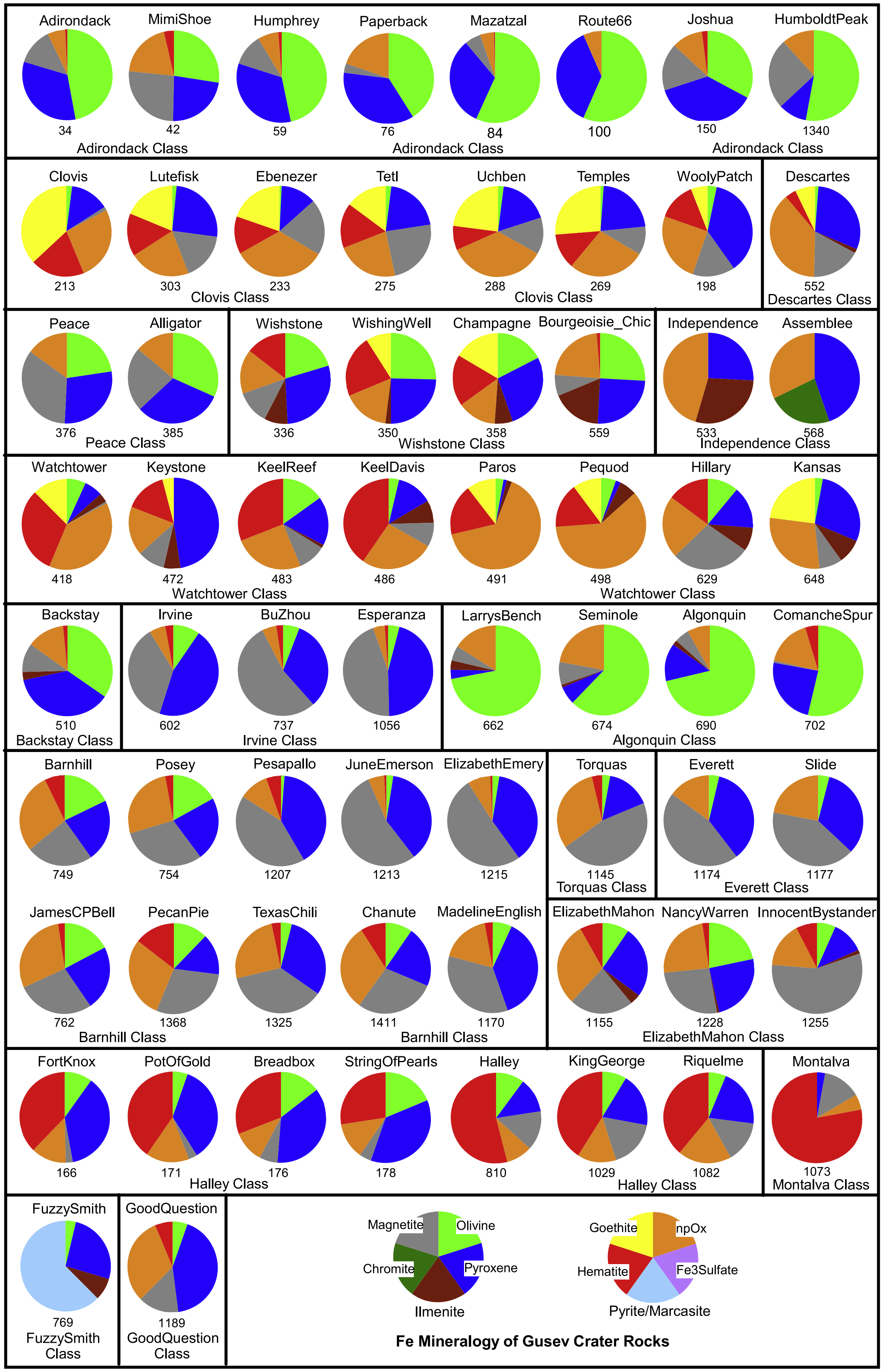

Figure 12. Pie diagrams for the Fe mineralogical composition of rocks according to their classification in Table 9. The number under each pie diagram is the sol that Mössbauer (MB) analysis began.

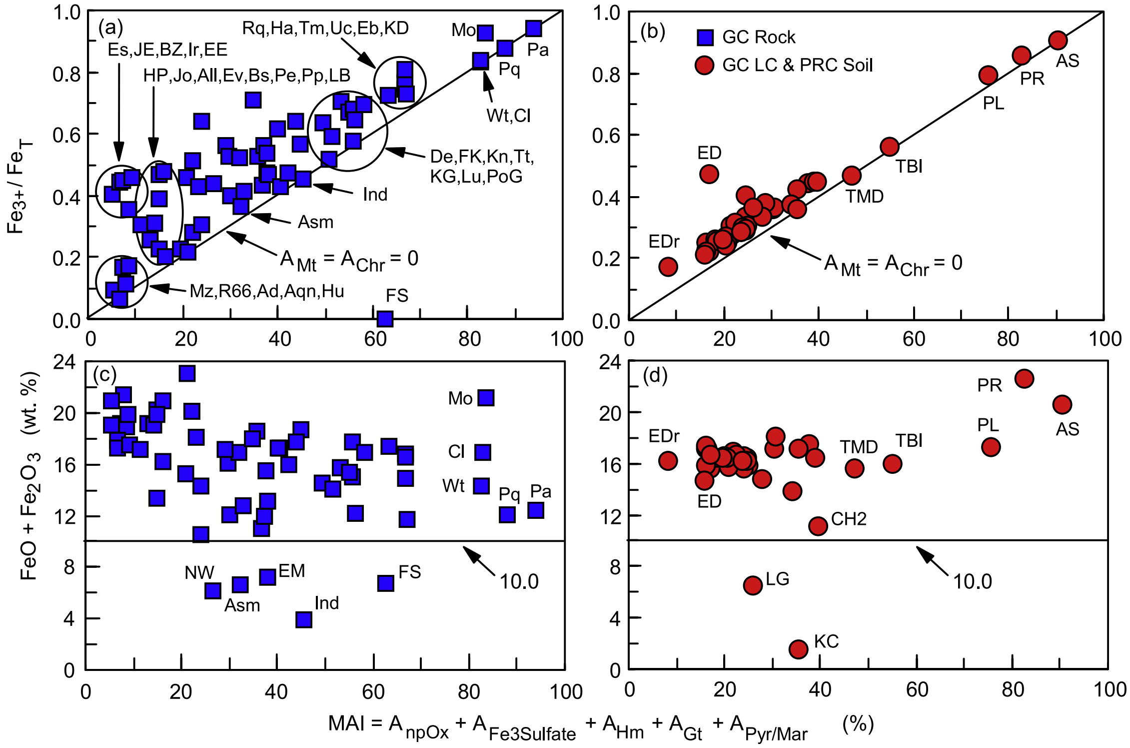

Figure 13. Total Fe concentration as FeO + Fe_2O_3 and Fe redox state as Fe^{3+}/Fe_T versus the Mineralogical Alteration Index (MAI) for Gusev Crater (a and c) rocks and (b and d) soils. The solid line in Figures 13a and 13b corresponds to $A_{Mt} = A_{Chr} = 0$. The horizontal solid line in Figures 13c and 13d corresponds to FeO + Fe_2O_3 = 10.0 wt %. Rock names are Ad, Adirondack; All, Alligator; Aqn, Algonquin; Asm, Assemblee; Bs, Backstay; BZ, Bu Zhou; Cl, Clovis; De, Descartes; Eb, Ebenezer; EE, Elizabeth Emery; EM, Elizabeth Mahon; Es, Esperanza; Ev, Everett; FK, Fort Knox; FS, Fuzzy Smith; Ha, Halley; HP, Humboldt Peak; Hu, Humphrey; Ind, Independence; Ir, Irvine; JE, June Emerson; Jo, Joshua; KD, Keel Davis; KG, King George; Kn, Kansas; LB, Larrys Bench; Lu, Lutefisk; Mo, Montalva, Mz, Mazatzal; NW, Nancy Warren; Pa, Paros; Pe, Peace; PoG, Pot Of Gold; Pp, Pesapallo; Pq, Pequod; R66, Route 66; Rq, Riquelme; Tm, Temples; Tt, Tetl; Uc, Uchben; Wt, Watchtower. Soil names are AS, Arad Samra; CH2, Cliffhanger Hang2; ED, Eileen Dean; EDr, El Dorado Scuff Shadow; KC, Kenosha Comets; LG, Lefty Ganote; PL, Paso Robles Paso Light1; PR, Pasadena Paso Robles; TBI, Tyrone Berkner Island; and TMD, Tyrone Mount Darwin.

possible ilmenite) have unusually high A_{Px}/A_{Ol} ratios for soils (Table 5), which may be a signature of mixing with fragments of local rocks. The Mössbauer spectra for Whymper and Kansas are shown in Figures 21c and 23c, respectively.

5.6. Haskin Ridge and Northern Inner Basin

[59] Spirit crossed a distinct mineralogical boundary between sols 648 and 662, from highly altered outcrop rocks on SW and SE Husband Hill with little or no Fe from olivine to the olivine-rich (A_{Ol} = 50% to 70%) outcrop rocks on Haskin Ridge (Algonquin Class: Larrys Bench, Seminole, Algonquin, and Comanche Spur) (Figure 24a). The low normative olivine compared to the high values expected from the Fe mineralogy results from APXS analyses that preferentially sample a thin (1s to 10s of micrometers depending on element) surface layer whose elemental composition has been altered by weathering, according to *McSween et al.* [2008]. Mössbauer, which samples deeper (100s of microns), preferentially samples the relatively unaltered Ol-rich rock beneath the thin surface layer. Mössbauer spectra for Algonquin and Comanche Spur are shown in Figure 25.

[60] The Fe mineralogical composition of Comanche Spur pyroxene is different from that for any other rock analyzed to date at Gusev Crater (and Meridiani Planum), including the other three Algonquin Class rocks. Its MB parameters (labeled Px-C in Figure 2) are significantly offset from other pyroxene data (Px-A) to higher δ and lower ΔE_Q. It is possible that the Fe^{2+}-bearing phase is not pyroxene (see section 3.2.3).

[61] One rock (BuZhou) was analyzed in the northern Inner Basin. Although it was not analyzed by APXS, we classify the rock as Irvine Class on the basis of its Fe mineralogical composition (predominantly Px + Mt; Figure 24a) and a morphology resembling vesicular basalts, which have been shown by in situ and remote observations to be Irvine Class.

[62] Two soils were analyzed by MB during the traverse between the summit of Husband Hill and Home Plate (Figure 24b). The first analysis was an undisturbed surface on a low-albedo dune field called El Dorado [*Arvidson et*

Table 11. Classification of GC and MP Soils According to Chemical (APXS) and Fe Mineralogical (MB) Data and Average Subclass Values of the Distribution of Total Fe Among Fe-Bearing Phases, Oxidation State, and Total Fe as FeO + Fe_2O_3 for Each Subclass[a]

Class	Subclass	Soils in Subclass[b]	Ol(%)	Px(%)	Ilm(%)	Mt(%)	npOx(%)	Fe^{3+}Sulfate(%)	Hm(%)	Fe^{3+}/Fe_T(%)	FeO + Fe_2O_3(%)
Laguna	Panda	GC: Laguna Hollow_Floor3, Laguna Hollow_Wall, Bear Paw_Panda, Schreaded_Dark4, **Goldfinger_Jaws**, Penney_DS1, **Crumble_Almonds**, **El Dorado Scuff_Shadow**	40 ± 4	35 ± 2	0	9 ± 2	14 ± 3	0	2 ± 2	0.22 ± 0.03	16.4 ± 1.0
		MP: **Merlot_Tarmac**, **Fine Soil_Paydirt**, **Millstone_Dahlia**, Auk_AukRAT, **Rocknest_Void Mod**, Trench_Scruffy	37 ± 4	40 ± 4	0	6 ± 2	14 ± 2	0	3 ± 2	0.21 ± 0.03	18.1 ± 1.5
	Liberty	GC: **Mimi Tracks_Middle**, **Laguna Hollow_Trout1**, **Mazatzal Flats_Soil1**, **Big Hole_MayFly**, Mount Hillyer_Horse Flats, Take A Break_Coffee, Yams_Turkey, Pase Robles2_Paso Dark, **Liberty_Bell**, **Enderbyland_Mawson**, Low Ridge_Progress1, Low Ridge_Progress2, Bear Island_Bear Island1	36 ± 3	34 ± 3	0	9 ± 2	18 ± 2	0	3 ± 2	0.28 ± 0.03	16.3 ± 0.4
		MP: **Meringue_MBone**, **Black Forest_Brians Choice**, **Dog Park_Jeffs Choice**, **Hill Top_McDonnell**, Trench Site_Left Of Peanut	33 ± 2	37 ± 2	0	7 ± 2	17 ± 2	0	5 ± 2	0.27 ± 0.03	19.2 ± 1.6
	Gobi	GC: **First Soil**, **Desert_Gobi**, **Waffel Flats_Soil1**, Cutthroat_Owens, **Cookie Cutter_Shortbread**, Conjunction_Disturbance, **Lambert_Whymper**, Cliffhanger_Lands End, **Low Ridge_Progress**	30 ± 4	33 ± 5	0	10 ± 5	25 ± 4	0	2 ± 2	0.35 ± 0.05	16.1 ± 0.7
		MP: Big Dig_Hema Trench1, Big Dig_Hema TrenchWall2, **Mont Blanc_Les Hauches**, No Feature Name_Westport, Trench_Powell	26 ± 4	32 ± 3	0	5 ± 2	30 ± 7	0	7 ± 2	0.41 ± 0.08	19.2 ± 1.2
	Boroughs	GC: Big Hole_RS2, Boroughs_Mill Basin, Boroughs_Hells Kitchen	28 ± 2	29 ± 2	0	8 ± 2	33 ± 4	0	1 ± 2	0.41 ± 0.04	17.6 ± 0.5
	Doubloon	GC: **Pequod_Doubloon, Cliffhanger_Hang2**	20 ± 10	33 ± 11	4 ± 6	6 ± 2	26 ± 6	0	11 ± 2	0.41 ± 0.05	12.5 ± 2.0
Gertrude Weise		GC: Eastern Valley_Kenosha Comets, Eastern Valley_Lefty Ganote	25 ± 3	29 ± 6	8 ± 11	7 ± 9	30 ± 6	0	0	0.36 ± 0.03	4.0 ± 3.6
Eileen Dean		GC: Eastern Valley_Eileen Dean	18 ± 3	20 ± 3	2 ± 3	43 ± 3	12 ± 3	0	5 ± 3	0.47 ± 0.03	16.7 ± 0.3
Paso Robles		GC: Pasadena_Paso Robles, Paso Robles2_Paso Light1, Arad_Samra, Tyrone_Berkner Island1, Tyrone_Mount Darwin	10 ± 8	11 ± 8	0	3 ± 3	0	65 ± 18	11 ± 7	0.78 ± 0.15	19.1 ± 3.0
Berry	Nougat	MP: **Berry Flats_Freckles**, **HematiteSlope_Hema2**, **Goal3Field_Vanilla2**, **Mud Pie_Coconut2**, **Black Patch_Munter**, PhotoTIDD_Nougat, **Trench Ripple_Cavair Tweaked**, Purgatory_Track2, **Alicante**	30 ± 7	28 ± 4	0	6 ± 2	15 ± 7	0	21 ± 8	0.40 ± 0.06	24.0 ± 5.1
	Moess Berry	MP: **Berry Bowl_Moess Berry**, **Goal5 Work Volume_Panaluu**, **Whitestreak_Cleo3**, **Seas_Aegean Crest**, **Dog Park_Jack Russell**, **Nullarbor_Great Sandy**, **Photo TIDD_Fred Ripple**, **Berry Stop_Leahs Choice**, **Berry Survey_Cluster3**, **Trench Ripple_Ripple Crest2b**, **Matts Choice_Mobarak**, **Ripple_Norooz**, **Ripple_Mayberooz**, **Recovery Soil_Cure**, **Alamogordo Creek**	15 ± 3	17 ± 3	0	3 ± 3	10 ± 3	0	56 ± 6	0.68 ± 0.06	31.2 ± 2.3

[a]Uncertainties are the larger of standard deviation of the average and the measurement uncertainty, which are ±2% for subspectral areas, ±0.03 for Fe^{3+}/Fe_T, and a maximum of ~0.3 wt % for FeO + Fe_2O_3. GC, Gusev Crater; MP, Meridiani Planum.

[b]Bold typeface, undisturbed surface soil; normal typeface, disturbed surface soil or trench soil.

Table 12. Average Mössbauer Parameters δ and ΔE_Q (200–270 K) and Their Standard Deviations for Ol, Px, and npOx for GC and MP Soils[a]

		Ol (Fe2D1)				Px (Fe2D2)				npOx (Fe3D1)			
		δ		ΔE_Q		δ		ΔE_Q		δ		ΔE_Q	
Class/Subclass Name	N[b]	Average (mm/s)	SD (mm/s)	Average (mm/s)	SD (mm/s)	Average (mm/s)	SD (mm/s)	Average (mm/s)	SD (mm/s)	Average (mm/s)	SD (mm/s)	Average (mm/s)	SD (mm/s)
Panda (GC)	7	1.15	0.02	3.00	0.02	1.14	0.02	2.12	0.02	0.38	0.03	0.89	0.05
Panda (MP)	6	1.15	0.02	2.99	0.02	1.15	0.02	2.13	0.02	0.38	0.02	0.89	0.03
Liberty (GC)	13	1.15	0.02	3.00	0.03	1.15	0.02	2.12	0.04	0.38	0.02	0.86	0.06
Liberty (MP)	4	1.16	0.02	2.98	0.02	1.15	0.02	2.11	0.02	0.37	0.02	0.85	0.05
Gobi (GC)	8	1.15	0.02	2.99	0.03	1.15	0.02	2.12	0.02	0.37	0.02	0.86	0.06
Gobi (MP)	5	1.15	0.02	3.01	0.02	1.15	0.02	2.14	0.02	0.37	0.02	0.88	0.04
Boroughs (GC)	3	1.15	0.02	2.96	0.02	1.15	0.02	2.08	0.02	0.37	0.02	0.86	0.06
Doubloon (GC)	2	1.15	0.02	3.01	0.02	1.16	0.02	2.21	0.02	0.36	0.02	0.86	0.02
Gertrude Weise (GC)	0	[1.16][c]	–	[3.00]	–	[1.15]	–	[2.11]	–	[0.37]	–	[0.86]	–
Eileen Dean (GC)	1	[1.16]	–	[3.00]	–	1.14	0.02	2.12	0.02	[0.37]	–	[0.86]	
Nougat (MP)	5	1.15	0.02	2.98	0.03	1.15	0.02	2.11	0.05	0.38	0.02	0.89	0.03

[a]Values of δ are with respect to metallic iron foil at the same temperature as the sample. GC, Gusev Crater; MP, Meridiani Planum.
[b]N, number of measurements for calculation of average and standard deviation; not the number of soils in a subclass.
[c]MB parameters in brackets are constraints used in the fitting procedure.

al., 2008]. The MB spectrum of El Dorado Scuff Shadow (Figure 21d) is similar to the ubiquitous basaltic soil in Gusev Crater, except that it has a higher proportion of Fe from Ol (A_{Ol} = 47%) and corresponding lower proportions of Fe from Px and especially npOx (A_{npOx} = 8%) (Table 5). The Ol-rich nature of El Dorado Scuff indicates accumulation of olivine as a lag deposit on dune surfaces. This measurement is important because the El Dorado dune field is large enough to be used as ground truth for the orbiting CRISM visible and near-IR hyperspectral spectrometer [*Arvidson et al.*, 2008].

[63] The second soil analysis was the subsurface Paso Robles Class soil Arad Samra (Figure 21e). It was exposed by the action of rover wheels in soft soil, and it has the largest Fe^{3+}-sulfate content measured at Gusev Crater to date ($A_{Fe3Sulfate}$ = 86%). It also has the highest SO_3 content measured on Mars (~35 wt %) [*Ming et al.*, 2008].

5.7. Home Plate

[64] Home Plate was traversed four times by the Spirit rover [*Arvidson et al.*, 2008] for a time span covering 750 sols. As of sol 1544, only rocks have been analyzed (Figure 26), and Spirit is parked on the north facing edge of Home Plate near the rock target Chanute for its third Martian winter [*Arvidson et al.*, 2008].

[65] Fuzzy Smith and Humboldt Peak are float rocks on Home Plate. Fuzzy Smith proved to be unique. Its MB spectrum (Figure 27a) is dominated ($A_{Pyr/Mar}$ = 63%) by a doublet whose parameters ($\delta = 0.28 \pm 0.02$ mm/s and $\Delta E_Q = 0.68 \pm 0.02$ mm/s) are consistent with an assemblage of pyrite and marcasite (FeS_2 polymorphs) [*Squyres et al.*, 2007]. As noted by the authors, there is not sufficient S from APXS analysis to accommodate the stoichiometric FeS_2 composition. However, this situation could result from the different sampling depths of MB and APXS. A surface layer of S-depleted material that was thick with respect to APXS analysis but thin with respect to MB analysis would accommodate the observed APXS results and the FeS_2 interpretation of the MB data. Fuzzy Smith is the first high-SiO_2 rock analyzed by Spirit (~68% [*Squyres et al.*, 2007]). Humboldt Peak is an Ol-rich rock (Figure 27b). On the basis of chemistry Humboldt Peak is an alkaline basalt that is Adirondack Class on the basis of its bulk major element composition [*Ming et al.*, 2008].

[66] Three outcrop rocks (Barnhill Subclass: Barnhill, Posey, James Cool Papa Bell) having very similar Fe mineralogical compositions (A_{Ol} ~18%, A_{Px} ~23%, A_{Mt} ~28%, A_{npOx} ~28%, and minor Hm) were analyzed by MB in the NW corner of Home Plate (Figure 26). On the eastern side of Home Plate, MB spectra were acquired for the outcrop rocks Pesapallo, June Emerson, and Elizabeth Emery (Pesapallo Subclass). They are assemblages of subequal proportions of Fe from Px and Mt. Two outcrop rocks (Texas Chili and Chanute) were analyzed on a line running approximately north to south through the interior of Home Plate. Pecan Pie was analyzed on the western edge of Home Plate. Texas Chili is classified Pesapallo Subclass because of its low Fe from Ol; Pecan Pie and Chanute are Barnhill Subclass because they have more Fe from Ol. Mössbauer spectra for Barnhill, Pesapallo, and Chanute are shown in Figure 28.

[67] Home Plate MB data (Figure 26) show evidence for a systematic variation in the Fe mineralogy of outcrop rocks normal to a line that passes northeast to southwest across the center of the structure [*Schröder et al.*, 2008; *Schmidt et al.*, 2008b]. Rocks furthest to the NW, with the most Fe from Ol and npOx, are Barnhill (Figure 27a), Posey, and James Cool Pappa Bell. With increasing distance from the NW, the rocks become progressively depleted in Fe from Ol and npOx and enriched in Fe from Px. Rocks furthest to the SE are the Ol-poor and Px-rich rocks Pesapallo (Figure 28c), June Emerson, and Elizabeth Emery. Rocks with intermediate Fe mineralogical compositions occur near the centerline (Texas Chili and Chanute (Figure 28b)), and Pecan Pie at the western edge of Home Plate has a composition similar to Barnhill Class.

5.8. Low Ridge and Eastern Valley

[68] Spirit explored Low Ridge (Figure 1), where it spent its second winter (approximately sols 805 to 1035), and Eastern Valley between sols ~800 and ~1250 [*Arvidson et al.*, 2008]. An attempt was made to explore Tyrone, an area

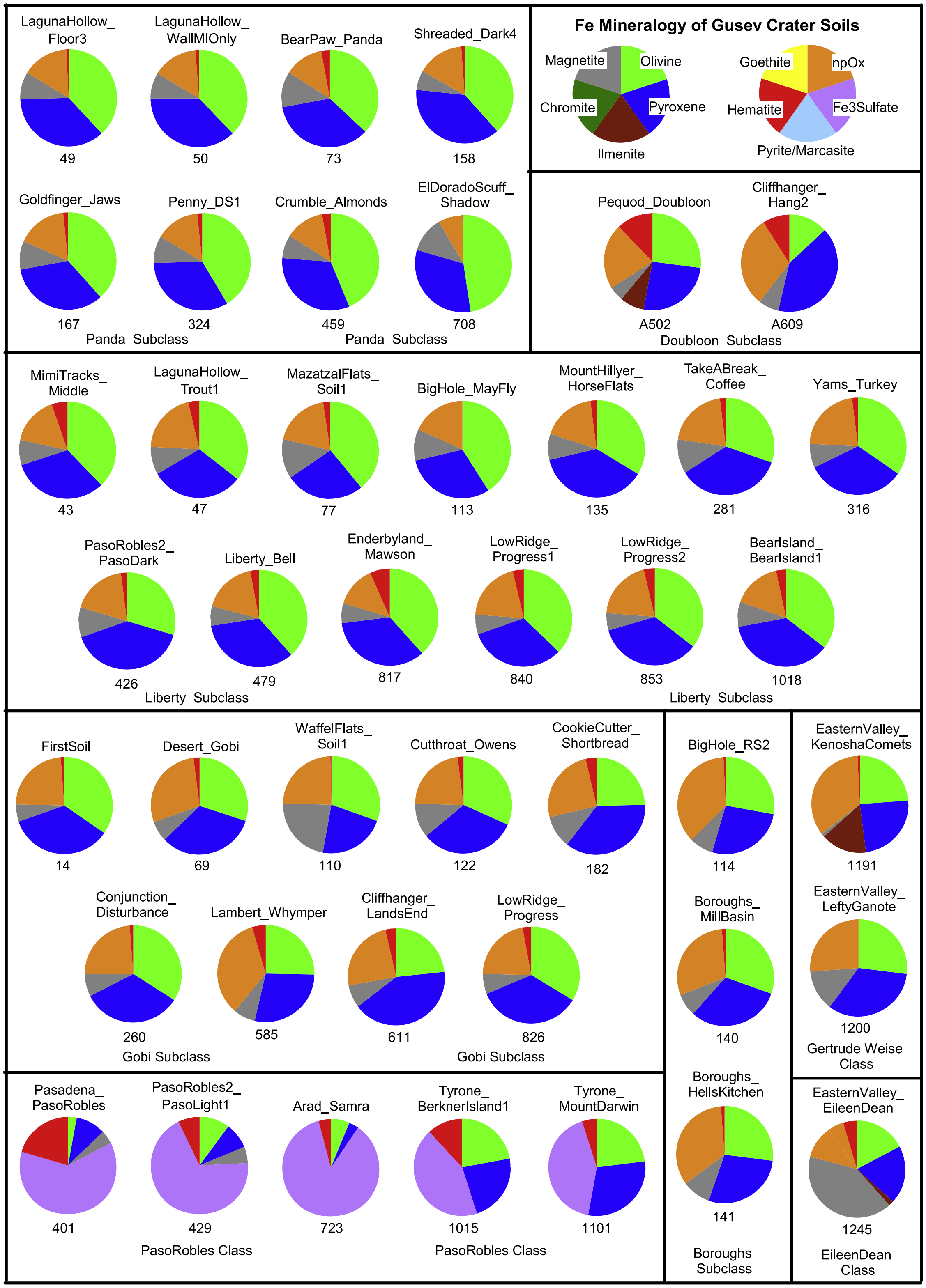

Figure 14. Pie diagrams for the Fe mineralogical composition of soils according to their classification in Table 11. The number under each pie diagram is the sol of the MB analysis.

to the SE toward McCool Hill, but the soil was too soft to traverse [*Arvidson et al.*, 2008].

[69] At Low Ridge and just to the northeast, Spirit acquired MB spectra on outcrop and soil (Figure 29). Surprisingly, the outcrop rocks (Halley, King George, Montalva, and Riquelme) are very Hm rich, with 40 to 78% of their total Fe from Hm. According to *Arvidson et al.* [2008], the rocks are all samples from the same

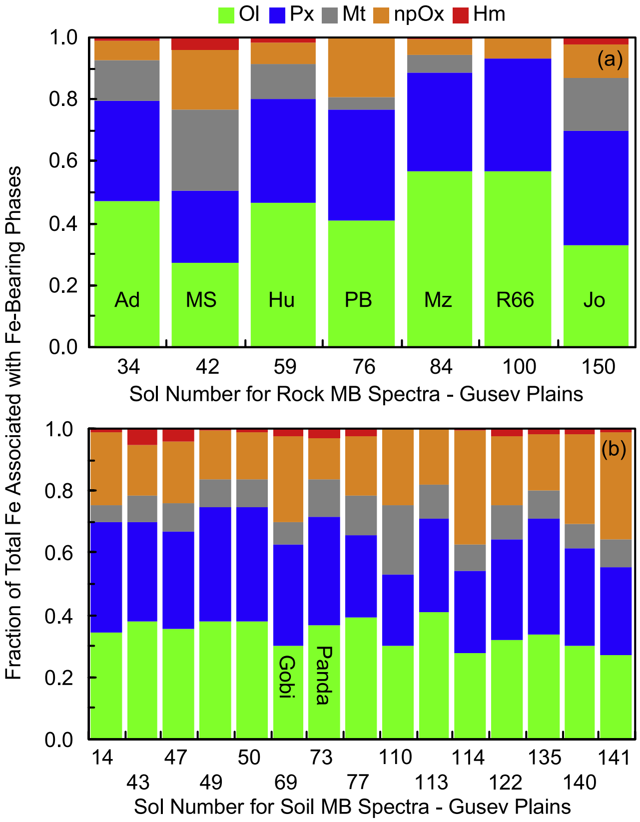

Figure 15. Histograms showing fraction of total Fe associated with Fe-bearing phases for (a) rocks and (b) soils on the Gusev plains (sol 0 to ~155). The category axis is the sol number the MB analysis began. Fe-bearing phase names are Ol, olivine; Px, pyroxene; Mt, magnetite; npOx, nanophase ferric oxide; and Hm, hematite. Rock names are Ad, Adirondack; MS, Mimi Shoe; Hu, Humphrey; PB, Paperback; Mz, Mazatzal; R66, Route 66; and Jo, Joshua.

horizon. Five of the seven soils (Mawson, the three Progress soils, and Bear Island) are typical basaltic soils (Ilm-free Laguna Class) and have an Fe mineralogy of subequal proportions of Fe from Ol (A_{Ol} ~38%) and Px (A_{Px} ~30%) with ~8% from Mt, ~15–20% from npOx, and minor hematite (A_{Hm} < 5%). The other two soils (Berkner Island1 and Mount Darwin) are mixtures of local basaltic soil and the light-toned soils carried from Tyrone in the cowling of the rover wheels. The observed Fe from Fe3Sulfate in Berkner Island1 and Mount Darwin ($A_{Fe3Sulfate}$ ~30%) is thus a lower limit for the Fe from Fe3Sulfate actually present at Tyrone. The vesicular float rock Esperanza, located near Montalva, is an Irvine Class rock with ~45% Fe from each of Px and Mt. Mössbauer spectra for Progress1, four of the Hm-rich outcrop rocks, and Esperanza are shown in Figures 21f, 30, and 18c, respectively.

[70] Eight rocks (all outcrop) and three soils were analyzed in Eastern Valley (Figure 29), which is located between Home Plate and Mitcheltree Ridge (Figure 1). The rocks are distinctly less altered (MAI = 24 to 38%) compared to Low Ridge (MAI = 55 to 84%) outcrop rocks (Table 8). Compare, for example, the large difference in Hm contents (Figure 29a). The rock closest to Mitcheltree Ridge (Torquas) is primarily an assemblage of Fe from Mt and npOx ($A_{Mt} + A_{npOx}$ ~80%). Other analyzed rocks (Elizabeth Mahon, Madeline English, Everett, Slide, Good Question, Nancy Warren, and Innocent Bystander) are located near the upslope edge of Home Plate. Their Fe^{2+} silicate mineralogy is dominated by Px over Ol, except for Nancy Warren which has subequal proportions of Fe from the two phases. Like Irvine Class rocks, Mt plus Px is the dominant Fe-bearing phase ($A_{Px} + A_{Mt}$ = 50 to 80%), although there is more Fe from npOx (A_{npOx} = 20 to 40%) compared to Irvine Class. Elizabeth Mahon and Nancy Warren, like Fuzzy Smith, are enriched in SiO_2 (~72 wt %) and depleted in FeO + Fe_2O_3 (~6 wt %) relative to basaltic compositions [*Ming et al.*, 2008]. Good Question and Innocent Bystander are enriched in SiO_2 to a lesser extent (53 to 62 wt %). Mössbauer spectra for Torquas, Everett, Nancy Warren, and Innocent Bystander are shown in Figure 31.

[71] Lefty Ganote and Kenosha Comets are subsurface, light-toned, SiO_2-rich (74 and 90 wt %, respectively), and Fe-poor (FeO + Fe_2O_3 = 6.5 and 1.5 wt %, respectively)

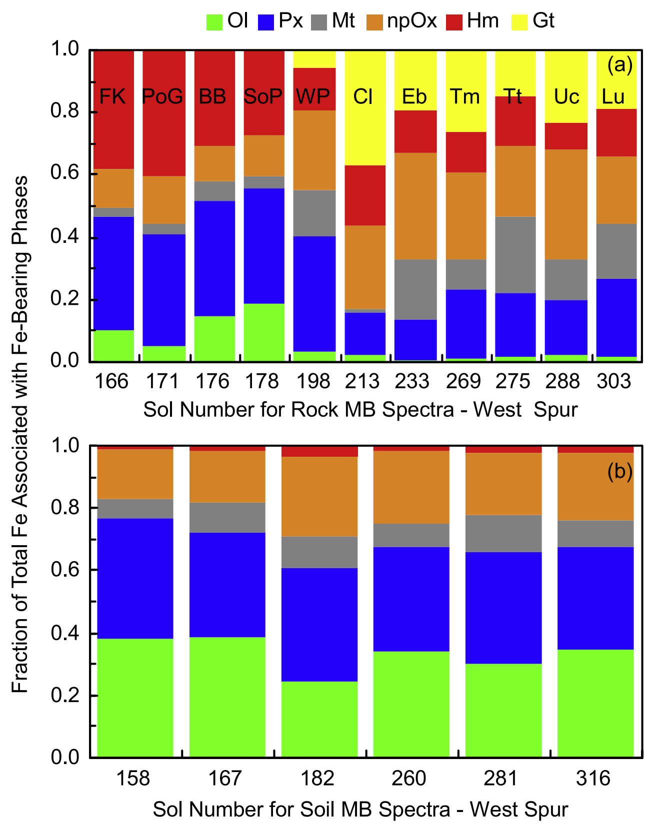

Figure 16. Histograms showing fraction of total Fe associated with Fe-bearing phases for (a) rocks and (b) soils at West Spur (sol ~155 to ~318). The category axis is the sol number the MB analysis began. Fe-bearing phase names are Ol, olivine; Px, pyroxene; Mt, magnetite, npOx, nanophase ferric oxide; Hm, hematite; and Gt, goethite. Rock names are FK, Fort Knox; PoG, Pot Of Gold; BB, Bread Box; SoP, String Of Pearls; WP, Wooly Patch; Cl, Clovis; Eb, Ebenezer; Tm, Temples; Tt, Tetl; Uc, Uchben; and Lu, Lutefisk.

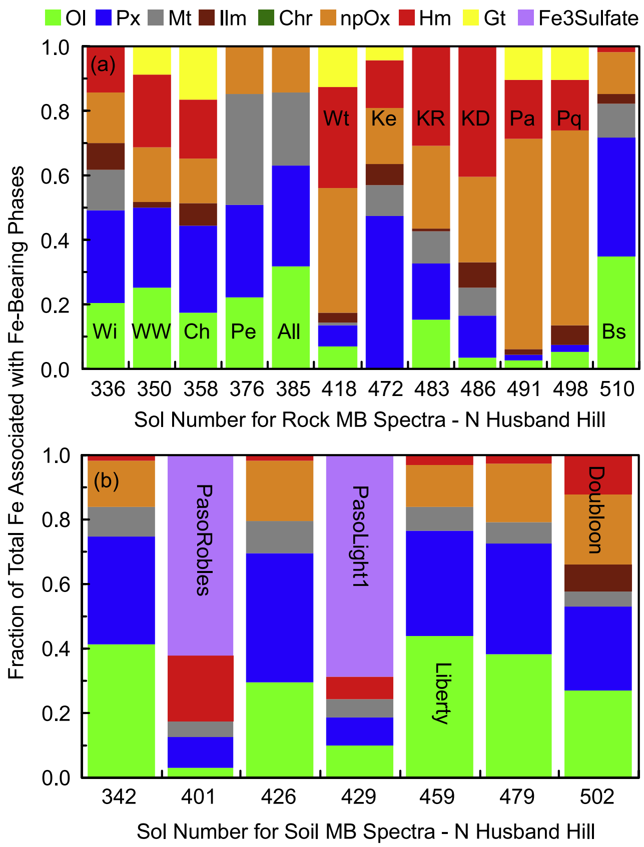

Figure 17. Histograms showing fraction of total Fe associated with Fe-bearing phases for (a) rocks and (b) soils on north Husband Hill (sol ~318 to ~533). The category axis is the sol number the MB analysis began. Fe-bearing phase names are Ol, olivine; Px, pyroxene; Mt, magnetite; Ilm, ilmenite; Chr, chromite; npOx, nanophase ferric oxide; Hm, hematite; Gt, goethite; and Fe3Sulfate, Fe^{3+}-bearing sulfate. Rock names are Wi, Wishstone; WW, Wishing Well; Ch, Champagne; Pe, Peace; All, Alligator; Wt, Watchtower; Ke, Keystone; KR, Keel Reef; KD, Keel Davis; Pa, Paros; Pq, Pequod; and Bs, Backstay.

soils uncovered by Spirit's frozen wheel [*Squyres et al.*, 2008]. Their low total Fe content, low MB source activity at this time in the mission, and limited integration time produced MB spectra with poor counting statistics. Nevertheless, Fe from Ol, Px, Ilm, and npOx was detected in Kenosha Comets, and the same for Lefty Ganote except that Mt was detected instead of Ilm. Eileen Dean (Figure 29b), which is also a light-toned subsurface soil, has a basaltic bulk composition similar to that for the rock Everett [*Ming et al.*, 2008]. This correspondence plus an abnormally high value (for a soil) of Fe from Mt (A_{Mt} ~40%) are evidence that Eileen Dean is the top of a friable rock or perhaps a weakly consolidated ash deposit. Mössbauer spectra for these light-toned soils are shown in Figure 32.

[72] In section 10, we expand the arguments made by *Squyres et al.* [2008] that the clan of high-SiO_2 rocks (Fuzzy Smith, Elizabeth Mahon, Nancy Warren, Good Question, and Innocent Bystander) and soils (Lefty Ganote and Kensoha Comets) in Eastern Valley is the result of aqueous leaching of basaltic precursors under acid sulfate conditions.

6. Fe-Bearing Mineralogical Markers for Aqueous Alteration

6.1. Goethite (α-FeOOH) and Acid Sulfate Alteration

[73] The ferric oxyhydroxide goethite is a common product of alteration and weathering on Earth [e.g., *Cornell and Schwertmann*, 1996]. It is a mineralogical marker for aqueous alteration on Mars because it has hydroxide as a part of its structure and thus can only form in the presence

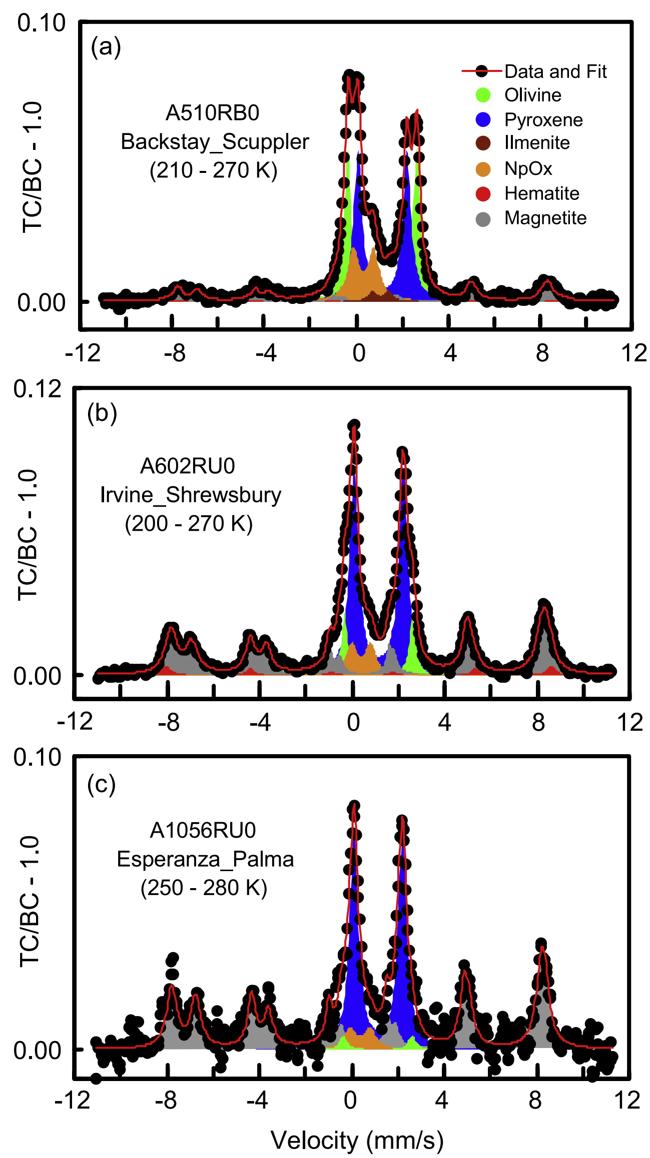

Figure 18. Mössbauer spectra and subspectra obtained by least squares analysis for rocks (a) Backstay on north Husband Hill, (b) Irvine on SW Husband Hill, and (c) Esperanza near Home Plate. Spectra were obtained by summing individual spectra over the specified temperature interval. Zero velocity is referenced with respect to metallic Fe foil at the same temperature as the Martian surface target. Backstay, Irvine, and Esperanza are relatively unaltered rocks.

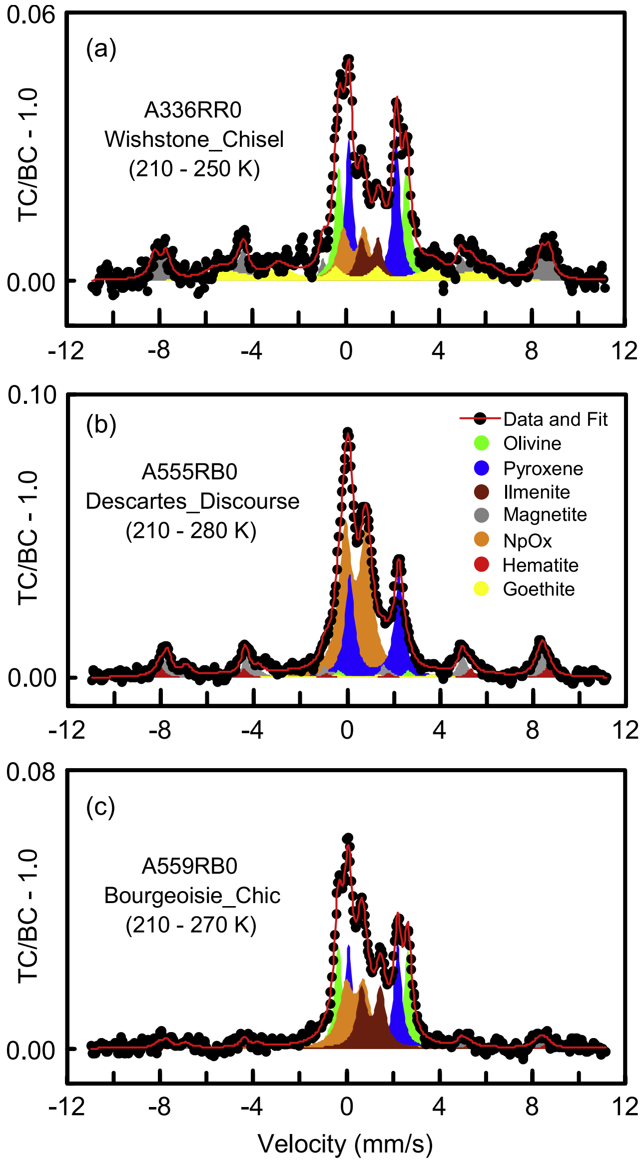

Figure 19. Mössbauer spectra and subspectra obtained by least squares analysis for rocks (a) Wishstone on north Husband Hill, (b) Descartes, and (c) Bourgeoisie Chic on SW Husband Hill. Spectra were obtained by summing individual spectra over the specified temperature interval. Zero velocity is referenced with respect to metallic Fe foil at the same temperature as the Martian surface target. Bourgeoisie Chic is a clast of Wishstone Class rock in Voltaire Outcrop as represented by the rock Descartes.

of H_2O (solid, liquid, or gas). The geographic extent of Gt-bearing rocks (Clovis, Wishstone, and Watchtower Classes) as of *Morris et al.* [2006a] (sol 602) was West Spur and the NW slope of Husband Hill to a point near, but downslope from, its summit. After summiting on sol ~618, Spirit found Gt downslope on the SE side of Husband Hill in the rock Kansas on sol ~648 (Figures 22a and 23c). *McCoy et al.* [2008] map an antiformal stratification for rocks exposed on Husband Hill, and Crumpler et al. (manuscript in preparation, 2008) show that Wishstone and Watchtower represent the topmost stratum exposed. Thus it is not surprising to find Gt-bearing rocks on the NW and SE sides of Husband Hill. The stratigraphic and structural relationships between West Spur and Husband Hill are not clear. An alternate interpretation is that Gt formed at the exposed edges (outcrops) of the strata by alteration of some precursor material that is still present (perhaps just locally) in its unaltered form within Husband Hill and possibly West Spur. As discussed by *Morris et al.* [2007], this precursor might be disseminated pyrrhotite. A pyrrhotite precursor also may provide an explanation for the unusually high values of ΔE_Q for npOx (~1.0 mm/s) in goethite-bearing rocks (see

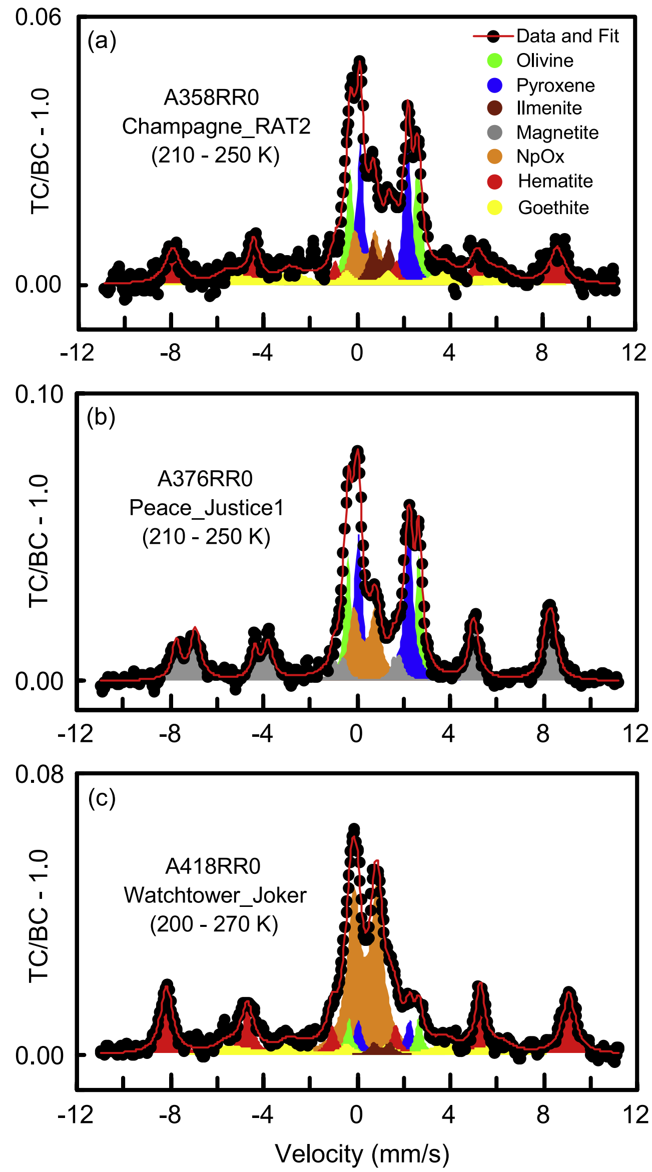

Figure 20. Mössbauer spectra and subspectra obtained by least squares analysis for rocks (a) Champagne, (b) Peace, and (c) Watchtower on north Husband Hill (modeled after *Morris et al.* [2006a]). Spectra were obtained by summing individual spectra over the specified temperature interval. Zero velocity is referenced with respect to metallic Fe foil at the same temperature as the Martian surface target.

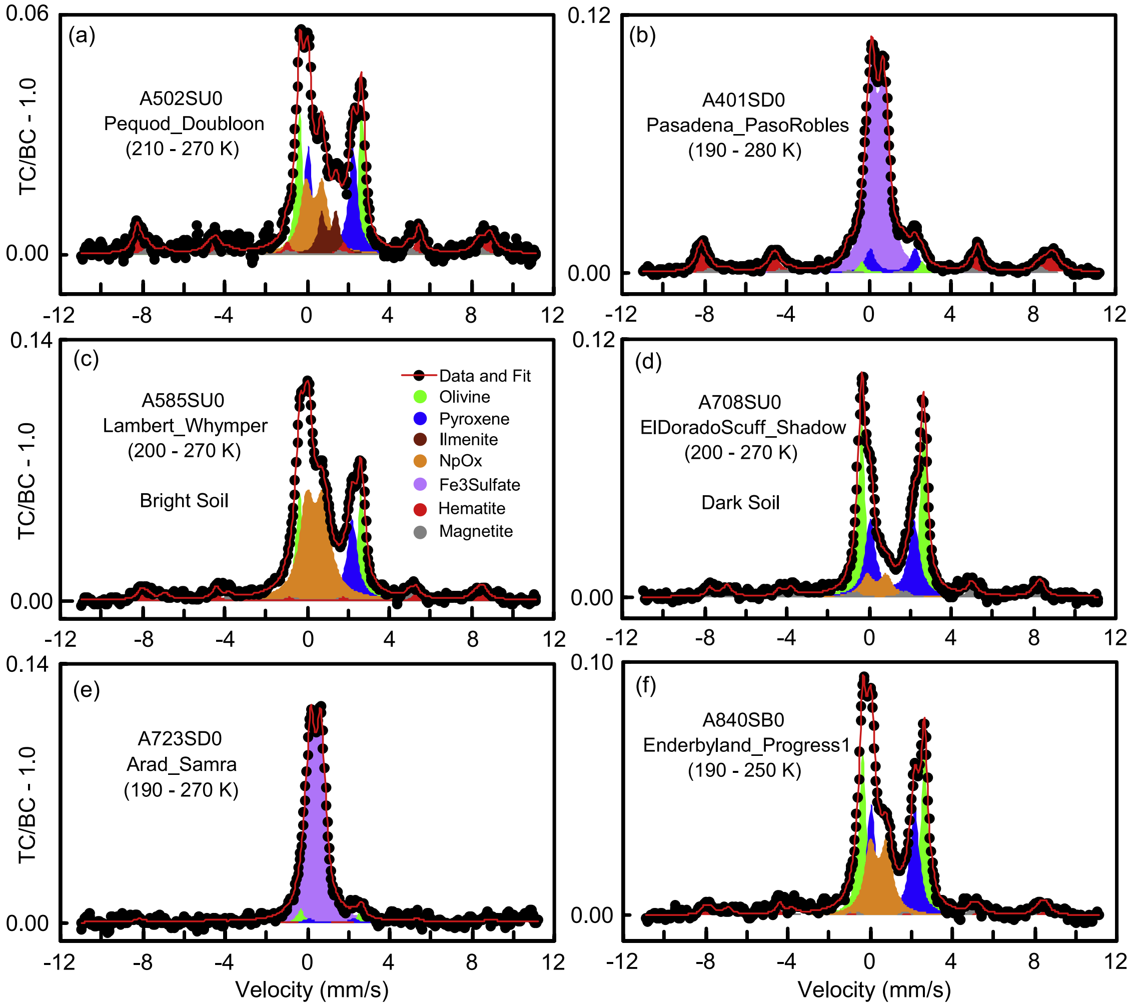

Figure 21. Mössbauer spectra and subspectra obtained by least squares analysis for soils (a) Pequod Doubloon, (b) Pasadena Paso Robles, (c) Lambert Whymper (d) El Dorado Scuff Shadow, (e) Arad Samra, and (f) Enderbyland Progress1. Spectra were obtained by summing individual spectra over the specified temperature interval. Zero velocity is referenced with respect to metallic Fe foil at the same temperature as the Martian surface target. Doubloon and Paso Robles are on north Husband Hill, Whymper is on SE Husband Hill, El Dorado is on a duneform in the northern Basin, Samra is in the northern Inner Basin, and Progress1 is on Low Ridge near Home Plate. Whymper and El Dorado, with high and low proportions of npOx, are examples of bright and dark soils. Doubloon is an example of incorporation of local rock material (Wishstone Class rock with Ilm) into typical basaltic soil like Progress1. Paso Robles and Samra represent two of the three occurrences (the third is Tyrone) of light-toned, subsurface deposits of high-S soil rich in Fe^{3+}-sulfate.

section 3.7.2). In the experiments of *Morris et al.* [2007], pyrrhotite under conditions of low H_2O to rock ratios altered to poorly crystalline goethite and hydronium jarosite (H-jarosite), the latter with $\Delta E_Q \sim 1.0$ mm/s. We continue to assign the Fe3D1 ferric doublet for the Gt-bearing rocks to npOx because the H-jarosite identification is equivocal in these rocks and because variations in the chemical and mineralogical composition of npOx (in response to local conditions) are consistent with its generic usage.

[74] On the basis of chemical composition, *Ming et al.* [2006] infer that Clovis Class rocks have undergone leaching by acidic vapor and/or fluids. If the presence of Gt and npOx as a H-jarosite-like phase are indicative of disseminated pyrrhotite (or some other sulfide) in the unaltered precursor, acid sulfate conditions can occur within the rock with access to neutral liquid and/or vapor H_2O. This removes the requirement for acidic interacting fluids/vapors. Once soluble salts precipitate from internal acid sulfate solutions or surface film, they are susceptible to leaching and passive Al_2O_3 enrichment, producing the corundum normative composition now observed for some rocks (e.g., Wooly Patch, Ebenezer, and Watchtower).

6.2. Fe3Sulfate and Hydrothermal Acid Sulfate Alteration

[75] Fe-bearing sulfate was identified by MB at high concentrations in subsurface soil deposits (Figures 17, 24, and 29) at three locations [*Arvidson et al.*, 2008] in Gusev

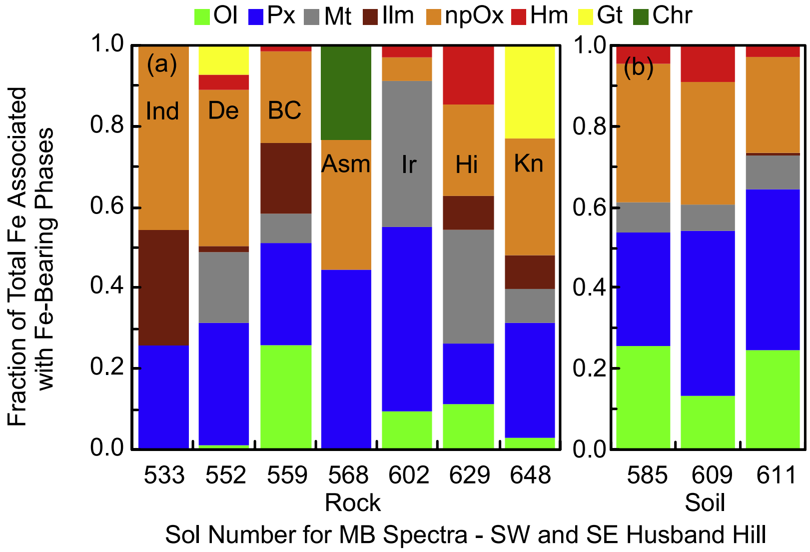

Figure 22. Histograms showing fraction of total Fe associated with Fe-bearing phases for (a) rocks and (b) soils on SW and SE Husband Hill (sol ~533 to ~650). The category axis is the sol number the MB analysis began. Fe-bearing phase names are Ol, olivine; Px, pyroxene; Mt, magnetite; Ilm, ilmenite; npOx, nanophase ferric oxide; Hm, hematite; Gt, goethite; and Fe3Sulfate, Fe^{3+}-bearing sulfate. Rock names are Ind, Independence; De, Descartes; BC, Bourgeoisie Chic; Asm, Assemblee; and Ir, Irvine; Hi, Hillary; and Kn, Kansas.

Crater: Paso Robles (Paso Robles and Paso Light1) on the NW slope of Husband Hill, at Arad (Samra) in the northern Inner Basin between Husband Hill and Home Plate, and at Tyrone (Berkner Island and Mount Darwin) SE of Home Plate. These soils (Paso Robles Class) are described by *Yen et al.* [2008] as likely having formed under oxidizing, acid sulfate conditions as hydrothermal and fumarolic condensates derived from any combination of magma degassing and alteration of crustal Fe sulfide deposits. On the basis of APXS analyses, these soils have H_2O contents ranging from 6 to 19 wt % [*Campbell et al.*, 2008], implying H_2O/OH-bearing Fe^{3+}-sulfate.

7. Isochemical Aqueous Alteration (Low Water-to-Rock Ratios)

7.1. Earth-Based Analogues

[76] Titanium is considered to be a relatively immobile element in the terrestrial weathering environment under a wide range of environmental conditions because it is generally not susceptible to leaching [e.g., *Hutton*, 1977; *Tilley and Eggleton*, 2005]. After dissolution, it immediately precipitates essentially in place as an insoluble phase (e.g., the TiO_2 oxide anatase), resulting in passive enrichment in the residue material as other elements are removed by leaching. This behavior is shown (Figure 33a) in basaltic terrain in a variety of alteration environments on Mauna Kea and Kilauea volcanoes, Hawaii (data from *Morris et al.* [2000a, 2000c]). The chemical data are normalized to a water-free basis so they can be directly compared with APXS data. Palagonitic tephra from Mauna Kea underwent supergene alteration at ambient temperatures. SiO_2 but not TiO_2 was leached (line P in Figure 33a), resulting in passive enrichment of TiO_2 and depletion of SiO_2. Samples from steam vents at Sulfur Bank underwent hypogene alteration at temperatures elevated compared to palagonitic tephra. Again, SiO_2 but not TiO_2 was leached (line S in Figure 33a). In both cases, Fe was also passively enriched [*Morris et al.*, 2000a]. For the bleached rock from Sulfur Bank, which underwent acid sulfate alteration, a different behavior was observed. Both SiO_2 and TiO_2 are passively enriched. In fact, all other elements are leached because line A extrapolates through the origin. Lines P, S, and A radiate from a common point in Figure 33a because the unaltered precursor basalts have the same concentrations of TiO_2 (~2.5 wt %) and SiO_2 (~53 wt %).

7.2. Outcrop Rocks on Husband Hill

[77] The TiO_2 versus SiO_2 diagram for Gusev Crater rocks is shown in Figure 33b. Rocks with MAI < 50% and MAI > 50% are represented by squares and circles, respectively. Solid vertical lines are drawn at 45 and 50 wt % SiO_2. We defer discussion of the rocks with >50 wt % SiO_2, which all occur at Home Plate and Eastern Valley, to section 8. The remaining rocks, independent of MAI value, generally have ~45 wt % SiO_2 and variable TiO_2 concentrations between 0.2 and 3.0 wt %. This is the signature of either (1) unaltered basalts that have a limited range in SiO_2 concentrations and a relative wide range in TiO_2 concentrations or (2) their isochemically altered equivalents. The relative low SiO_2 concentrations for rocks Larrys Bench, Algonquin, and Comanche Spur (~41 wt % [*Ming et al.*, 2008]) reflects their Ol-rich nature (Figure 24) and not an alteration process. The rock Peace has the lowest SiO_2 concentration because it is cemented by Mg-sulfate salts that result in reduced SiO_2 and TiO_2 concentrations by dilution [*Ming et al.*, 2006]. We find no clear evidence for leaching of Martian rocks that resulted in TiO_2 passive

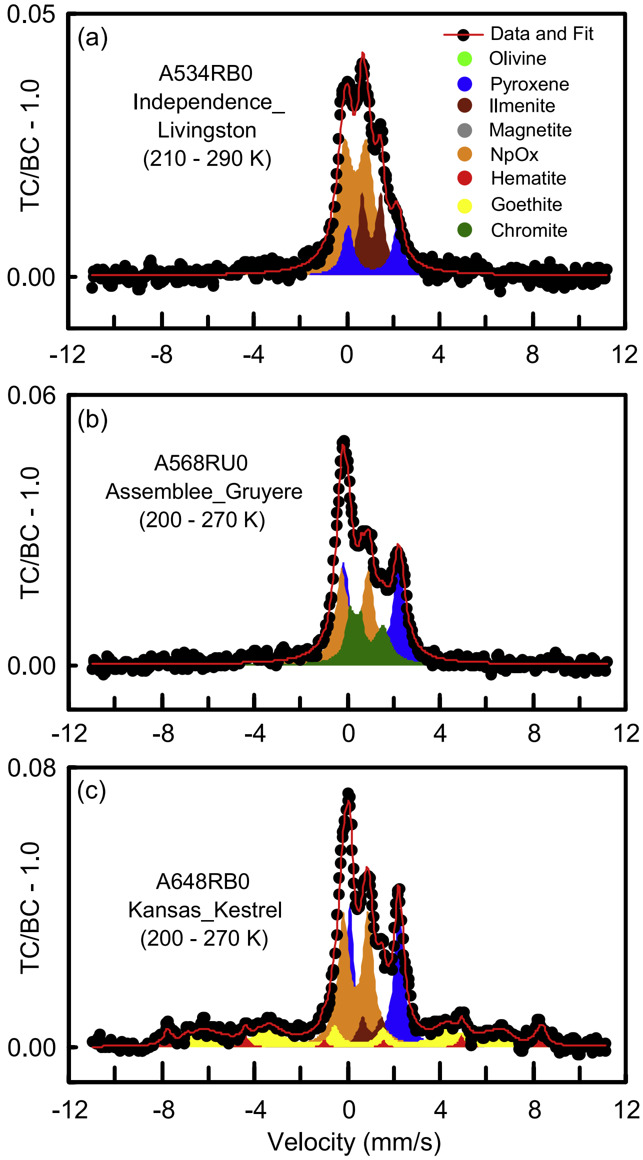

Figure 23. Mössbauer spectra and subspectra obtained by least squares analysis for rocks (a) Independence, (b) Assemblee on the SW Husband Hill (modeled after *Clark et al.* [2007]), and (c) Kansas on the SE Husband Hill. Spectra were obtained by summing individual spectra over the specified temperature interval. Zero velocity is referenced with respect to metallic Fe foil at the same temperature as the Martian surface target. Independence and Assemblee are strongly altered, having ~4 to 7 wt % Fe as FeO + Fe_2O_3. The only detection of chromite is for Assemblee. The rock Kansas shows that Gt is present in outcrop rocks on both sides of the summit of Husband Hill.

enrichment similar to that shown in Figure 33a for terrestrial analog samples with the exception for the Independence Outcrop rock. The absence or near absence of leaching implies low water-to-rock ratios.

[78] Perhaps the best instance of aqueous, isochemical alteration is the Watchtower Class rocks on Husband Hill [*Morris et al.*, 2006a; *Ming et al.*, 2006]. They have a nearly constant chemical composition and a Fe mineralogical composition that ranges from ~63% Fe from Ol, Px, Ilm, and Mt for Keystone to ~13% Fe from those phases for Pequod (Table 8 and Figure 12).

7.3. Palagonitic Tephra at Home Plate

[79] A number of outcrop rocks on Home Plate (Barnhill Subclass) and Mitcheltree Ridge (Torquas) have a Fe mineralogy of Ol, Px, Mt, and npOx where Fe from npOx is ~29% (Table 8). This amount of npOx is significantly higher than that observed for rocks with the same assemblage of Fe-bearing phases (i.e., relatively unaltered with minimal Hm, no detectable Gt, and FeO + Fe_2O_3 > 13 wt %). Such rocks are Adirondack Subclass, Joshua Subclass, Backstay Class, Irvine Class, Everett Class, and Pesapallo Subclass, and they have average values of Fe from npOx equal to 9, 15, 13, 5, 18, and 14%, respectively (Table 9). This mineralogical observation and the textural observations of *Squyres et al.* [2007] that Barnhill Subclass is a pyroclastic deposit are consistent with deposition of glassy tephra in association with Home Plate volcanism and subsequent supergene aqueous alteration of the glassy tephra to palagonitic tephra, where (by analogy with terrestrial palagonitic tephra [*Morris et al.*, 2000a, 2001]) npOx and additional short-order and Fe-poor phases (e.g., allophane) are present.

[80] As shown in Figure 33a, the terrestrial palagonitic tephra underwent supergene alteration under conditions of high water-to-rock ratios because significant leaching (e.g., of SiO_2) took place. At Home Plate, in the absence of detectable leaching (Figure 33b), palagonitization progressed at low water-to-rock ratios.

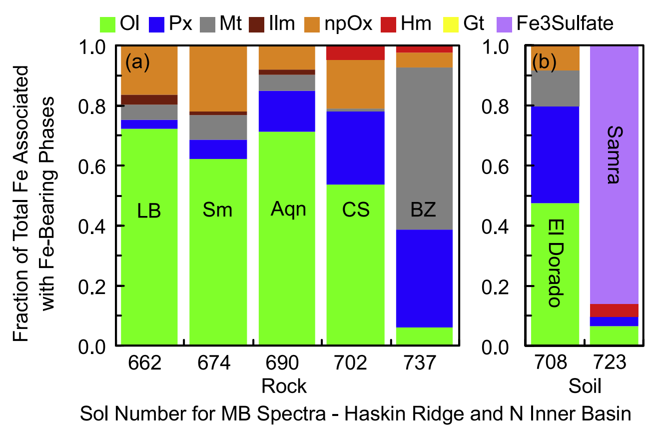

Figure 24. Histograms showing fraction of total Fe associated with Fe-bearing phases for (a) rocks and (b) soils on Haskin Ridge and the northern Inner Basin (sol ~650 to ~740). The category axis is the sol number the MB analysis began. Fe-bearing phase names are Ol, olivine; Px, pyroxene; Mt, magnetite; Ilm, ilmenite; npOx, nanophase ferric oxide; Hm, hematite; Gt, goethite; and Fe3Sulfate, Fe^{3+}-bearing sulfate. Rock names are LB, Larrys Bench; Sm, Seminole; Aqn, Algonquin; CS, Comanche Spur; and BZ, Bu Zhou.

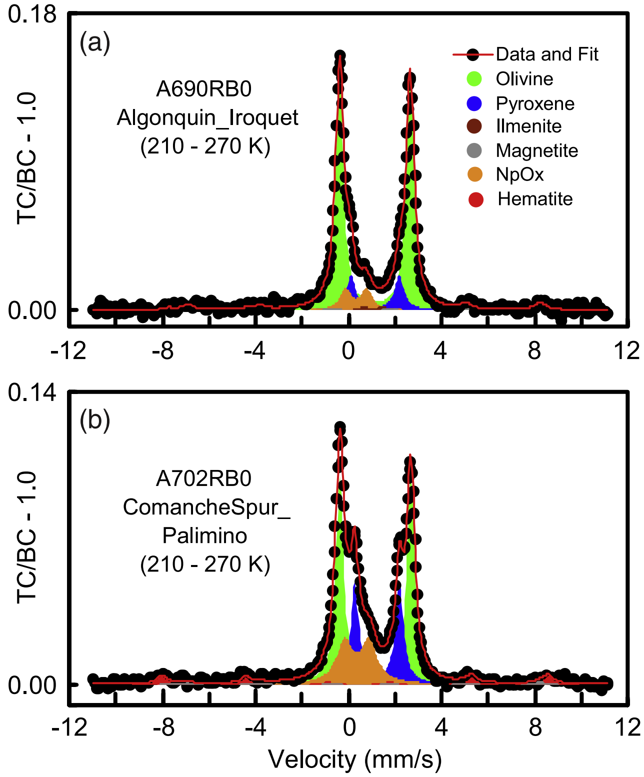

Figure 25. Mössbauer spectra and subspectra obtained by least squares analysis for rocks (a) Algonquin and (b) Comanche Spur on Haskin Ridge. Spectra were obtained by summing individual spectra over the specified temperature interval. Zero velocity is referenced with respect to metallic Fe foil at the same temperature as the Martian surface target. The Ol-rich rocks Algonquin and Comanche Spur may be part of an ultramafic sequence. The Mössbauer parameters for the Px subspectrum of Comanche Spur are unique to that rock.

7.4. Gusev Crater Soils

[81] The TiO_2 versus SiO_2 diagram for Gusev Crater soils is shown in Figure 33c. The soils with >49 wt % SiO_2 are discussed in section 8. With the exception of the Paso Robles Class soil, the soils have a relatively constant SiO_2 concentration (~45 wt %) and a variable TiO_2 concentration (~0.5 to ~2.0 wt %), which indicates variation in the composition of the source material and not aqueous alteration accompanied by leaching. Soils with the highest and lowest TiO_2 concentrations are Pequod Doubloon and El Dorado Scuff Shadow, respectively.

[82] Reaction of preexisting soil with acid sulfate waters in a closed system (i.e., local precipitation of reaction products, including sulfates) would produce a bulk composition that is enriched in SO_3 and depleted in all other elements because of the closure property. Thus, the concentration of all elements in the reacted soil would be between 0 wt % and their concentration in the preexisting soil.

[83] Line B in Figure 33c was drawn through the origin and the average TiO_2 and SiO_2 concentrations for the sulfate-rich soils at the Paso Robles location. Line C was drawn through the origin and the average TiO_2 and SiO_2 concentrations for the Arad and Tyrone sulfate-rich soils. Line B and line C intersect the vertical line at 45 wt % SiO_2 at TiO_2 concentrations of ~1.5 and ~0.6 wt %, respectively, for the presumed precursor materials. The extrapolated TiO_2 concentrations are reasonable considering the locale of the high-sulfate deposits. The Paso Robles deposit is proximate to the high-Ti Wishstone Class and Watchtower Class rocks and the high-Ti soils (Doubloon). The Arad and Tyrone deposits are proximate to the low-Ti outcrop rocks in the vicinity of Home Plate. As discussed previously [*Ming et al.*, 2006; *Yen et al.*, 2008], the imprint of local chemical compositions on the bulk composition of the high-sulfate deposits means that the acid sulfate dissolution and precipitation occurred locally, perhaps in a hydrothermal, solfatara-like environment, without significant leaching (i.e., at low water-to-rock ratios).

[84] Hydrothermal conditions at low water-to-rock ratios are implied at Paso Robles and the other high-sulfate deposits because they promote closed-system dissolution of local precursor material that is followed by precipitation of Fe^{3+}-sulfate (detected by Mössbauer) and other phases as evaporite deposits. In contrast, neither hydrothermal conditions nor low water-to-rock ratios are indicated at Peace Outcrop (rocks Peace and Alligator), because the Fe mineralogy of the Mg-sulfate cemented rock does not have detectable Fe3Sulfate or any other Fe-sulfate and is instead characterized by an igneous-like assemblage of Ol, Px, Mt, and npOx (Figure 17) [*Morris et al.*, 2006a; *Ming et al.*, 2006].

8. Acid Sulfate Alteration at High Water-to-Rock Ratios in Eastern Valley

[85] We now focus on the high-SiO_2 rocks and soils in Eastern Valley and the high-SiO_2 float rock (Fuzzy Smith)

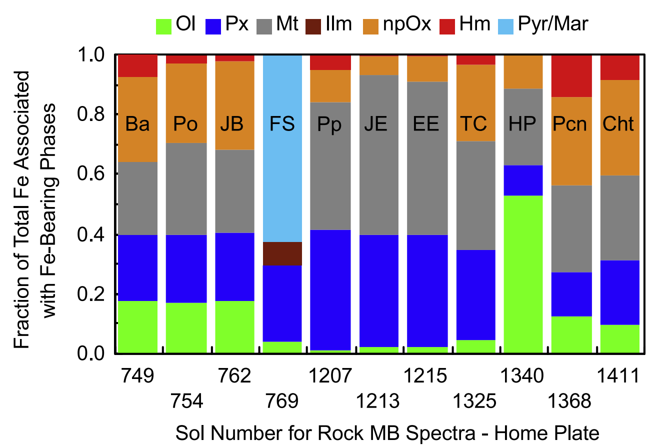

Figure 26. Histograms showing fraction of total Fe associated with Fe-bearing phases for rocks on Home Plate (four times between sol ~725 to ~1544). The category axis is the sol number the MB analysis began. Fe-bearing phase names are Ol, olivine; Px, pyroxene; Mt, magnetite; Ilm, ilmenite; npOx, nanophase ferric oxide; Hm, hematite; and Pyr/Mar, pyrite/marcasite. Rock names are Ba, Barnhill; Po, Posey; JB, James CP Bell; FS, Fuzzy Smith; Pp, Pesapallo; JE, June Emerson; EE, Elizabeth Emery; TC, Texas Chili; HP, Humboldt Peak; Pcn, Pecan Pie; and Cht, Chanute. The outcrop rocks on the NW side of Home Plate (Ba, Po, and JB) are Ol-rich compared to the outcrop rocks on the SE side of Home Plate (Pp, JE, and EE).

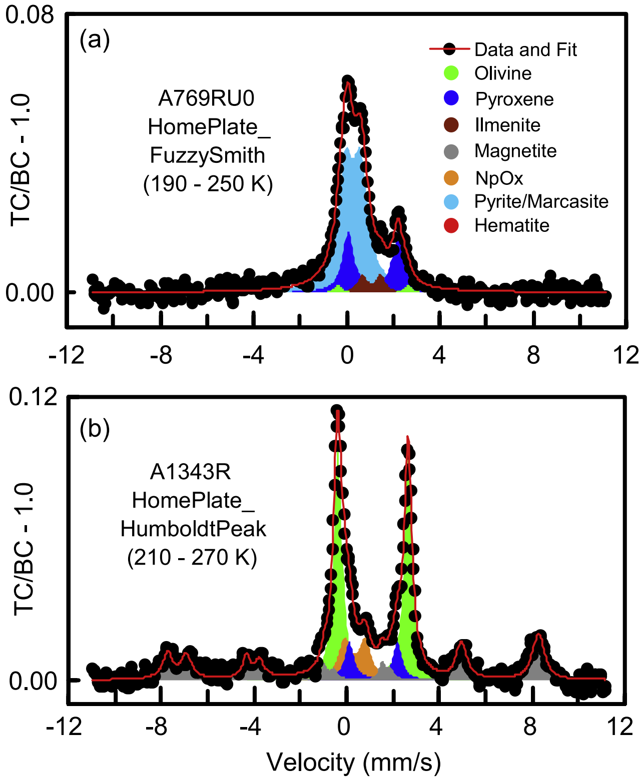

Figure 27. Mössbauer spectra and subspectra obtained by least squares analysis for float rocks (a) Fuzzy Smith and (b) Humboldt Peak on Home Plate. Spectra were obtained by summing individual spectra over the specified temperature interval. Zero velocity is referenced with respect to metallic Fe foil at the same temperature as the Martian surface target. Fuzzy Smith is the only rock that has a subspectrum that can be assigned to pyrite/marcasite (sulfide), and it is also a high-SiO_2 rock.

on Home Plate (Figure 34). Local Home Plate and Eastern Valley rocks and soils that do not have an apparent SiO_2 enrichment plot near the solid vertical line near SiO_2 = 45 wt %. Comparison to Figure 33a points to acid sulfate leaching of precursor basalt as a formation pathway for the Gusev high-SiO_2 materials. That is, all elements detected by APXS are removed by leaching except for SiO_2 and TiO_2 whose concentrations passively increase because they precipitate as insoluble phases, for example opal-A and anatase, respectively, on the basis of a terrestrial analog [*Morris et al.*, 2000c].

[86] By analogy with Figure 33a, we drew the two solid lines in Figure 34a that pass through the origin and the samples that give the maximum (Pesapallo) and minimum (Nancy Warren) TiO_2/SiO_2 ratios. At first look, it appears that the ensemble of high-SiO_2 materials can be explained by different extents of acid sulfate leaching of basaltic rock compositions found at Home Plate and Eastern Valley, as discussed by *Squyres et al.* [2008]. In Kenosha Comets, the leaching process has essentially proceeded to completion. However, we must look at other element correlations to confirm the observation (Figures 34b and 34c).

[87] Close examination of Figure 34 reveals an inconsistency with the proposition that all high-SiO_2 rocks and soils can be derived from known rock compositions at Home Plate. Elizabeth Mahon and Nancy Warren have chemical affinity for Slide and Everett on the basis of the TiO_2 $-SiO_2$ correlation (line A2 in Figure 34a). However, on the basis of $FeO + Fe_2O_3$ and especially MgO correlations with SiO_2,

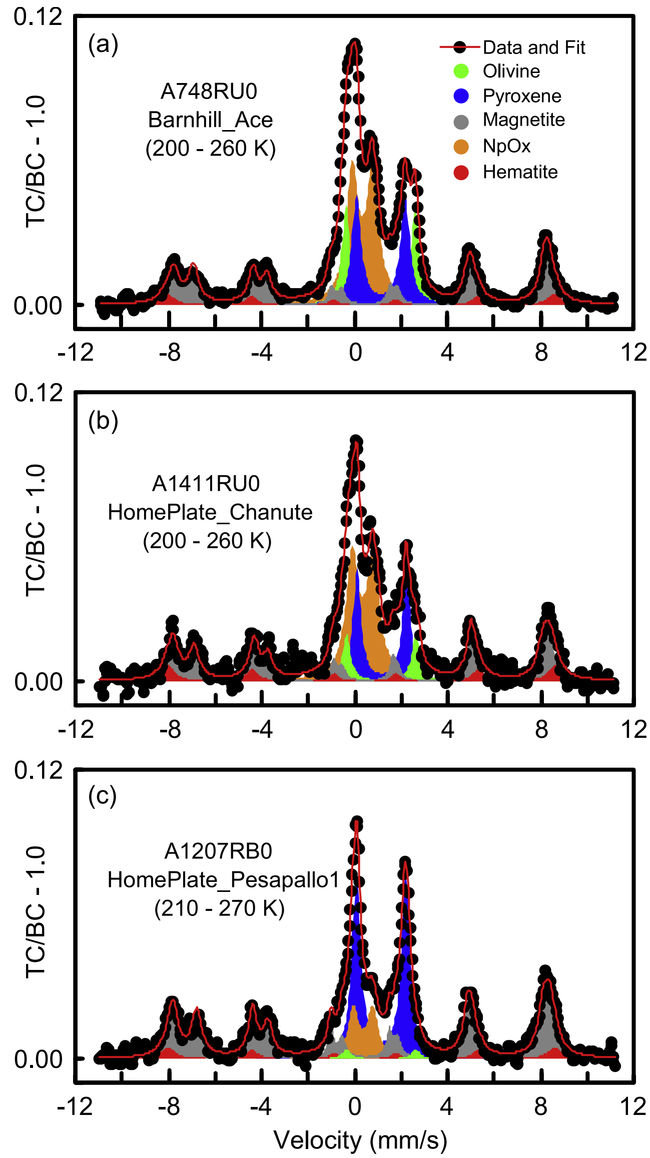

Figure 28. Mössbauer spectra and subspectra obtained by least squares analysis for outcrop rocks (a) Barnhill, (b) Chanute, and (c) Pesapallo on Home Plate. Spectra were obtained by summing individual spectra over the specified temperature interval. Zero velocity is referenced with respect to metallic Fe foil at the same temperature as the Martian surface target. All three outcrop rocks are Mt-rich. The rocks on the NW side of Home Plate (e.g., Barnhill) have higher proportions of Fe from Ol and npOx than the rocks on the SE (e.g., Pesapallo) side of Home Plate that are rich in Fe from Px. Rocks at intermediate locations (e.g., Chanute) have intermediate Fe mineralogical compositions.

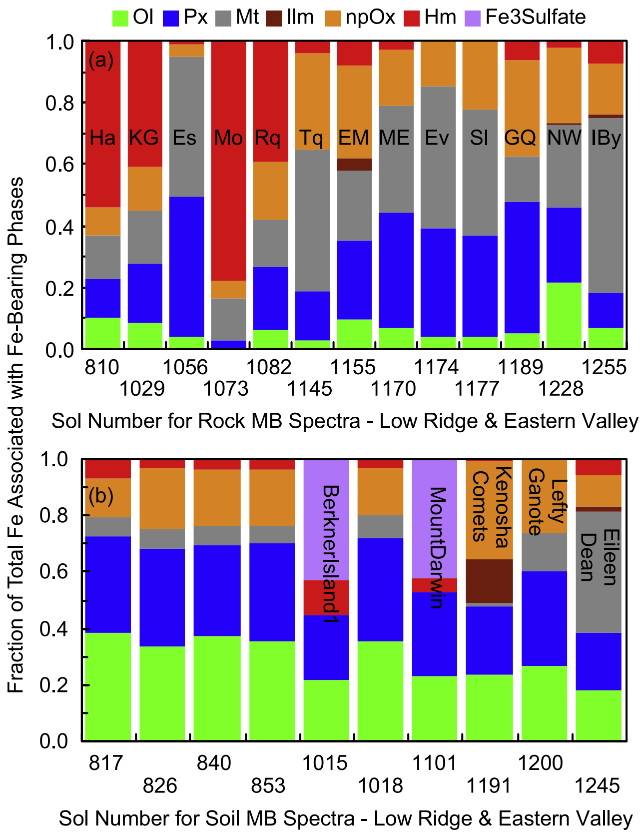

Figure 29. Histograms showing fraction of total Fe associated with Fe-bearing phases for (a) rocks and (b) soils at Low Ridge and in Eastern Valley (sol ~800 to ~1260). The category axis is the sol number the MB analysis began. Fe-bearing phase names are Ol, olivine; Px, pyroxene; Mt, magnetite; Ilm, ilmenite; npOx, nanophase ferric oxide; Hm, hematite; and Fe3Sulfate, Fe^{3+}-bearing sulfate. Rock names are Ha, Halley; KG, King George; Es, Esperanza; Mo, Montalva; Rq, Riquelme; Tq, Torquas; EM, Elizabeth Mahon; ME, Madeline English; Ev,Everett; Sl, Slide; GQ, Good Question; NW, Nancy Warren; and IBy, Innocent Bystander. Montalva is the most Hm-rich target (A_{Hm} = 78%) analyzed by the MER rovers. The Fe^{3+}-sulfate component in the soils Berkner Island1 and Mount Darwin was carried to the analysis site from Tyrone in the wheel cowling of the Spirit rover. High-SiO_2 materials are the rocks Elizabeth Mahon and Nancy Warren and the soils Kenosha Comets and Lefty Ganote.

they have chemical affinity for the rocks (e.g., Pesapallo) that have soil-like values of FeO + Fe_2O_3 and MgO (lines B2 and C2 in Figures 34b and 34c, respectively). The inconsistency is resolved if the basaltic precursor is igneous rock/tephra with MgO and TiO_2 concentrations equal to ~9 and ~0.4 wt %, respectively (Figure 34). Such compositions have not been observed or measured by Spirit, but they may be present in subsurface rocks/tephra or in unanalyzed surface materials.

[88] The water-to-rock ratio during the alteration that resulted in the high-SiO_2 materials must be high enough to support leaching (removal) of the soluble constituents of the rock and soils. We do not estimate a value for the ratio

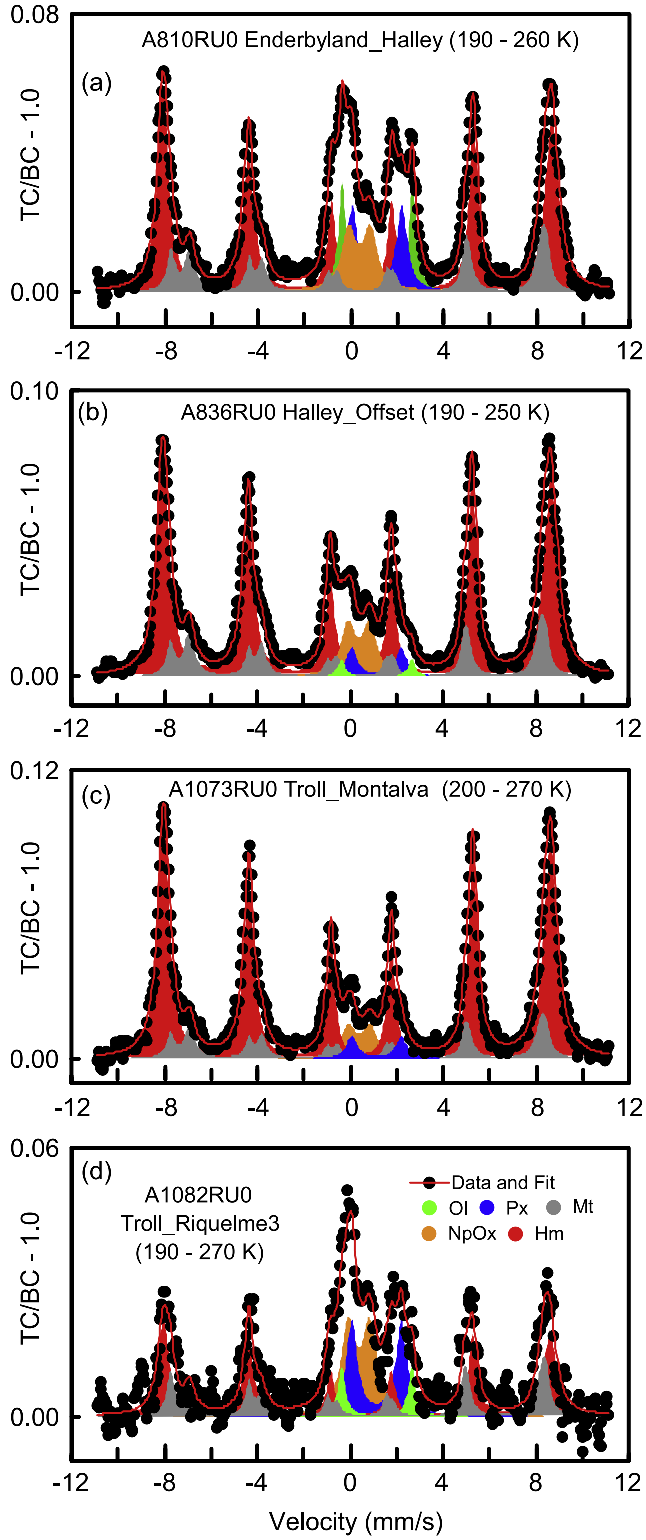

Figure 30. Mössbauer spectra and subspectra obtained by least squares analysis for rocks (a and b) Halley, (c) Montalva, and (d) Riquelme on and near Low Ridge SE of Home Plate. Spectra were obtained by summing individual spectra over the specified temperature interval. Zero velocity is referenced with respect to metallic Fe foil at the same temperature as the Martian surface target. All these rocks are rich in hematite and are located between Home Plate and the sulfate deposit at Tyrone.

except in a relative sense. The leaching that occurred during formation of the Eastern Valley high-SiO_2 rocks and soils must have occurred at water-to-rock ratios that are higher than the ratios implied by the isochemical or nearly isochemical alteration observed on Husband Hill for the Clovis Class, Wishstone Class, and Watchtower Class rocks. Furthermore, the geologic setting of Home Plate (a volcanic complex) and chemical data for terrestrial analogs imply acid sulfate alteration under hydrothermal conditions [*Morris et al.*, 2000a, 2000c; *Squyres et al.*, 2007, 2008; *Yen et al.*, 2008]. Such conditions could exist for long periods of time at high water-to-rock ratios within the reaction front where aggressive (acid sulfate) volcanic condensates dissolve basaltic rock and remove all but the insolubile components (SiO_2 and TiO_2) by leaching.

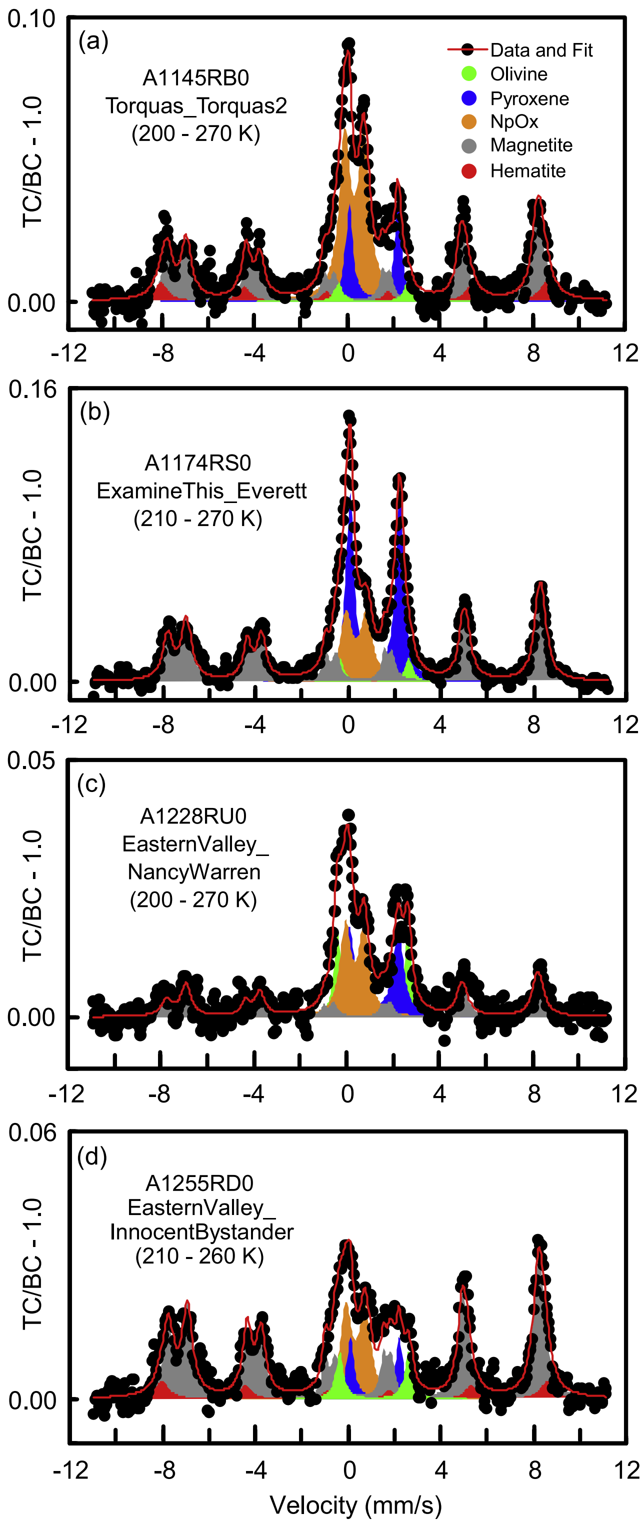

[89] *Squyres et al.* [2008] also consider a sinter origin for which dissolved Si (and Ti) is transported to Eastern Valley by aqueous solutions and subsequently precipitated as the SiO_2-rich material (e.g., a hot springs environment). The authors do not favor this pathway (and we concur) because of the evidence for acid sulfate leaching under hydrothermal conditions and because the diversity in the chemical composition of the high-SiO_2 materials is consistent with the diversity in the chemical composition of the rocks at Home Plate and Eastern Valley. In addition, we are not aware of terrestrial sinter deposits that have TiO_2 concentrations comparable to those observed for the Gusev high-SiO_2 deposits, although the discrepancy might result from different precursor bulk chemical compositions and/or different environmental parameters [e.g., *McAdam et al.*, 2008].

9. Aqueous Processes and Magnetite and Pyroxene

[90] Magnetite is firmly established as the strongly magnetic mineral in the region of Gusev Crater traversed by Spirit on the basis of Mössbauer measurements of rock, soil, and material collected by the capture magnet, as shown in this and previously published papers [e.g., *Morris et al.*, 2004, 2006a; *Goetz et al.*, 2005, 2008]. Throughout this paper we considered magnetite to originate from igneous processes (i.e., crystallization from a silicate liquid) as opposed to a product of oxidative weathering of primary Fe^{2+}-bearing silicate minerals (e.g., olivine and pyroxene). We show next that the magnetite detected by Spirit is most likely igneous in origin.

[91] Titanomagnetite in Martian meteorites has an igneous origin [e.g., *Stolper and McSween*, 1979; *Treiman*, 2005]. On the basis of electron microprobe data, three representative compositions for the titanomagnetite in the Martian meteorites are approximately $Fe_{2.27}Ti_{0.50}Al_{0.15}Mn_{0.02}O_4$ (MIL 03346), $Fe_{2.24}Ti_{0.41}Al_{0.30}Mg_{0.03}Mn_{0.01}O_4$ (Nakhla), and $Fe_{2.64}Ti_{0.31}Al_{0.03}Mn_{0.01}O_4$ (NWA817). One connection between these data and MER is through Mössbauer

Figure 31. Mössbauer spectra and subspectra obtained by least squares analysis for the rocks (a) Torquas, (b) Everett, (c) Nancy Warren, and (d) Innocent Bystander in Eastern Valley between Home Plate and Mitcheltree Ridge. Spectra were obtained by summing individual spectra over the specified temperature interval. Zero velocity is referenced with respect to metallic Fe foil at the same temperature as the Martian surface target. All but Innocent Bystander are outcrop rocks. The MB spectrum of Torquas, with its high percentage of npOx, resembles terrestrial palagonitic tephra. Nancy Warren is a high-SiO_2 rock. Innocent Bystander has an unusually high ratio of Fe from Fe-oxide to Fe from Fe-silicate; the analysis spot was an internal surface that was exposed when the rock was broken by Spirit's wheel.

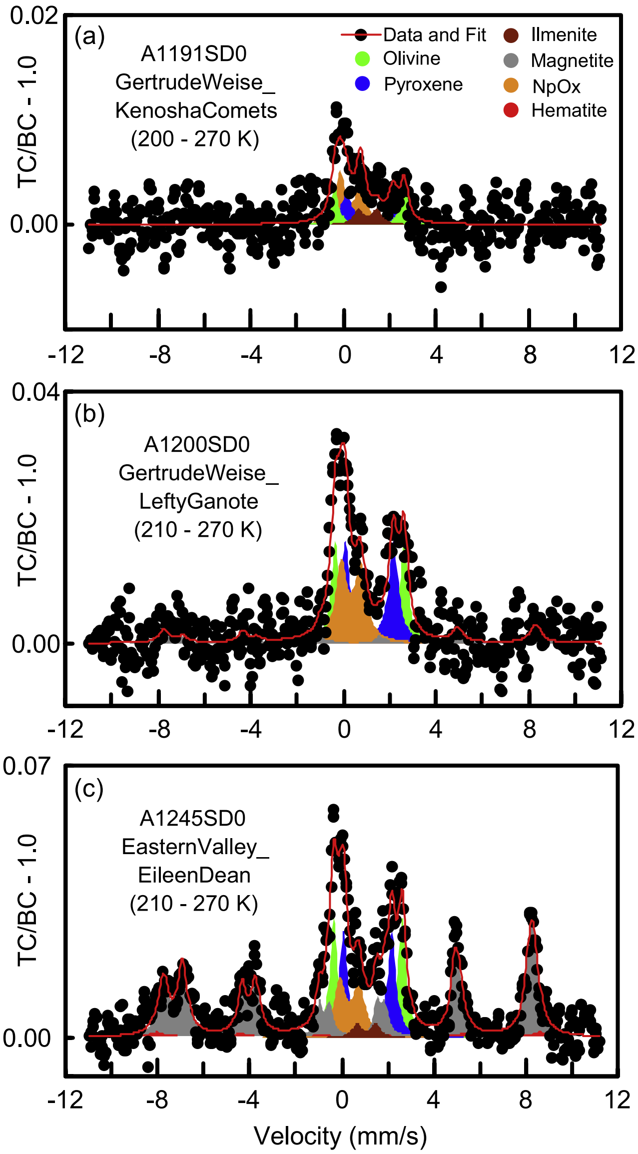

Figure 32. Mössbauer spectra and subspectra obtained by least squares analysis for the soils (a) Kenosha Comets, (b) Lefty Ganote, and (c) Eileen Dean in Eastern Valley. Spectra were obtained by summing individual spectra over the specified temperature interval. Zero velocity is referenced with respect to metallic Fe foil at the same temperature as the Martian surface target. Kenosha Comets and Lefty Ganote are high-SiO_2 soils. The extremely poor counting statistics for Kenosha Comets result from its very low Fe content (~1.5 wt % as FeO + Fe_2O_3) and available integration time. Eileen Dean may be the top of a friable rock that was crushed to a soil by the action of Spirit's wheel.

spectra. Mössbauer subspectra for titanomagnetite in MIL 03346 [*Morris et al.*, 2006c, 2008] (and also that for a titanomagnetite separate from Nakhla [*Vieira et al.*, 1986]) are equivalent to the MER Mössbauer subspectra for magnetite. All subspectra show the characteristic double sextet of magnetite. However, stoichiometric magnetite (i.e., no Ti substitution) is also characterized by a double sextet with similar Mössbauer parameters [e.g., *Morris et al.*, 1985]. The Martian meteorite and MER Mössbauer spectra are thus permissive of igneous magnetite at Gusev Crater (i.e., Ti-bearing magnetite), but they are not unequivocal evidence without supporting chemical data.

[92] Supporting chemical data were provided on sol 1352 by APXS measurements of material adhering to the Capture Magnet. According to *Ming et al.* [2008], the chemical composition of the magnetite is $Fe_{2.24}Ti_{0.56}Al_{0.07}Cr_{0.13}O_4$ after making corrections for the Al metal magnet substrate and unmixing the local soil component. This chemical composition is essentially identical to that for the igneous magnetite in the Martian meteorites discussed in the previous paragraph. We therefore conclude, in the absence of clear evidence to the contrary, that the magnetite detected by Spirit's Mössbauer spectrometer is predominantly igneous in origin.

[93] Another, indirect, way to look for evidence of nonigneous magnetite is to look for Fe-bearing phases that are produced in association with nonigneous magnetite. As a representative example, serpentization is the reaction of water with olivine (Mg, Fe)SiO_4 to form serpentine (Mg, Fe)$_3Si_2O_5(OH)_4$, brucite (Mg, Fe)OOH, and magnetite and to evolve H_2 gas. Is there evidence for serpentine or its Martian equivalent?

[94] We looked for Fe-bearing serpentine and for other alternatives to igneous pyroxene by examining the values of ΔE_Q as a function of sol number (Figure 35). The Px-A, Px-B, and Px-C groups (see section 3.2) are indicated by different symbols (Figure 35a). The horizontal line at ΔE_Q = 2.12 mm/s corresponds to the average value of ΔE_Q for Home Plate rocks with A_{Hm} < 10%. Because the Px-B group includes highly altered rocks, Px-B, especially for the rocks with ΔE_Q ~ 2.4 mm/s (Independence Class and Ebenezer and Uchben in Clovis Subclass), may be Fe^{2+}-bearing alteration products as opposed to pyroxene as discussed in section 3. Similarly, Px-C (Comanche Spur) has an unusually low value of ΔE_Q, which may implicate a phase other than pyroxene. We did not find either Px-B or Px-C associated with high-Mt rocks, so they cannot be coupled with Mt formation during serpentization. In fact, Mt was not detected in either Assemblee or Independence. Evidence for phyllosilicates (e.g., serpentine) in Mini-TES data has not been reported for Clovis and Independence Class rocks [*Ruff et al.*, 2006; *Clark et al.*, 2007].

[95] The Px-A group can be divided into three subgroups on the basis of values ΔE_Q, with each subgroup representing pyroxene with different mineralogical composition (Figure 35a). Only rocks whose values of ΔE_Q were obtained from the least squares fitting procedures are plotted in Figure 35a (and also Figure 2). In a practical sense, this means that only rocks with significant Fe from Px and good counting statistics are included in Figure 35a.

[96] One Px composition is primarily associated with Adirondack Class rocks (average ΔE_Q = 2.07 ± 0.02 mm/s) (Figure 35a). Note the sharp change in pyroxene composition (i.e., ΔE_Q) when Sprit crossed the boundary between the Gusev plains and West Spur near sol ~155. The second pyroxene has a larger ΔE_Q (average = 2.15 ± 0.03 mm/s) and is primarily associated with outcrop rocks

on the NW slope of Husband Hill (e.g., Wooly Patch Subclass, Peace Class, and Watchtower Class). The third pyroxene composition has an intermediate ΔE_Q (average = 2.12 ± 0.02 mm/s) and is associated with Home Plate Outcrop rocks, Irvine Class rocks (float rocks on Husband Hill and near Home Plate), and Backstay Class (a float rock on Husband Hill). The MB parameter δ is not useful as discriminator for the Px-A pyroxene compositions because all three groups have the same average value (δ = 1.16 ± 0.02 mm/s). At this point, it is premature to associate values of ΔE_Q with particular Px compositions, but we note (1) that Adirondack pyroxenes are associated with rocks that have Ol, minor Mt, and no detectable Ilm as their other Fe^{2+}-bearing phases, (2) that the Backstay, Irvine, and Home Plate pyroxenes generally are accompanied by Mt as a major Fe-bearing phase, and (3) that pyroxene associated with the West Spur and NW Husband Hill Outcrop rocks have a loose affinity with Ilm-bearing rocks (e.g., Wishstone).

[97] For soils (Figure 35b), the average value of ΔE_Q is 2.12 ± 0.03 mm/s. Below average values are associated with the Adirondack Class rocks (sol < 155). The soil with the lowest ΔE_Q (2.02 ± 0.02 mm/s) is Mazatzal Flats Soil1 on the apron of the Adirondack Class rock Mazatzal [*Morris et al.*, 2006a]. Above average values are associated with Ilm-bearing rocks. The soils with the highest values of ΔE_Q are Pequod Doubloon and Cliffhanger Hang2 (2.20 ± 0.02 and 2.22 ± 0.02 mm/s, respectively) (*Morris et al.* [2006a] and Table 1). Pequod Doubloon is the only soil for which there is a clear detection of Fe from Ilm (Table 5). These observations show that the Fe mineralogical composition of local basaltic soils is perturbed from some average composition by degradation of local rocks.

10. Hydrothermal System at Home Plate

[98] Many lines of evidence now point to the presence of an extinct hydrothermal system at Home Plate. Home Plate itself is considered to have an explosive origin when basaltic magma came into contact with groundwater or ice [*Squyres et al.*, 2007]. Proximate and to the north and to the SE of Home Plate are sulfate deposits (Arad and Tyrone) that, with respect to Fe mineralogy, are rich in Fe^{3+}-sulfate (Figures 24b and 28b). Another Fe^{3+}-sulfate deposit is located at Paso Robles ~1 km from Home Plate on the NW slope of Husband Hill (Figure 17 and *Morris et al.* [2006a]). Because of their proximity, the Arad and especially the Tyrone deposits are probable fumarolic and/or hydrothermal deposits associated with the volcanic activity at Home Plate [*Yen et al.*, 2008]. The Paso Robles deposit may also be associated with Home Plate volcanism. In any case, these deposits involve dissolution of local Fe-bearing

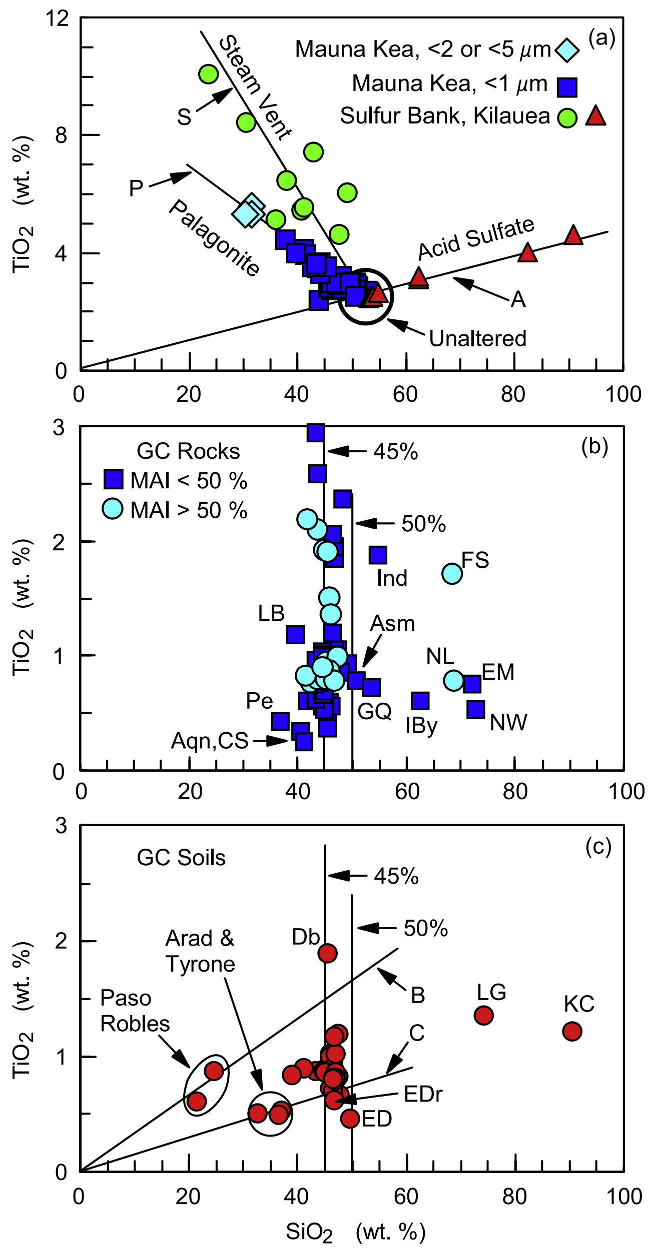

Figure 33. Plots of TiO_2 versus SiO_2 for (a) terrestrial analog basaltic material (Mauna Kea and Kilauea Volcanoes, Hawaii) weathered under supergene conditions (palagonite), in steam vents, and by acid sulfate leaching, (b) all Gusev Crater rocks, and (c) all Gusev Crater soils. In Figure 33a, data for weathered samples emanates from unaltered materials. SiO_2 is leached and TiO_2 is passively enriched during palagonitic and steam vent weathering. Both are passively enriched during acid sulfate weathering. In Figure 33b, the TiO_2–SiO_2 variation is largely controlled by differences in the bulk composition of the precursor basalts, except for the high-SiO_2 rocks (SiO_2 > 50 wt %) which have undergone acid sulfate leaching. In Figure 33c, the TiO_2–SiO_2 variation is controlled by differences in bulk composition (vertical line at SiO_2 = 45 wt %), dilution of both oxides by addition of S (Paso Robles, Arad, and Tyrone sulfate deposits), and alteration by acid sulfate leaching (Kenosha Comets and Lefty Ganote). MAI is the Mineralogical Alteration Index. Rock names are Aqn, Algonquin; Asm, Assemblee; CS, Comanche Spur; EM, Elizabeth Mahon; FS, Fuzzy Smith; GQ, Good Question; IBy, Innocent Bystander; Ind, Independence; LB, Larrys Bench; NL, Norma Luker; NW, Nancy Warren; and Pe, Peace. Soil names are Db, Pequod Doubloon; ED, Eastern Valley Eileen Dean; EDr, El Dorado Scuff Shadow; LG, Eastern Valley Lefty Ganote; and KC, Eastern Valley Kenosha Comets.

rocks and soils by sulfate-bearing hydrothermal solutions and subsequent precipitation of Fe^{3+}-sulfates and other sulfate salts [*Ming et al.*, 2006, 2008; *Yen et al.*, 2008].

[99] The high-SiO_2 soils in Eastern Valley between Home Plate and Mitcheltree Ridge are evidence for a different manifestation of an acid sulfate hydrothermal environment. In this case, basaltic precursor rocks/tephra are leached under acid sulfate hydrothermal conditions leaving behind the high-SiO_2 and high-TiO_2 fingerprint of the process (section 8 and *Squyres et al.* [2008]). Perhaps not coincidentally, there are very Hm-rich outcrop rocks (Halley, King George, Riquelme, and Montalva; Figures 28b and 29) located between Home Plate and the Fe^{3+}-sulfate deposit at Tyrone. A possible sequence of events is deposition of Mt-rich basaltic material like that further to the north in Eastern Valley during active Home Plate volcanism followed by some combination of (1) thermal oxidation (dry heating) of preexisting Mt plus exsolution and/or reprecipitation of Hm from Fe^{2+}-bearing silicate phases and (2) an isochemical aqueous process (low water-to-rock ratios) involving dissolution of Fe-bearing phases and precipitation of hematite and Fe-poor phases. Hematite formation reasonably occurred in association with the event or sequence of events that formed the Tyrone sulfate deposit.

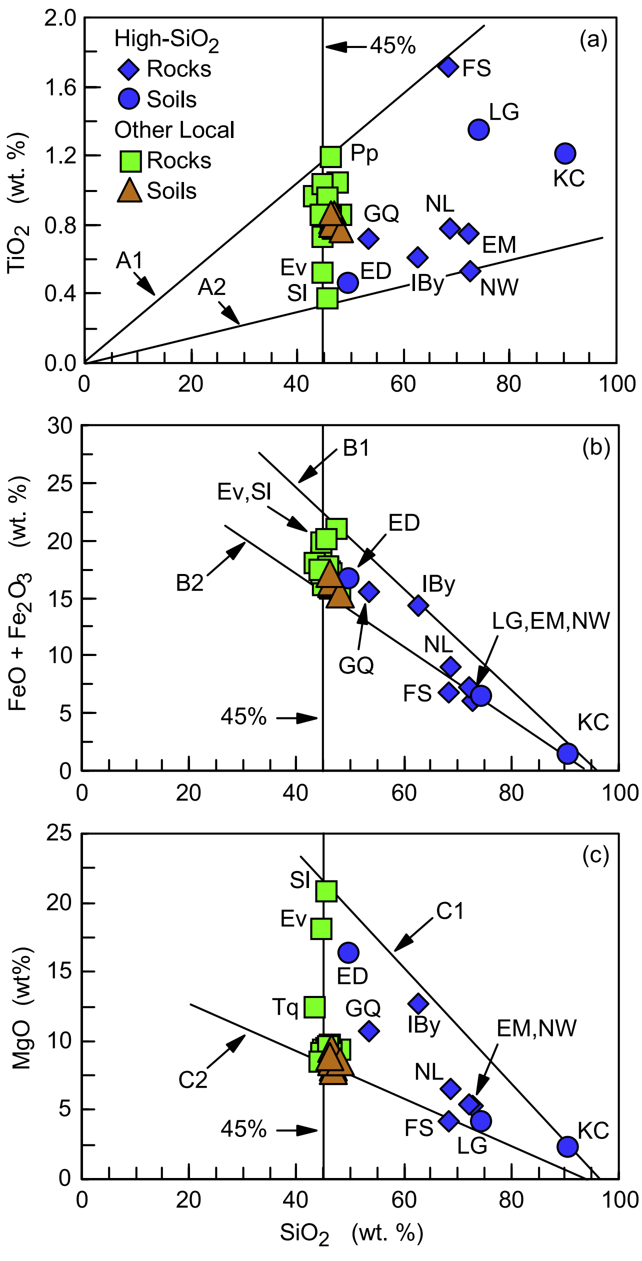

11. Summary

[100] The Mössbauer spectrometer on the Spirit rover provided spectra for determination of the Fe mineralogical composition and Fe redox state (as Fe^{3+}/Fe_T) of ~71 rocks and ~43 soils as of sol 1544. Some rocks were analyzed multiple times as undisturbed surfaces, surfaces cleaned by the RAT brush, and interior surfaces exposed by RAT grinding. Major results and interpretations since sol 520 are summarized next.

[101] 1. The Fe bearing phases detected by Spirit are olivine, pyroxene, ilmenite, magnetite, chromite, nanophase ferric oxide, Fe^{3+}-sulfate, hematite, goethite, and pyrite/marcasite. Chromite and Pyr/Mar have one occurrence each in different rocks (Assemblee and Fuzzy Smith, respectively). Fe^{3+}-sulfate occurs only in soils.

[102] 2. Relatively unaltered rocks occur as float rocks on Husband Hill and Home Plate (e.g., Irvine, Backstay, Esperanza, and Humboldt Peak), as Ol-rich outcrop rocks on Haskin Ridge, and as outcrop rocks at Home Plate and its vicinity. Backstay and Humboldt Peak are Ol-rich basalts with subordinate Mt and npOx. The Fe mineralogy of Irvine and Esperanza is dominated by Fe from Px and Mt. The outcrop rocks on Haskin Ridge are extremely Ol-rich (A_{Ol} = 50% to 75%) and are the best exposure of ultramafic rocks examined by Spirit. The unaltered outcrop rocks on Home Plate range from Ol-rich basalt on the western side (e.g., Barnhill) to Px- and Mt-rich rocks on the eastern side (e.g., Pesapallo). Px- and Mt-rich rocks are also found in the central and northern areas of Eastern Valley (e.g., Everett).

Figure 34. (a) TiO_2, (b) $FeO + Fe_2O_3$, and (c) MgO versus SiO_2 for high-SiO_2 rocks and soils, relatively unaltered outcrop rocks, and Eileen Dean and local Laguna Class soil at Home Plate and in Eastern Valley. The solid lines labeled A1 and A2 in Figure 34a are drawn through the origin and the two rocks with SiO_2 ~ 45% and with the extreme TiO_2 concentrations (Pp and Sl). By analogy with Figure 33a, all the high-SiO_2 rocks and soils can be derived by acid sulfate leaching of basaltic precursors known at Home Plate, at least with respect to TiO_2 and SiO_2 concentrations (but see text). The solid lines labeled B1 and B2 in Figure 34b and C1 and C2 in Figure 34c are drawn through the extreme values of the $FeO + Fe_2O_3$ and MgO concentrations at SiO_2 ~ 45% and their inferred values for fully leached basaltic rock ($FeO + Fe_2O_3$ = MgO = 0.0 wt % and SiO_2 ~ 95 wt %). As in Figure 34a, all high-SiO_2 rocks plot within or near the wedges defined by the solid lines. Rock names are EM, Elizabeth Mahon; Ev, Everett; FS, Fuzzy Smith; GQ, Good Question; IBy, Innocent Bystander; NL, Norma Luker; NW, Nancy Warren; Pp, Pesapallo; Sl, Slide; and Tq, Torquas. Soil names are ED, Eastern Valley Eileen Dean; KC, Eastern Valley Kenosha Comets; and LG, Eastern Valley Lefty Ganote.

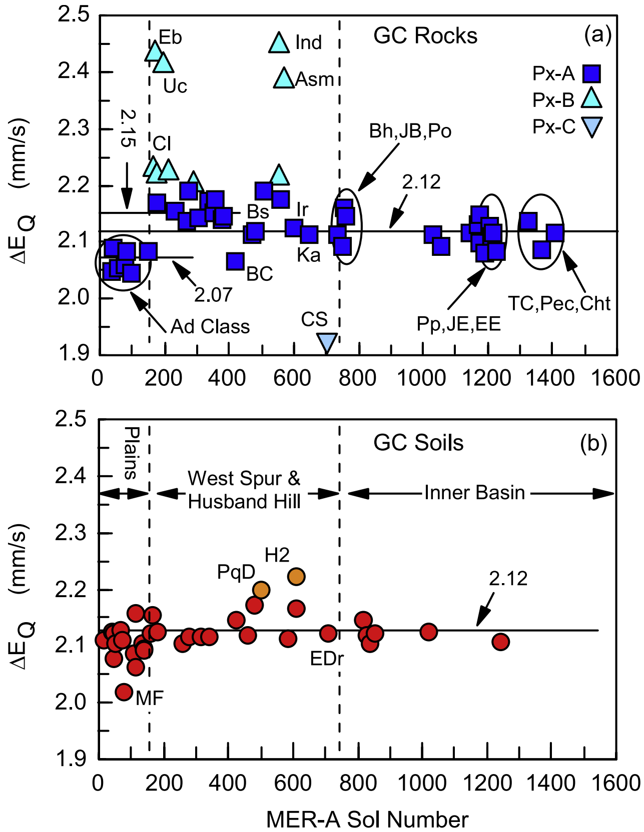

Figure 35. Plots of quadrupole splitting (ΔE_Q) versus Spirit sol number for the pyroxene doublet in MB spectra of Gusev Crater (a) rocks and (b) soils. The solid horizontal line at ΔE_Q = 2.12 mm/s is the average value of ΔE_Q for Home Plate rocks (Barnhill Class). Three pyroxene compositions are possibly represented in the Px-A group: Adirondack Class rocks with ΔE_Q ~2.07 mm/s (Gusev plains), Wooly Patch Subclass, Peace Class, and Watchtower Class with ΔE_Q ~2.15 mm/s, and Barnhill Class, Irvine Class, and Backstay Class with ΔE_Q ~2.12 mm/s. Rock names: Ad, Adirondack; Asm, Assemblee; Bh, Barnhill; BC, Bourgeoisie Chic; Bs, Backstay; Cht, Chanute; Cl, Clovis; CS, Comanche Spur;Eb, Ebenezer; EE, Elizabeth Emery; Ind, Independence; Ir, Irvine; JB, James CP Bell; JE, June Emerson; Ka, Kansas; Pec, Pecan Pie; Po, Posey; Pp, Pesapallo; TC, Texas Chili; and Uc, Uchben. Soil names are PqD, Pequod Doubloon; EDr, El Dorado Scuff Shadow; H2, Cliffhanger Hang2; and MF, Mazatzal Flats.

[103] 3. The Px subspectrum for the Ol-rich rock Comanche Spur has unusual MB parameters for pyroxene, which may permit a mineralogical assignment other than Px. Comanche Spur is the only occurrence.

[104] 4. There is evidence for three pyroxene compositions for the relative unaltered Gusev Crater rock on the basis of different quadrupole splittings (ΔE_Q). They are associated with (1) Adirondack Class rocks, (2) Home Plate Outcrop (Barnhill Class) and float rocks in Irvine Class and Backstay Class, and (3) Ti-bearing Columbia Hill rocks.

[105] 5. Pervasively altered rocks containing Gt occur on both sides of the Husband Hill summit. Gt (α-FeOOH) is a marker mineral for aqueous alteration because it can form only in the presence of H_2O. Isochemical alteration (low water-to-rock ratios) is a characteristic of the Gt-bearing rocks (Clovis, Wishstone, and Watchtower Classes).

[106] 6. Pervasively altered outcrop rocks (Independence and Assemblee) with Fe from Px, npOx and either Ilm or Chr but no detectable Fe from Ol, Mt, Hm, and Gt are found on the SW slope of Husband Hill. The Ilm and Chr are interpreted as residual phases of aqueous leaching (high water-to-rock ratios) which also resulted in low total Fe concentrations.

[107] 7. Subsurface Fe^{3+}-sulfate deposits were detected by MB near Home Plate at Arad and Tyrone. The sulfates are likely fumarolic and/or hydrothermal deposits associated with the volcanic activity at Home Plate.

[108] 8. The Hm-rich outcrop rocks with up to ~78% of total Fe from Hm (e.g., Halley and Montalva) are located between Home Plate and the Tyrone sulfate deposit. The hematite may be a manifestation of oxidative heating of previously unaltered basaltic materials by the event or sequence of events that lead to the formation of the Tyrone sulfate deposit. Low water-to-rock ratios or possibly dry heating (i.e., no or limited leaching) is implied by basaltic bulk chemical composition.

[109] 9. The silica-rich rocks and soils in Eastern Valley are interpreted as a product of acid sulfate leaching of precursor basalt having a range of bulk chemical compositions.

[110] 10. The only strongly magnetic phase detected by Mössbauer at Gusev is magnetite. The percentage of total Fe that is present as Mt ranges from 40 to 56% for a significant number of rocks (e.g., Irvine Class, Pesapallo Subclass, Everett Class, Torquas, and Innocent Bystander). An igneous origin is indicated by the presence of Ti in the magnetite-rich sample collected by the MER capture magnet.

[111] **Acknowledgments.** R.V.M. and D.W.M. acknowledge support of the NASA Mars Exploration Rover Project and the NASA Johnson Space Center. C.S. acknowledges support by an appointment to the NASA Postdoctoral Program at the Johnson Space Center, administered by Oak Ridge Associated Universities through a contract with NASA. The MER MIMOS II Mössbauer spectrometers were developed and built with funding provided by the German Space Agency under contract 50QM 99022 and with additional support from the Technical University of Darmstadt and the University of Mainz. A portion of the work described in this paper was conducted at the Jet Propulsion Laboratory, California Institute of Technology under a contract with NASA. We acknowledge the unwavering support, dedication, and attention to detail of JPL engineering and MER operations staff and the MER Athena Science Team. We thank D. Agresti and Brad Jolliff for thoughtful and detailed reviews of the manuscript.

References

Allen, C. C., J. L. Gooding, M. Jercinovic, and K. Keil (1981), Altered basaltic glass: A terrestrial analog to the soil of Mars, *Icarus*, *45*, 347–369, doi:10.1016/0019-1035 (81)90040-3.

Allen, C. C., R. V. Morris, H. V. Lauer Jr., and D. S. McKay (1993), Microscopic iron metal on glass and minerals: A tool for studying regolith maturity, *Icarus*, *104*, 291–300, doi:10.1006/icar.1993.1102.

Arvidson, R. E., et al. (2004), Localization and physical properties experiments conducted by Spirit at Gusev Crater, *Science*, *305*, 821–824, doi:10.1126/science.1099922.

Arvidson, R. E., et al. (2006), Overview of the Spirit Mars Exploration Rover Mission to Gusev Crater: Landing site to Backstay Rock in the Columbia Hills, *J. Geophys. Res.*, *111*, E02S01, doi:10.1029/2005JE002499.

Arvidson, R. E., et al. (2008), Spirit Mars Exploration Rover mission to Gusev Crater, Columbia Hills: Mission overview and selected results from the Cumberland Ridge to Home Plate, *J. Geophys. Res.*, *113*, E12S33, doi:10.1029/2008JE003183.

Bell, J. F., III, et al. (2000), Mineralogic and compositional properties of Martian soil and dust: Results from Mars Pathfinder, *J. Geophys. Res.*, *105*, 1721–1755, doi:10.1029/1999JE001060.

Bell, J. F., III, et al. (2004), Pancam multispectral imaging results form the Spirit rover at Gusev Crater, *Science*, *305*, 800–806, doi:10.1126/science.1100175.

Bibring, J.-P., et al. (2006), Global mineralogical and aqueous Mars history derived from OMEGA/Mars Express data, *Science*, *312*, 400–404, doi:10.1126/science.1122659.

Bouska, V., and J. F. Bell III (1993), Assumptions about the presence of natural glasses on Mars, *J. Geophys. Res.*, *98*, 18,719–18,725, doi:10.1029/93JE01959.

Burns, R. G., and T. C. Solberg (1990), Crystal structure trends in Mössbauer spectra of ^{57}Fe-bearing oxide, silicate, and aluminosilicate minerals, in *Spectroscopic Characterization of Minerals and Their Surfaces*, edited by L. M. Coyne et al., pp. 262–283, Am. Chem. Soc., Washington, D.C.

Cabrol, N. A., et al. (2008), Soil sedimentology at Gusev Crater from Columbia Memorial Station to Winter Haven, *J. Geophys. Res.*, *113*, E06S05, doi:10.1029/2007JE002953.

Campbell, J. L., R. Gellert, M. Lee, C. L. Mallett, J. A. Maxwell, and J. M. O'Meara (2008), Quantitative in situ determination of hydration of bright high-sulfate Martian soils, *J. Geophys. Res.*, *113*, E06S11, doi:10.1029/2007JE002959.

Clark, B. C., et al. (2007), Evidence for montmorillonite or its compositional equivalent in the Columbia Hills, Mars, *J. Geophys. Res.*, *112*, E06S01, doi:10.1029/2006JE002756.

Cornell, R., and U. Schwertmann (1996), *The Iron Oxides: Structure, Properties, Reactions, Occurrences, and Uses*, VHC, New York.

Dang, M.-Z., D. G. Rancourt, J. E. Dutrizac, G. Lamarche, and R. Provencher (1998), Interplay of surface conditions, particle size, stoichiometry, cell parameters, and magnetism in synthetic hematite-like minerals, *Hyperfine Interact.*, *117*, 271–319, doi:10.1023/A:1012655729417.

Farrand, W. H., J. F. Bell III, J. R. Johnson, R. E. Arvidson, L. Crumpler, J. A. Hurowitz, and C. Schröder (2008), Rock spectral classes observed by the Spirit Rover's Pancam on the Gusev Crater Plains and in the Columbia Hills, *J. Geophys. Res.*, doi:10.1029/2008JE003237, in press.

Gellert, R., et al. (2006), Alpha Particle X-Ray Spectrometer (APXS): Results from Gusev Crater and calibration report, *J. Geophys. Res.*, *111*, E02S05, doi:10.1029/2005JE002555.

Goetz, W., et al. (2005), Indication of drier periods on Mars from the chemistry and mineralogy of atmospheric dust, *Nature*, *436*, 62–65, doi:10.1038/nature03807.

Goetz, W., et al. (2008), Search for magnetic minerals in Martian rocks: Overview of the Rock Abrasion Tool (RAT) magnet investigation on Spirit and Opportunity, *J. Geophys. Res.*, *113*, E05S90, doi:10.1029/2006JE002819.

Hutton, J. T. (1977), Titanium and zirconium minerals, in *Minerals in Soil Environments*, edited by J. B. Dixon et al., pp. 673–688, Soil Sci. Soc. of Am., Madison,Wis.

Johnson, J. H. (1977), Jarosite and akaganeite from White Island volcano, New Zealand: An X-ray and Mossbauer study, *Geochim. Cosmochim. Acta*, *41*, 539–544.

Jouglet, D., F. Poulet, R. E. Milliken, J. F. Mustard, J.-P. Biebring, Y. Langevin, B. Gondet, and C. Gomez (2007), Hydration state of the Martian surface as seen by Mars Express OMEGA: 1. Analysis of the 3 μm hydration feature, *J. Geophys. Res.*, *112*, E08S06, doi:10.1029/2006JE002846.

Klingelhöfer, G., et al. (2003), Athena MIMOS II Mössbauer spectrometer investigation, *J. Geophys. Res.*, *108*(E12), 8067, doi:10.1029/2003JE002138.

Lichtenberg, K. A., et al. (2007), Coordinated analyses of orbital and Spirit rover data to characterize surface materials on the cratered plains of Gusev Crater, Mars, *J. Geophys. Res.*, *112*, E12S90, doi:10.1029/2006JE002850.

McAdam, A. C., M. Y. Zolotov, M. V. Mironenko, and T. G. Sharp (2008), Formation of Martian silica-rich deposits through rock alteration: A theoretical assessment, *Lunar Planet. Sci.* [CD-ROM], *XXXIX*, Abstract 2371.

McCammon, C. (1995), Mössbauer spectroscopy of minerals, in *Mineral Physics and Crystallography: A Handbook of Physical Constants*, edited by T. J. Ahrens, pp. 332–347, AGU, Washington, D.C.

McCoy, T. J., et al. (2008), Structure, stratigraphy, and origin of Husband Hill, Columbia Hills, Gusev Crater, Mars, *J. Geophys. Res.*, *113*, E06S03, doi:10.1029/2007JE003041.

McKay, G., J. Wagstaff, and S.-R. Yang (1986), Clinopyroxene REE distribution coefficients for shergottites: The REE content of the Shergotty melt, *Geochim. Cosmochim. Acta*, *50*, 927–937, doi:10.1016/0016-7037(86)90374-1.

McSween, H. Y., et al. (2006a), Characterization and petrologic interpretation of olivine-rich basalts at Gusev Crater, Mars, *J. Geophys. Res.*, *111*, E02S10, doi:10.1029/2005JE002477.

McSween, H. Y., et al. (2006b), Alkaline volcanic rocks from the Columbia Hills, Gusev Crater, Mars, *J. Geophys. Res.*, *111*, E09S91, doi:10.1029/2006JE002698.

McSween, H. Y., et al. (2008), Mineralogy of volcanic rocks in Gusev Crater, Mars: Reconciling Mössbauer, Alpha Particle X-Ray Spectrometer, and Miniature Thermal Emission Spectrometer spectra, *J. Geophys. Res.*, *113*, E06S04, doi:10.1029/2007JE002970.

Milliken, R. E., J. F. Mustard, F. Poulet, D. Jouglet, J.-P. Bibring, B. Gondet, and Y. Langevin (2007), Hydration state of the Martian surface as seen by Mars Express OMEGA: 2. H_2O content of the surface, *J. Geophys. Res.*, *112*, E08S07, doi:10.1029/2006JE002853.

Ming, D. W., et al. (2006), Geochemical and mineralogical indicators for aqueous processes in the Columbia Hills of Gusev Crater, Mars, *J. Geophys. Res.*, *111*, E02S12, doi:10.1029/2005JE002560.

Ming, D. W., et al. (2008), Geochemical properties of rocks and soils in Gusev Crater, Mars: Results of the Alpha-Particle X-Ray Spectrometer from Cumberland Ridge to Home Plate, *J. Geophys. Res.*, doi:10.1029/2008JE003195, in press.

Morris, R. V., H. V. Lauer Jr., C. A. Lawson, E. K. Gibson Jr., G. A. Nace, and C. Stewart (1985), Spectral and other physicochemical properties of submicron powders of hematite (α-Fe_2O_3), maghemite (γ-Fe_2O_3), magnetite (Fe_3O_4), goethite (α-FeOOH), and lepidocrocite (γ-FeOOH), *J. Geophys. Res.*, *90*, 3126–3144, doi:10.1029/JB090iB04p03126.

Morris, R. V., D. G. Agresti, H. V. Lauer Jr., J. A. Newcomb, T. D. Shelfer, and A. V. Murali (1989), Evidence for pigmentary hematite on Mars based on optical magnetic and Mössbauer studies of superparamagnetic (nanocrystalline) hematite, *J. Geophys. Res.*, *94*, 2760–2778.

Morris, R. V., et al. (2000a), Mineralogy, composition, and alteration of Mars Pathfinder rocks and soils: Evidence from multispectral, elemental, and magnetic data on terrestrial analogue, SNC meteorite, and Pathfinder samples, *J. Geophys. Res.*, *105*, 1757–1817, doi:10.1029/1999JE001059.

Morris, R. V., L. Le, M. D. Lane, D. C. Golden, T. D. Shelfer, G. E. Lofgren, and P. R. Christensen (2000b), Multidisciplinary study of synthetic Mars golbal average soil glass, *Lunar Planet. Sci.* [CD-ROM], *XXXI*, Abstract 1611.

Morris, R. V., T. Graff, M. D. Lane, C. S. Schwandt, T. D. Shelfer, D. W. Ming, S. A. Mertzman, J. F. Bell III, J. Crisp, and P. R. Christensen (2000c), Acid sulfate alteration products of a tholeiitic basalt: Implications for interpretation of Martian thermal emission spectra, *Lunar Planet. Sci.* [CD-ROM], *XXXI*, Abstract 2014.

Morris, R. V., D. C. Golden, D. W. Ming, T. D. Shelfer, L. C. Jorgensen, J. F. Bell III, T. G. Graff, and S. A. Mertzman (2001), Phyllosilicate-poor palagonitic dust from Mauna Kea Volcano (Hawaii): A mineralogical analogue for magnetic Martian dust?, *J. Geophys. Res.*, *106*, 5057–5083, doi:10.1029/2000JE001328.

Morris, R. V., et al. (2004), Mineralogy at Gusev Crater from the Mössbauer spectrometer on the Spirit rover, *Science*, *305*, 833–836, doi:10.1126/science.1100020.

Morris, R. V., et al. (2006a), Mössbauer mineralogy of rock, soil, and dust at Gusev Crater, Mars: Spirit's journey through weakly altered olivine basalt on the plains and pervasively altered basalt in the Columbia Hills, *J. Geophys. Res.*, *111*, E02S13, doi:10.1029/2005JE002584.

Morris, R. V., et al. (2006b), Mössbauer mineralogy of rock, soil, and dust at Meridiani Planum, Mars: Opportunity's journey across sulfate-rich outcrop, basaltic sand and dust, and hematite lag deposits, *J. Geophys. Res.*, *111*, E12S15, doi:10.1029/2006JE002791.

Morris, R. V., G. A. McKay, D. W. Ming, G. Klingelhöfer, C. Schröder, D. Rodionov, and A. Yen (2006c), Magnetite in Martian meteorite MIL 03346 and Gusev Adirondack Class basalt: Mössbauer evidence for variability in the oxidation state of Adirondack lavas, *Lunar Planet. Sci.* [CD-ROM], *XXXVII*, Abstract 1594.

Morris, R. V., et al. (2007), Possible evidence for iron sulfates, iron sulfides, and elemental sulfur at Gusev Crater, Mars, from MER, CRISM, and analog data, in *Seventh Internation Conference on Mars* [CD-ROM], Abstract 3933, Jet Propul. Lab., Pasadena, Calif.

Morris, R. V., G. A. McKay, D. G. Agresti, and L. Le (2008), Mössbauer and electron microprobe studies of density separates of Martian Nakhlite MIL03346: Implication for interpretation of Mössbauer spectra acquired by the Mars Exploration Rovers, *Lunar Planet. Sci.* [CD-ROM], *XXXIX*, Abstract 2458.

Murad, E., and J. H. Johnston (1987), Iron oxides and oxyhydroxides, in *Mössbauer Spectroscopy Applied to Inorganic Chemistry*, vol. 2, edited by G. J. Long, pp. 507–582, Plenum, New York.

Ruff, S. W., P. R. Christensen, D. L. Blaney, W. H. Farrand, J. R. Johnson, J. R. Michalski, J. E. Moersch, S. P. Wright, and S. W. Squyres (2006), The rocks of Gusev Crater as viewed by the Mini-TES instrument, *J. Geophys. Res.*, *111*, E12S18, doi:10.1029/2006JE002747.

Schmidt, M. E., et al. (2008a), Hydrothermal origin of halogens at Home Plate, Gusev Crater, *J. Geophys. Res.*, *113*, E06S12, doi:10.1029/2007JE003027.

Schmidt, M. E., W. H. Farrand, R. Gellert, J. Hurowitz, J. R. Johnson, T. J. McCoy, and the Athena Science Team (2008b), Lateral mineralogical and chemical variations at Home Plate: Implications for fluid flow and hydrothermal alteration, *Lunar Planet. Sci.* [CD-ROM], *XXXIX*, Abstract 2024.

Schröder, C., K. Di, R. V. Morris, G. Klingelhöfer, R. Li, and the Athena Science Team (2008), An east to west mineralogical trend in Mars Exploration Rover Spirit Mössbauer spectra of Home Plate, *Lunar Planet. Sci.* [CD-ROM], *XXXIX*, Abstract 2153.

Squyres, S. W., et al. (2003), Athena Mars rover science investigation, *J. Geophys. Res.*, *108*(E12), 8062, doi:10.1029/2003JE002121.

Squyres, S. W., et al. (2004), The Spirit rover's Athena science investigation at Gusev Crater, Mars, *Science*, *305*, 794–799, doi:10.1126/science.3050794.

Squyres, S. W., et al. (2006), Rocks of the Columbia Hills, *J. Geophys. Res.*, *111*, E02S11, doi:10.1029/2005JE002562.

Squyres, S. W., et al. (2007), Pyroclastic activity at Home Plate in Gusev Crater, Mars, *Science*, *316*, 738–742, doi:10.1126/science.1139045.

Squyres, S. W., et al. (2008), Detection of silica-rich deposits on Mars, *Science*, *320*, 1063–1067.

Stevens, J. G., A. M. Khasanov, J. W. Miller, H. Pollak, and Z. Li (1998), *Mössbauer Mineral Handbook*, Biltmore Press, Ashville, N.C.

Stolper, E., and H. Y. McSween Jr. (1979), Petrology and origin of the shergottite meteorites, *Geochim. Cosmochim. Acta*, *43*, 1475–1498, doi:10.1016/0016-7037(79)90142-X.

Tilley, D. B., and R. A. Eggleton (2005), Titanite low-temperatue alteration and Ti mobility, *Clays Clay Miner.*, *53*, 100–107, doi:10.1346/CCMN.2005.0530110.

Treiman, A. H. (2005), The nakhlite meteorites: Augite-rich igneous rocks from Mars, *Chem. Erde*, *65*, 203–270, doi:10.1016/j.chemer.2005.01.004.

Van Cromphaut, C., V. G. de Resende, E. De Grave, A. Van Alboom, R. E. Vandenberghe, and G. Klingelhöfer (2007), Characterisation of the magnetic iron phases in Clovis Class rocks in Gusev Crater from the MER Spirit Mössbauer spectrometer, *Geochim. Cosmochim. Acta*, *71*, 4814–4822, doi:10.1016/j.gca.2007.07.024.

Vieira, V. W. A., T. V. V. Costa, H. G. Jensen, J. M. Knudsen, and M. Olsen (1986), Oxidation state of iron in SNC meteorites as studied by Mössbauer spectroscopy, *Phys. Scr.*, *33*, 180–186, doi:10.1088/0031-8949/33/2/016.

Wang, A., et al. (2006), Sulfate deposition in subsurface regolith in Gusev Crater, Mars, *J. Geophys. Res.*, *111*, E02S17, doi:10.1029/2005JE002513.

Yen, A. S., B. C. Murray, and G. R. Rossman (1998), Water content of the Martian soil: Laboratory simulations of reflectance spectra, *J. Geophys. Res.*, *103*, 11,125–11,133, doi:10.1029/98JE00739.

Yen, A. S., et al. (2008), Hydrothermal processes at Gusev Crater: An evaluation of Paso Robles Class soil, *J. Geophys. Res.*, *113*, E06S10, doi:10.1029/2007JE002978.

R. E. Arvidson, Department of Earth and Planetary Sciences, Washington University, Campus Box 1169, 1 Brookings Drive, St. Louis, MO 63130, USA.

B. C. Clark, Lockheed Martin Corporation, Littleton, CO 80127, USA.

B. A. Cohen, NASA Marshall Space Flight Center, Huntsville, AL 35812, USA.

L. S. Crumpler, New Mexico Museum of Natural History and Science, 1801 Mountain Road NW, Albuquerque, NM 87104, USA.

P. A. de Souza Jr., Tasmanian ICT Centre, CSIRO, Castray Esplanade, Hobart, Tas, 7000, Australia.

I. Fleischer, G. Klingelhöfer, and D. S. Rodionov, Institut fur Anorganische und Analytische Chemie, Johannes Gutenberg Universität, Staudinger Weg 9, Mainz, D-55128, Germany.

R. Gellert, Department of Physics, University of Guelph, Guelph, ON N1G 2W1, Canada.

T. J. McCoy and M. E. Schmidt, Department of Mineral Sciences, Smithsonian Institution, Washington, DC 20560-0119, USA.

D. W. Ming, D. W. Mittlefehldt, R. V. Morris, and C. Schröder, NASA Johnson Space Center, Houston, TX 77058, USA. (richard.v.morris@nasa.gov)

S. W. Squyres, Department of Astronomy, Cornell University, Ithaca, NY 14853, USA.

A. S. Yen, Jet Propulsion Laboratory, California Institute of Technology, 4800 Oak Grove Drive, Pasadena, CA 91109, USA.